FABRICATION AND STUDY OF PATTERNED POLYMER BRUSHES FOR CONTROLLING CELL BEHAVIOR

CHEN Lina
Ph.D

The Hong Kong Polytechnic University
2017

The Hong Kong Polytechnic University

Institute of Textiles and Clothing

Fabrication and Study of Patterned Polymer Brushes for Controlling Cell Behavior

CHEN Lina

A Thesis Submitted in Partial Fulfillment of the Requirements for the Degree of Doctor of Philosophy

May 2017

Certificate of Originality

I hereby declare that this thesis is my own work and that, to the best of my knowledge and belief, it reproduces no material previously published or written, nor material that has been accepted for the award of any other degree or diploma, except where due acknowledgement has been made in the text.

_____ *(Signed)*

Lina Chen

May 2017

ABSTRACT

Thorough understanding of how to control cell behaviors including cell adhesion, proliferation, orientation, migration, and differentiation on an artificial surface is critical in materials and life sciences such as biomedical engineering, tissue engineering, and cell-based bioassay. *In vivo*, extracellular matrix (ECM) consists of a combination of proteoglycans, glycosaminoglycans, fibrous proteins and adhesion proteins, which not only provide mechanical support to cells but also profoundly affect cell behaviors and cell functions. The three major cues in ECM, namely chemical, topographical and mechanical cues, can interact and communicate with cells to influence cell behaviors. Functional polymer brushes, which exhibit excellent mechanical properties, abundant chemical species, and remarkable capability to form various topographical surfaces, have superior advantages over many other materials for generating artificial ECM.

This thesis studies the fabrication of biomimetic binary polymer brush patterns and their applications in controlling cell behaviors. Two new approaches are developed to generate binary polymer brush patterns for controlling cell behaviors. One is two-dimensional bench-top parallel dip-pen nanodisplacement lithography (DNL) (2D p-DNL) technique, by which the nano-micro binary polymer brush patterns are prepared. The nano-micro binary polymer brush patterns consist of lateral patterned centimeter-sized nanolines of gelatin-modified poly (glycidyl methacrylate) (gelatin-PGMA) brushes which are spaced by microstripes of poly (N-isopropylacrylamide) (PNIPAm) brushes. Cells can adhere and align well with the binary polymer brush patterns, and detach from the substrate with well-preserved ECM and aligned morphology upon the external thermal stimulus. Another method is microcontact printing (μCP) which is applied to generate a micropatterned binary polymer brush systems based on the serendipitous initiator-sticky ability of poly [oligo (ethylene glycol) methyl ether methacrylate] (POEGMA), poly (2-hydroxyethyl methacrylate) (PHEMA), and PGMA brushes. Briefly, initiator micropatterns are printed onto three kinds of polymer brush

surfaces, and vertically patterned second-layer polymer brushes are then grown from the pre-patterned initiators. Cell micropatterning and orientation can be realized on the binary polymer brush patterns.

For the content, the research background, challenges, objectives, and originality are introduced at the beginning of the thesis. Subsequently, a comprehensive literature review on polymer brushes for controlling cell behaviors and state-of-the-art lithography techniques for preparing patterned polymer brushes is presented. Chapter 3 gives a general description of research methodologies. In chapter 4, the DNL technique and the fabrication of single-component 3D-patterned polymer brushes are elaborately presented. Chapter 5 states the fabrication of binary 3D polymer brush structures by DNL. Chapter 6 focuses on the fabrication of nano-micro binary polymer brush patterns and the application in manipulating cell behaviors. Chapter 7 described a binary polymer brush micropatterns fabricated based on the initiator stickiness for cell micropatterning and orientation. Finally, the conclusions and outlook of this thesis are presented in Chapter 8.

LIST OF PUBLICATIONS

Related Journal Publications

1. **Chen, L.**, Xie, Z., Gan, T., Wang, Y., Zhang, G., Mirkin, C. A., Zheng, Z.* Biomimicking Nano-Micro Binary Polymer Brushes for Smart Cell Orientation and Adhesion Control. Small, 2016, 12 (25), 3400-3406.

2. **Chen, L.**, Yan, C., Zheng, Z.*. Functional Polymer Surfaces for Controlling Cell Behaviors. Materials Today, 2017. (Accepted, DOI https://doi.org/10.1016/j.mattod. 2017.07.002).

3. **Chen, L**.†, Wei, X.†, Zhou, X., Li, K., Niu, L., Ruan, Q., Zhen, H., Chen, C., Xie, Z., Wang, J., Mirkin, C. A., Zheng, Z.* Large-Area Patterning of Metal Nanostructures by Dip-pen Nanodisplacement Lithography for Optical Applications. Small, 2017. (Accepted, DOI: 10.1002/smll.201702003).

Other Journal Publications

1. Yu, Y., Xiao, X., Zhang, Y., Li, K., Yan, C., Wei, X., **Chen, L.**, Zhen, H., Zhou, H., Zhang, S., Z. J. Zheng. (2016). Photoreactive and Metal-Platable Copolymer Inks for High-Throughput, Room-Temperature Printing of Flexible Metal Electrodes for Thin-Film Electronics. Advanced Materials, 2016, 28 (24), 4926-4934.

Conference Participation

1. **Lina Chen**, Zijian Zheng, "Fabrication of Two-Component 3D Polymer Brush Structures by Parallel Dip-Pen Nanodisplacement Lithography for Cell Orientation Control" (Oral Presentation), 2016 MRS Spring Meeting, March 28th-April 1st, 2016, Phoniex, Arizona, USA.

2. **Lina Chen**, Zijian Zheng, "Biomimicking Nano-Micro Binary Polymer Brushes for Smart Cell Orientation and Adhesion Control", ITC Research Seminar 2016, The Hong Kong Polytechnic University, Hong Kong SAR, China.

3. **Lina Chen**, Zijian Zheng, “Thermoresponsive Nano-Micro Binary Polymer Brush Patterns for Controlling Cell Orientation and Smart Detachment” (Poster), Young Giants of Nanosicence 2016, The Hong Kong Polytechnic University, Hong Kong SAR, China.

ACKNOWLEDGEMENTS

First, I would like to express my greatest gratitude to my chief supervisor, Prof. Zijian Zheng, for giving me the chance to join his research group. I am very grateful to all patience and support of Prof. Zijian Zheng and his constant guidance, encouragements, words and deeds given on my PhD study. The things he has taught me, are not only about knowledge and professional training, but also contain the writing, presentation, and even communicating skills. His insight-suggestion and enthusiasm in guidance, rigorous and honest attitudes in academic research, have been always great inspirations for me.

I would also like to acknowledge my co-supervisors, Prof. Tao and Prof. Wang. They have provided enormous help to support my research topic, especially Prof. Wang who has helped me a lot in cell culture experiments.

Also, I am very grateful to all my colleagues in Dr. Zheng's group. They help me a lot in my research and daily life, especially Dr. Xuechang Zhou, Dr. Zhuang Xie, Dr. Liyong Niu, Dr Xiaoling Wei, Dr. You Yu, Dr Xuqiang Liu, Dr. Hongyu Zhen, Dr Dongrui Wang, Dr. Dongdong Chen, Mr Yaokang Zhang, Miss Miya Ng, Miss Casey Yan and Mr Chaojian Chen.

In addition, I would like to acknowledge all the laboratory officers and technicians in the Institute of Textiles and Clothing. And I would like to thank Miss Wendy Liu at the Hong Kong Baptist University for helping me with the XPS characterization, and Miss Fangyuan Dong in Prof. Wang's group for helping me a lot in cell culture experiments.

I also gratefully acknowledge financial support from The Hong Kong Polytechnic University, the General Research Fund of Hong Kong, National Natural Science Foundation of China and Research Student Attachment Programme of HKPolyU.

Finally, I wish to express my deepest gratitude to my dear parents, sister and brother for their endless love and support.

TABLE OF CONTENTS

LIST OF FIGURES

to 20 °C and grafted onto a damaged cornea of a patient suffering from Saltzman syndrome. Photographs were taken before and after the surgical operation. c) Cell adhesion and detachment on thermal-responsive P (OEGMA-co-MEO_2MA) modified gold substrates. The scale bars are 100 μm. d) Images of human fibroblasts detached from P(TEGMA-EE) modified substrates at 17.5 °C. Scale bar: 100 μm. e) Representative fluorescence microscopic images of Live/Dead viability staining adhered cells on different surfaces following photoirradiation. The green fluorescent cells indicate living cells and the red fluorescent cells indicate cell death. Scale bar: 20 μm.

Figure 2.8. a) The biofunctional block-copolymer brushes (PAAm/bisAAm-bPAA) architecture. The crosslinking is implemented in the initially polymerized PAAm block, while the adhesion peptide RGD, conjugated to the subsequently polymerized PAA block, affords the signaling. b) Number of cells per mm^2 (NIH-3T3 cells, and PaTu 8988t cells) on peptide-functionalized polymer brushes (green RGD, red RAD) compared to cells attached to a tissue culture poly styrene (TCPS) dish after 24 hours of culture. c) Fluorescence microscopy images of NIH-3T3 and PaTu 8988t cells on PAAm-b-PAA-RGD brushes with different moduli of the PAAm block. The immunostaining method is included in the Supporting Information.

Figure 2.9. a) Surface SEM images for (left) the unmodified PVDF membrane and (right) PHEMA modified PVDF membrane. Scale bar: 50 μm. b) Fluorescence and SEM images of L02 and BEL-7402 cells on surfaces. Spreading cells on the GNPL surface are marked by red ovals in B3 and D3. Scale bar: 50 μm. The shape and filopodia of the cells on POEGMA-modified surfaces were observed by confocal microscopy and are shown as insets in A2, A4, C2, and C4 (scale bar: 10 μm).

Figure 2.10. a) Chemical structures of polymers prepared. b) schematic image (lower right) of cellular response to non-contacting nanoscale sublayer, and microscopic images of adhered L929 on TCPS (upper left), poly(MPC) (upper middle), poly(AEMA) (upper right), PMbA50 (lower left), and PMbA15 (lower middle) after 72 h from seeding.

Figure 2.11. a) Schematic presentation of PL process. b) The fluorescence images of adherent fibroblasts on nonpatterned PNIPAm and patterned copolymer brushes surfaces (Actin: red and nuclei: blue. Scale bar: 100 μm), and the photograph of a cell sheet harvested from patterned surfaces showing orientation. c) Schematic of preparation of nanopatterned brushes by IL and SIP. First, nanopatterns of ATRP initiators are fabricated via IL. Second, brushes (e.g., PNIPAAm) are grafted from the nanopatterns of ATRP initiators. d) Procedure for preparing PNIPAAm surfaces with both micropatterns and nanopatterns. e) Contact-mode AFM height images obtained in air of nanopatterned PNIPAAm surfaces generated at a constant polymerization time (6 min, corresponding to tPNIPAAm = 78.8 ± 3.5 nm). f) The fluorescence images of viable NIH-3T3 fibroblasts located exclusively on the nanopatterned regions after 72 h. Cells were treated with LIVE/DEAD stain prior to imaging.

Figure 2.12. a) Schematic presentation of EBL process. b) From left to right: phase-contrast, fluorescence, and SEM microscopy images, of hippocampal neurons on PPy. A-C) Cells cultured on 2 μm wide and 200 nm deep PPy microchannels; D-F) cells cultured on unmodified PPy. The green labeling (Alexa 488) corresponds to Tau-1 (axonal marker) immunostaining. Cells polarized more readily on microchannels than on unmodified PPy. The scale bar is 20 μm (A, B, D, E) and 5 μm (C, F). c) A quantitative analysis of the axon angle. Histograms for axon angle distribution on unmodified PPy/PDMS substrates (left) and 2 μm PPy/PDMS microchannels (right).

Figure 2.13. a) Schematic presentation of the procedure for micropatterning cells inside a microfluidic device using cell-adhesive or non-adhesive substrates. b) Schematic presentation of the formation of ECM protein/POEGMA patterns on glass or gold substrates by μCP and SI-ATRP, and fluorescence microscope images of single cells (scale bar: 30 μm) spreading on 50 μm islands after 3 hrs (F-actin: red and nucleus: blue) and the corresponding projected single cell area measured from F-actin staining images (*$P < 0.01$). The substrates used were APTS-coated glass (APTS), LBL-coated glass with macro-initiator printing (Macro) and gold (Gold).

Figure 2.14. Evolution of SPL-directed organic transformations involving metal catalyzed, enzyme catalyzed, thermal, redox, force, and light induced reactions.

cells/mL. (b) Optical image of NIH-3T3 cells incubated on gelatin modified PGMA brushes-coated Au-glass substrate (thickness of PGMA: 70 nm) for 24 h. Seeding density: 1 x 10^5 cells/mL. Scale bar: 100 μm.

Figure 6.4. (a) Designed pattern parameters for the nanoline array. (b-c) Optical images and AFM topographic view of the gelatin-PGMA@PNIPAm sample. (d-e, g) Optical images of NIH-3T3 incubated on gelatin-PGMA@PNIPAm surface for 24 hrs and 48 hrs. (d) 24 hrs; (e, g) 48 hrs. (f) Fluorescence microscopy images of NIH-3T3 incubated on the gelatin-PGMA@PNIPAm surface for 48 hrs. Red and blue colors were the cell cytoskeleton and nucleus respectively. Scale bar of d-g: 100 μm.

Figure 6.5. Optical image of NIH-3T3 cells incubated on patterned PGMA without gelatin immobilization on PNIPAm brushes-coated Au-glass substrate for 24 h. Seeding density: 3 x 10^5 cells/mL. Scale bar: 100 μm.

Figure 6.6. (a-b) Underwater AFM topographic view, the corresponding cross-sectional profile and the contact angles of nanoline arrays of the gelatin-PGMA@PNIPAm sample in 37 °C and 26 °C of water. (a) 37 °C; (b) 26 °C. (c) Schematic illustration of the transformation of cell attachment and detachment with temperature variation. (d) Images of NIH-3T3 cells on gelatin-PGMA@PNIPAm substrate incubating in 26 °C. The cell film gradually fell off from the surface from the edges. Scale bars: 1 cm. (e) Optical image of detaching NIH-3T3 cells from the gelatin-PGMA@PNIPAm surface. Scale bar: 50 μm.

Figure 6.7. Optical image of oriented NIH-3T3 cells on reused gelatin-PGMA@PNIPAm surface. (a) Oriented cells on the surface reused for two times. (b) Oriented cells on the surface reused for three times. Scale bars: 50 μm.

Figure 6.8. (a-e) Optical images of NIH-3T3 incubated on different nanoline space of gelatin-PGMA@PNIPAm surface for 24 hrs. (a) 2 μm; (b) 4 μm; (c) 6.7 μm; (d) 10 μm; (f) 20 μm. Scale bar: 100 μm. (f) Histogram of orientation effect on different nanoline space of the gelatin-PGMA@PNIPAm surface. (g) Mechanism schematic of the influence of nanoline space on cell orientation control effect.

Figure 7.1. Schematic illustration of fabrication of vertically micropatterned binary polymer brush systems by μCP.

Figure 7.2. (a-c) ATR-FTIR spectra of MUDBr SAM and various polymer brushes coated-Au substrates.

Figure 7.3. (a-f) Optical microscopic images of (a) POEGMA, (b) PHEMA, (c) PGMA (d) PMMA, (e) PMETAC and (f) PNIPAm brushes coated-Au substrates after microcontact printing of initiator and SI-ATRP process. (g) Optical microscopic images of PGMA grid on POEGMA surface, called PGMA@POEGMA. (h) ATR-FTIR spectra of POEGMA brushes coated Au substrate and PGMA@POEGMA sample. (i) AFM topographic view, corresponding phase view and cross-sectional profile of the PGMA grid on POEGMA surface.

Figure 7.4. (a-f) Optical microscope images of the patterned PGMA brushes grid with a different contact time of PDMS stamp on POEGMA brushes coated Au substrate. (a) 5 s, (b) 10 s, (c) 15 s, (d) 20 s, (e) 45 s and (f) 60 s. (g-h) The stability of binary PGMA@POEGMA substrate in mix solution with ultrasonic. (g) 10 min of ultrasonic, (h) 40 min of ultrasonic.

Figure 7.5. (a-d) Optical microscope images of the various binary system. (a) POEGMA dot array on POEGMA surface, called POEGMA@POEGMA, (b) PNIPAm square array on POEGMA surface, called PNIPAm@POEGMA, (c) PMMA grid on POEGMA surface, called PMMA@POEGMA and (d) PMETAC grid on POEGMA surface, called PMETAC@POEGMA. (e-f) Optical microscope images of copper deposition on PMETAC@POEGMA substrate. (e) 5X. (f) 50X.

Figure 7.6. (a-c) Optical microscope images of (a) gelatin modified PGMA@POEGMA substrate, called gelatin-PGMA@POEGMA and (b-c) cell micropatterning of NIH-3T3 cells on gelatin-PGMA@POEGMA for 24 hrs. (d-f) CLSM images of NIH-3T3 cells incubated on the gelatin-PGMA@PNIPAm surface for 48 hr. Red and blue colors were the cell cytoskeleton and nucleus respectively.

Figure 7.7. (a-c) The optical images, AFM topography and cross-section profiles of gelatin-PGMA stripes (5-, 40, 100-μm width) on POEGMA-glass. (d-i) The optical images of NIH-3T3 cells cultured on gelatin-PGMA stripes (5-, 40, 100-μm width) for 24 hrs (d-f) and 48 hrs (g-i).

LIST OF TABLES

LIST OF ABBREVIATION

μCP	Microcontact Printing
1D	One-Dimensional
2D	Two-Dimensional
3D	Three-Dimensional
AFM	Atomic Force Microscope
AGET	Activators (Re)Generated by Electron Transfer
ATR-FTIR	Attentuated Total Reflectance Fourier Transform Infrared Spectroscopy
ATRP	Atomic Transfer Radical Polymerization
DMD	Digital Mirror Device
DNL	Dip-Pen Nanodisplacement Lithography
DPN	Dip-Pen Nanolithography
EBL	Electron Beam Lithography
ECM	Extracellular Matrix
ELD	Electroless Deposition
LCST	Lower Critical Solution Temperature
LFM	Lateral Force Microscopy
MHA	16-Mercaptohexadecanoic Acid
MUDBr	Ω-Mercaptoundecyl Bromoisobutyrate
PAAm	Polyacrylamide
PDMS	Polydimethylsiloxane
P-DNL	Parallel Dip-Pen Nanodisplacement Lithography
PEG	Poly (Ethylene Glycol)
PET	Poly (Ethylene Terephthalate)
PGMA	Poly (Glycidyl Methacrylate)
PGMA	Poly (Glycidyl Methacrylate)
PHEMA	Poly (2-Hydroxyethyl Methacrylate)
PL	Photolithography
PMAA	Poly (Methylacrylic Acid)
PMANa	Poly (Methacrylic Acid, Sodium Salt)
PMETAC	Poly[(2-(Methacryloyloxy) Ethyl) Trimethylammonium Chloride]
PMETAC	Poly[2-(Methacryloyloxy)Ethyl-Trimethylammonium Chloride]
PMMA	Poly (Methyl Methacrylate)
PNIPAm	Poly (N-Isopropylacrylamide)
POEGMA	Poly [Oligo (Ethylene Glycol) Methyl Ether Methacrylate]
PPL	Polymer Pen Lithography
PSPMAK	Poly (3-Sulfopropyl Methacrylate) Potassium Salt
SAMs	Self-Assembled Monolayers
SEM	Scanning Electron Microscopy

SI-ATRP	Surface-Initiated Atom Transfer Radical Polymerization
SI-NMP	Surface-Initiated Nitroxide-Mediated Polymerization
SIP	Surface-Initiated Polymerization
SI-PIMP	Surface-Initiated Photoiniferter-Mediated Polymerization
SI-RAFT	Surface-Initiated Reversible Addition-Fragmentation Chain Transfer Polymerization
SL	Soft Lithography
SPL	Scanning Probe Lithography
XPS	X-Ray Photoelectron Spectrometer

CHAPTER 1 INTRODUCTION

1.1 Background and Challenges

With many revolutionary breakthroughs in recent researches on cell regeneration and tissue engineering for repair and transplant, tissue cells are cultured, and their behaviors are manipulated *in vitro* to obtain desired functional cells. To date, a thorough understanding of how to control cell behaviors on an artificial surface becomes even more crucial in materials and life science, cell biology, tissue engineering and regenerative medicine. Controlling cell behaviors with the aid of artificial biomaterials comes into the spotlight, thanks to the rapid advance of nanobiotechnology and the successful optimization of many artificial biological systems [1-3]. The importance of biocompatibility of these artificial biomaterials, interfacial interactions between cells with the artificial surface as well as the environment that cells are cultured in are further recognized in recent decades [4-5].

Controlling cell behaviors is one critical step that paves the way for future advanced cell engineering. Cell behaviors are regarded as cell activities, such as adhesion, proliferation, differentiation, migration, which ultimately determine cell functions and vitality [6]. Cell behaviors can be profoundly affected by the surrounding environment. *In vivo*, living cells are surrounded by a dynamic and complex environment which consist of various components such as surrounding cells, extracellular matrix (ECM) molecules as well as other bound or soluble factors. Designed by nature, such a dynamic environment is almost perfect for any cell activities, where cells not only sustainably gather information from the dynamic environment but also generate a response to subsequent cell signaling events to control cell functions, shapes and behaviors [7-11]. Among these components in the complex microenvironment, ECM is found to be one major entity to signal and control cell behaviors [12]. ECM

consists of a combination of proteoglycans, glycosaminoglycans, fibrous proteins and adhesion proteins, etc. of micro- to nanoscale three-dimensional (3D) conformation [13]. By interacting and communicating with the three major cues in ECM, namely 1) chemical, 2) topographical and 3) mechanical cues, cells generate response accordingly.

However, *in vitro*, culturing cells and controlling their behaviors both require precise control on materials and incubation conditions. Since cell-ECM interactions majorly determine all of the cell behaviors *in vivo*, artificial ECM must be first designed that mimics natural ECM to control cell behaviors *in vitro*. From the materials' point of view, artificial ECM can also be regarded as a kind of material. To artificially mimic cell-ECM interaction, it should be noted that not only the properties of the ECM must be mimicked; the entire cell-material interaction at the cell/material interface must also follow the one that naturally occurs. Thus, fabrication of such a cell-material system becomes significantly challenging in recent cell research, where many criteria are required to construct a well-defined surface mimicking the complex cell-ECM interaction. For example, first, the mimicked material should be precisely designed and possess the quality for biocompatibility. Second, as mentioned earlier, the three major cues (chemical, topographical, and mechanical cues) of material surfaces have great influence on controlling cell behaviors. These cues in the mimicked material surface must be previously adjusted, and the properties of these cues must be fully exhibited which can be easily recognized by the cultured cells.

To address these challenges, extensive biocompatible materials have been utilized for the preparation of artificial ECM for controlling cell behaviors. By decorating the material surface with suitable cues (chemical, topographical, and mechanical cues), cell-material interaction and in turn cell behaviors can be manipulated. Among these biocompatible materials, polymer brushes, which refer to polymer chains tethered by one end to a substrate [14], have attracted increasing attention for a range of biomedical applications. Among them, polymer brushes possess superior advantages such as long-term stability, excellent mechanical and chemical robustness, and convenient processability [15]. Importantly, the utilization of polymer brushes densely grafted on a substrate surface provides versatility on surface morphology control. Varying degrees

of the topology of the substrates affect multiple cellular properties including cell morphology, orientation, migration, gene expression profile and cell differentiation, etc. [16-18]. With various lithography techniques, patterned polymer brush integrates the three cues (chemical, topographical, and mechanical cues) on a substrate to mimic the real ECM for controlling cell behaviors with high efficiency.

Future developments in this field will focus on the complexity of the current brush-based platforms containing as more chemical, topographical, and mechanical cues as possible. For example, enabling multiscale patterning or multi-component, and designing dynamic or responsive substrates to improve current polymer brush based biomimicking ECM for better controlling cell behaviors. Moreover, the exact mechanism of the patterned surfaces influences the cells still need to be explored further.

To address the challenges, we would like to design artificial ECM with multiscale patterned binary polymer brushes by easy and cheap lithography techniques. Among the various lithography techniques, scanning-probe-based lithography, such as dip-pen nanodisplacement lithography (DNL), fulfill the requirements for convenient generation of arbitrary multiscale patterning, binary or multi-component, and smart polymer brush substrates for controlling cell behaviors. Otherwise, the microcontact printing (μCP) is also a cheap and simple lithography method, which can be developed to fabricate binary or multi-component polymer brush patterns to meet the requires.

1.2 Research Objectives

This study is concerned with generating binary 2D and 3D polymer brush structures for controlling cell behaviors:

1. To develop the parallel-DNL (p-DNL) techniques for preparation of 2D and 3D polymer brush structures with high-resolution, large-areas, and serials fabrication.
2. To improve the p-DNL techniques for fabricating binary 3D polymer brush structures.
3. To generate nano-micro binary cell-adhesive polymer brush patterns with lateral intersection for regulating cell orientation and smart attachment/detachment.

4. To develop vertically micropatterned binary polymer brushes by extremely simple μCP and explore their applications in cell micropatterning.

1.3 Research Originality

The originality of the project is not only developing the polymer brush as resist layer in the p-DNL technique but also improving the high-throughput preparation of nano-micro binary polymer brush patterns with the pattern area large to square centimeter. Such laterally patterned binary polymer brushes are thermal sensitive composed by cell-adhesive materials, which successfully regulate cell adhesion, orientation, and detachment.

On the other hand, the vertically micropatterned binary polymer brushes are prepared by extremely simple μCP based on the initiator sticky-ability of some polymer brushes. It is the first to report unmodified initiator can easy adsorbed by polymer brushes via facile contact.

1.4 Outlines of the Thesis

The thesis is organized as the following:

Chapter 1 introduces the importance of controlling cell behaviors, how to realize artificial ECM for regulating cell behaviors and current challenges. Then the research objectives and originality are stated.

Chapter 2 first gives a brief introduction of polymer brush, cell-polymer brush interaction, and how the cell-inert and cell-adhesive polymer brushes to control cell behaviors. Further, introduces the lithography techniques for preparing patterned polymer brush.

Chapter 3 elaborates the research methodology, including substrate modification, lithography process, cell culture conditions, and characterization techniques.

In chapter 4, the single-tip DNL, 1D p-DNL, and 2D p-DNL techniques and the resulted well-defined polymer brush patterns are elaborately presented.

In chapter 5, the fabrication of binary 3D polymer brush structures is demonstrated

by *in-suit* repeated 1D p-DNL and SI-ATRP.

In chapter 6, the thermoresponsive nano-micro binary polymer brush patterns are generated by 2D p-DNL and SI-ATRP. The applications of the binary polymer brush patterns in cell orientation, and smart detachment are demonstrated.

In chapter 7, a newly and extremely simple method based on initiator stickiness for fabricating binary polymer brush micropatterns via μCP and SI-ATRP is developed. The cell micropatterning and orientation on the fabricated binary polymer brush micropatterns are studied.

Last but not the least, chapter 8 summarizes the conclusions of this thesis and give some future outlooks.

CHAPTER 2 LITERATURE REVIEW

2.1 Introduction of Polymer Brushes

Tailoring the surface chemical properties of materials is a convenient way to adjust its nano- or microscale interactions with its environment [19-20]. For nearly half a century, polymer brushes that covalently tethered one end on a substrate surface [14] has attracted a lot of scientific attention in many areas for their versatility as surface coatings. The common applications include but are not limited to actuators [21-22], microfluidic devices [23-25], surface wettability tuning [26], chromatographic separation [27], lithium batteries [28], non-fouling surfaces [29-30], bio-surfaces (biosensors and implants) [31-33], protein adsorption and controlling cell behaviors [34-38], nanoparticles assembly [39] and metal coating [40-44]. The interactions between the tethered polymer chains and the substrate surface are much stronger than physically adhered bulk polymer thin films [45]. Thus, the surface-tethered polymer brushes are remarkable stable to the environment, which is very important for many applications. Polymer brushes has a high degree of synthetic flexibility towards the introduction of a variety of functional groups [15]. Using functional polymer brushes to prepare responsive surfaces for biological applications has attracted increasing research interest, in which the responsive polymer brushes surface can reversibly change its physical property (hydrophilicity and biocompatibility) based on an external stimulus such as temperature, salt concentration, and pH. For instance, thermoresponsive poly (N-isopropylacrylamide) (PNIPAm) brushes is hydrophobic (cell-adhesive) at a temperature above its lower critical solution temperature (LCST) while hydrophilic (cell-inert) at a temperature below LCST. By varying temperatures, switchable cell-adhesive and cell-inert properties exhibited in PNIPAm can be used in controlling cell adsorption and desorption. Thus various cell behaviors can be controlled [46].

The tethered polymer brushes typically shows three conformations according to the grafting density of polymer chains: ‘mushroom’ or ‘pancake’ regime at low density, while ‘brushes’ regime at high density (Figure 2.1a) [47]. Polymer brushes has a high degree The polymer brushes can be fabricated on a variety of surfaces via two methods (Figure 2.1b), respectively called “grafting to” [48] and “grafting from” [49-50] methods. In the “grafting to” approach, functional polymer chains are directly attached to a modified substrate surface. However, the steric repulsion of polymer chains and the low attaching efficiency can lead to the low brushes grafting density [51]. As a result, preparing dense and thick polymer brushes via ‘‘grafting-to’’ strategies is somewhat undesirable for effective brushes grafting.

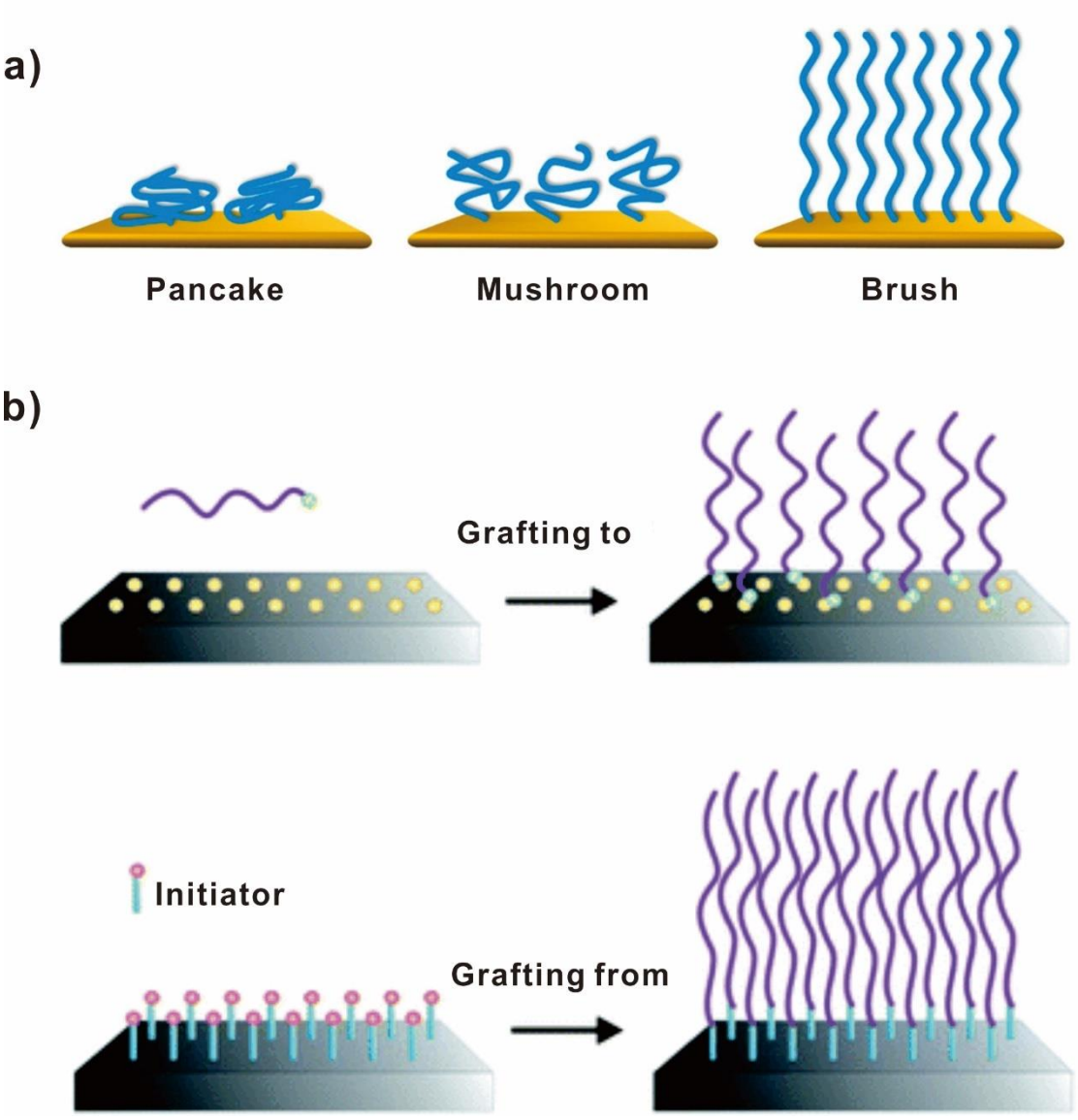

Figure 2.1. a) Schematic illustration of three different types of conformations of

surface-attached polymers: pancake, mushroom, and brushes-type surface-anchored polymers [47]. b) Synthetic strategies of polymer brushes [45].

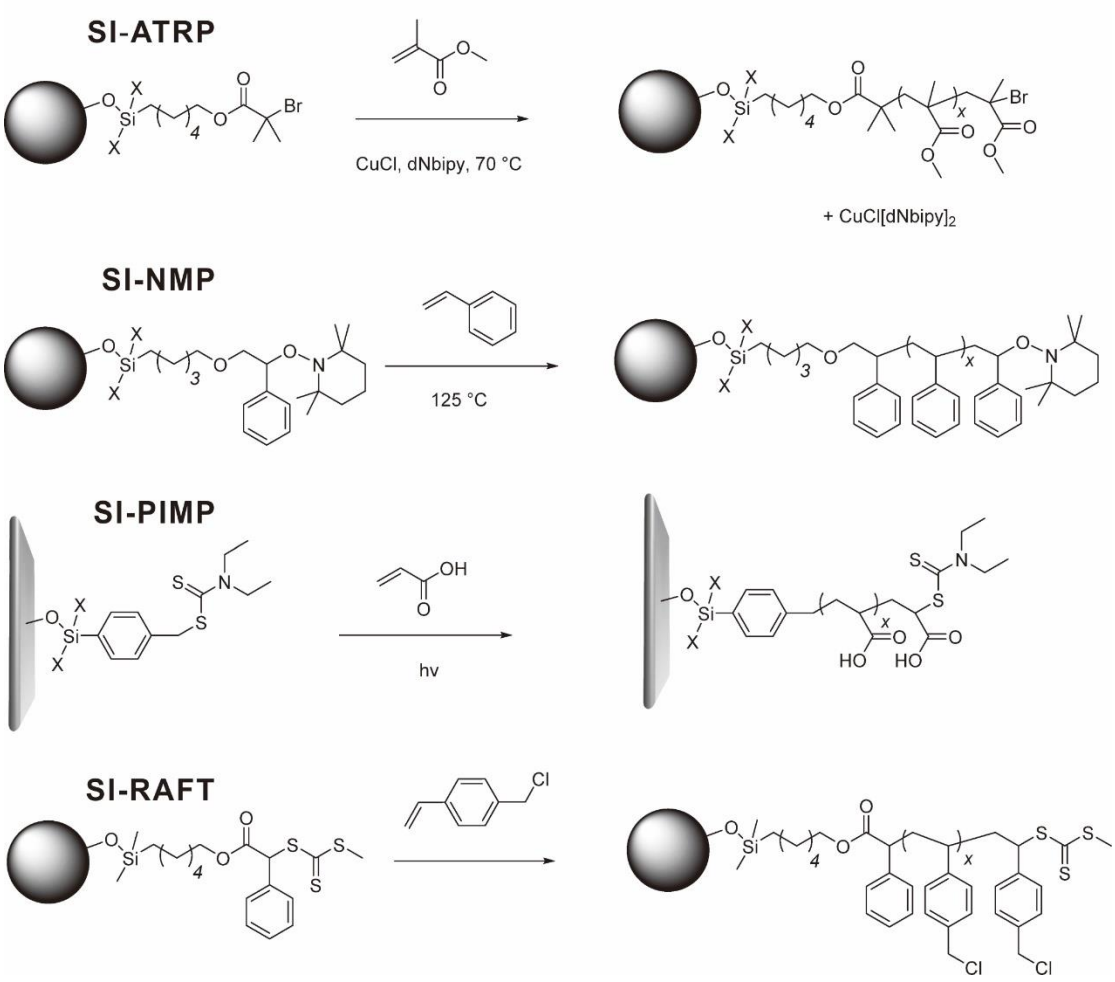

Figure 2.2. Overview of the four most prominent SIP Strategies [47]. Illustrated by SI-ATRP of methl methacrylate (MMA), SI-NMP of styrene, SI-PIMP of acrylic acid, and SI-RAFT of 4-vinylbenzyl chloride (VBC).

To solve this problem, "grafting-from" is preferably adopted as in this strategy, polymer brushes are synthesized *in-situ* from the initiator-modified substrate surface (such as initiator SAMs) via surface-initiated polymerization (SIP) [15]. Polymerization of polymer chains is imitated from the surface-deposited initiators. Common SIP methods (Figure 2.2) include surface-initiated atom transfer radical polymerization (SI-ATRP) [52-54], surface-initiated reversible addition-fragmentation chain transfer polymerization (SI-RAFT) [55-56], surface-initiated nitroxide-mediated polymerization (SI-NMP) [57-58] and surface-initiated photoiniferter-mediated polymerization (SI-PIMP)

[59-60]. The “grafting-from” is widely used than the “grafting-to” due to its precise control of polymer brushes thickness, composition, grafting density and architecture for fabrication of well-defined micro- and nanoarrays of polymer brushes. With the development of SIP, the traditional process of the polymerization has been improved. For example, some researchers have reported an activators (re)generated by electron transfer (AGET) ATRP, which depends on an added reducing agent (such as ascorbic acid) to make the active transition metal complex (such as CuBr) regenerate by reduction of higher oxidation state transition metal complex (such as $CuBr_2$) [53, 61-62]. This regenerated process decreases the reaction while increase the reaction efficiency.

2.2 Cell-Polymer Brushes Interaction: The Principles

To have a better understanding of cell-polymer brushes interaction, the principles are briefly explained. The cell-polymer brushes interaction consists of early events, such as adsorption of proteins, followed by cell adhesion and spreading, and late events, related to matrix deposition, cell proliferation, differentiation and cell function [63]. Cell adhesion is thus the first step of other cell behaviors, which is the process that cells occur interaction and bind to a material surface or another cell, essential in cell communication and regulation, and organ formation and tissue maintenance [64]. *In vitro*, occurring interaction with the material surface via [65]. Therefore, according to adhesion happening, there are three kinds of cell-polymer brushes interactions (Figure 2.3), namely 1) non-adhesive interaction, 2) passive adhesion interaction and 3) active adhesion interaction [66].

Non-adhesive interaction refers to a material surface that cells (i.e. non-adsorbed cells) cannot interact with and adhere to a polymer brushes surface during desired time. On the other hand, passive adhesion interaction is an interfacial response controlled by the physicochemical interactions between the polymer brushes, adsorbed proteins and adhering cells [67]. In such interaction, cells (i.e. adsorbed cells) remain to interact with and adhere onto but easily detach from the polymer brushes surface once suffering from a minimal or negligible damage [68-69]. This kind of interaction is therefore reversible.

Importantly, there are no metabolic signaling or morphological changes within the cells. Finally, active adhesion interaction, as the name suggests, is a kind of interaction in which cells strongly attach on the polymer brushes surface. Here, the interaction between the receptors on the cell membrane and polymer brushes are spontaneously activated, leading to transforming cell morphology to spread and commence signaling processes typically of ttachment-dependent phenotypes. The adhered, spread cells barely detach from these surfaces without strong external influence. The enzymatic digestion of extracellular matrix proteins (e.g., trypsinization), mechanically scraping and switchable cell attachment/detachment polymer brushes are therefore used to turn to detachment behavior of actively adherent cells.

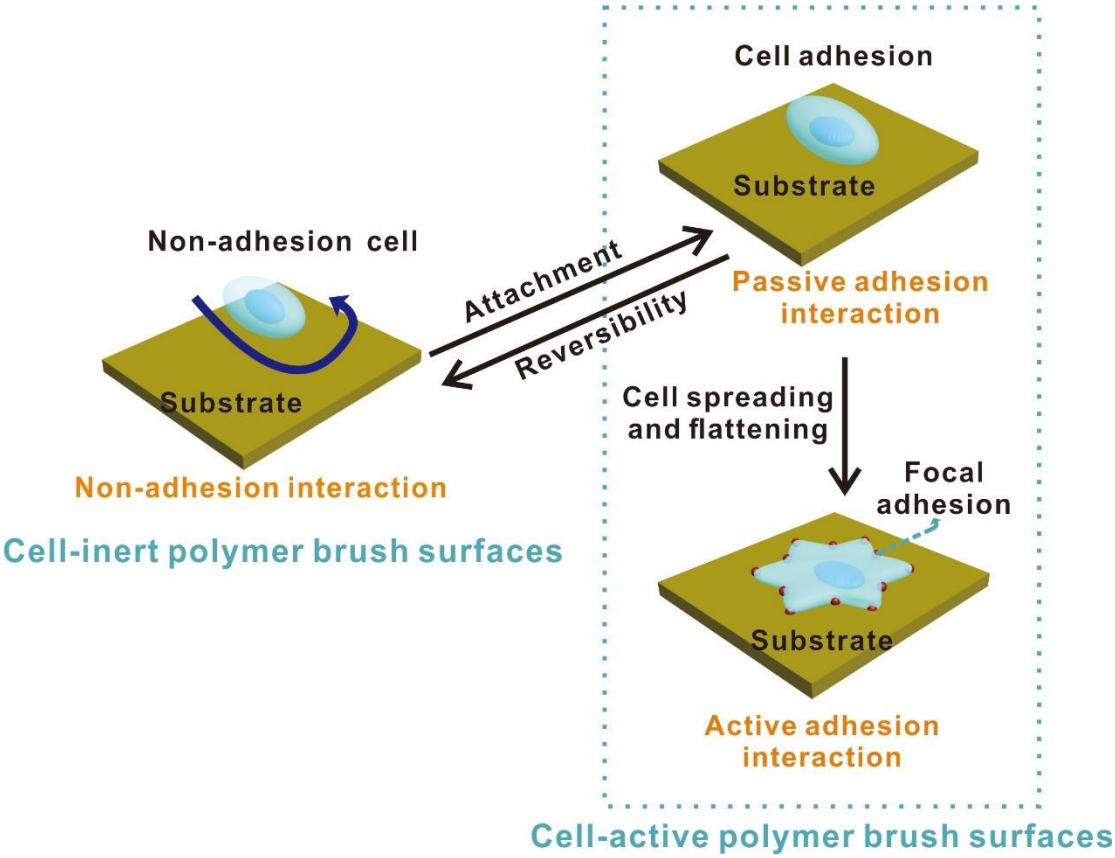

Figure 2.3 Schematic diagrams for possible interactions of materials surfaces with cells.

Base on the various cell-polymer brushes interactions mentioned above, there are two categories of polymer brushes for controlling cell behaviors. The first item is cell-inert polymer brushes, which is dominated by non-adhesion interaction. It is well known that cell adhesion on a biocompatible polymer brushes surface is mediated by a

protein (such as fibronectin, vitronectin, and fibrinogen) layer. The protein layer is previously adsorbed onto the polymer brushes surface from either the physiological fluids in vivo or intentionally deposited in vitro (e.g., the adsorption of serum proteins or even after chemical attachment to the polymer brushes surface [70-72]). As a matter of fact, cells cultured on the polymer brushes surface do not directly interact with the brushes itself, but instead, interact with the protein layer on the brushes surface through transmembrane receptors (e.g., integrins), improving cell anchorage and triggering the subsequent cellular response and behaviors. However, the cell-inert polymer brushes is protein repellent, which prevents the adsorption of protein layer at the top of the brushes surfaces by strong surface hydration, or low surface energy, or electrostatic repulsion [73-75], and then inhibits cell adhesion.

Table 1. Cell adhesion process on cell-active polymer brushes [64].

Cell adhesion phase	**Phase I**	**Phase II**	**Phase III**
Schematic diagram of cell adhesion	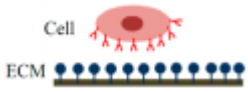	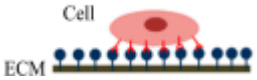	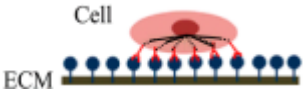
The transformation of cell shape	Initial attachment	 Flattening	 Fully spreading and structural organization
Cell adhesion intervention	Electrostatic interaction	Integrin binding	Focal adhesion
Adhesion stages	Sedimentation	Cell attachment	Cell spreading and stable adhesion

The second category is cell-adhesive polymer brushes on which cells can interact and adhere through passive and active adhesion. The cell adhesion process on a cell-adhesive polymer brushes surface is characterized by three phases (Table 1) [64]. At first, cell bodies adhere to the polymer brushes surface by combinations of complex physicochemical interactions including hydrophobic, coulombic, and van der Waals

forces [76] between the cell membrane and the polymer brushes surface (phase I). The interactions during this process are passive adhesion. Then active adhesion interactions occur leading to the arising of integrin bonding, and then cell bodies start to flatten (phase II). In phase III, the spreading process is the combination of continuing adhesion with the reorganization and distribution of the actin skeleton around the cell's body edge. The cytoskeleton is organized to form focal adhesion between the cell and the substrate.

2.3 Cell-Inert Polymer brushes for Controlling Cell Behaviors

Concentrated polymer brushes surfaces leading to cell-inert effect are usually either extremely low surface energy, or hydrophilic with strong surface hydration, or zwitterionic, etc. [77]. The regulated anti-adhesive effect of cell-inert polymer brushes contributes to maintain a healthy body and protect the body from trauma and foreign bodies. Importantly, cell-inert polymer brushes can prevent or reduce the thrombosis and immunological responses of most biomedical devices and implants, such as artificial blood vessels, cell encapsulation, and biosensing devices. Therefore, cell-inert polymers as adhesion barriers become a hot topic in both research and industrial fields [78].

Polymer brushes which have extremely low surface energy are cell repellent due to the very few protein adsorption of the polymer brushes surface, such as fluorinated polymer brushes poly (2-perfluorooctylethyl acrylate) (PFA-C8) [79]. Concentrated hydrophilic polymer brushes such as poly (ethylene glycol) (PEG), poly (2-hydroxyethyl methacrylate) (PHEMA) and their derivatives, and poly(2-oxazoline)s (POx)-based polymer brushes, can produce a strong hydrogen bonding between the polymer brushes chains and water molecules to form a water hydration barrier on the brushes surfaces [80-82]. The water barrier, i.e. strong surface hydration, prevent proteins to be adsorbed onto the polymer brushes surface, so that inhibit cell adhesion behavior. In detailed studies, Prime *et al*. reported on the protein-repellent properties of oligo (ethylene glycol)-terminated self-assembled monolayers (OEG-SAMs) on metals on

1991 [83] and since then, PEG brushes coated gold (Au) become a standard surface coating method for non-adhesive model surfaces [84]. However, there is increasing evidence that PEG has limited long-term stability, particularly in vivo. Later on, some researchers developed highly dense bottle-brushes brushes (BBBs) with POx as defined side chains to be as potential alternative polymer brushes for preparing protein- and cell-repellent surfaces [85-86] (Figure 2.4a).

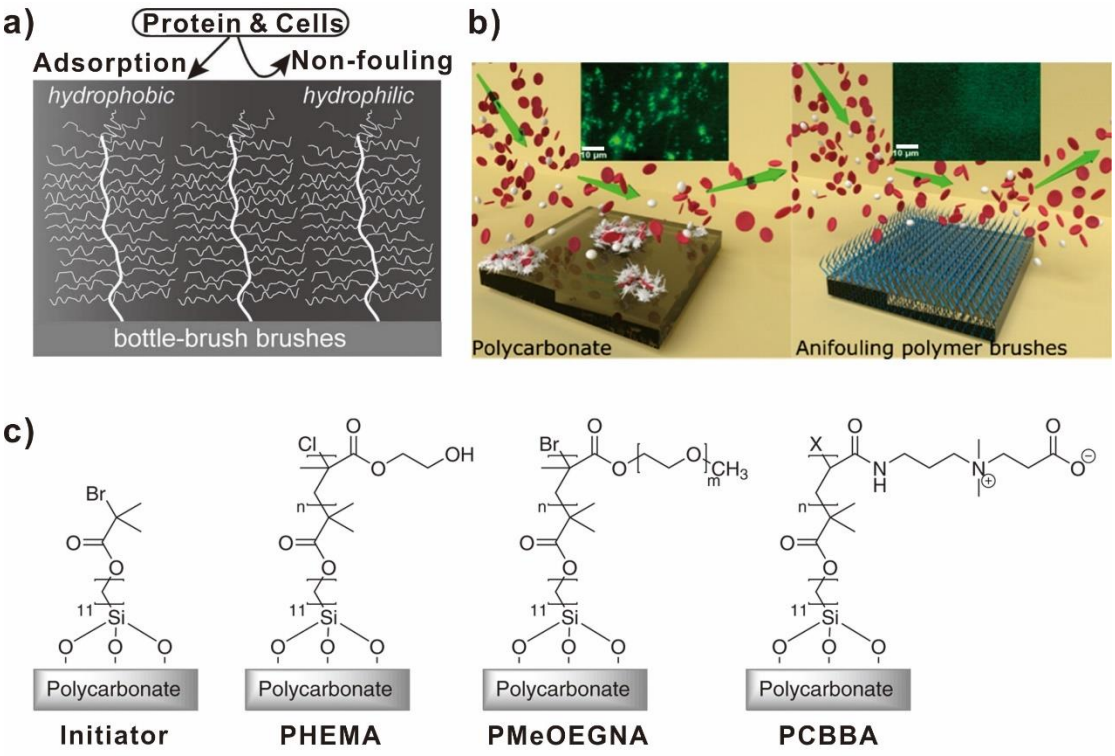

Figure 2.4. a) Schematic image for tailored POx bottle-brushes brushes (BBBs) to control protein adsorption and cell adhesion [87]. b) Schematic images for antifouling polymer brushes displaying antithrombogenic surface properties on polycarbonate substrates [88]. Scale bar: 20 µm. c) Chemical structures of the surface modifications performed on polycarbonate [88].

On the other hand, polyelectrolytes such as polyanion and zwitterionic polyelectrolytes also show similar cell-repellent properties. It is well known that the cell membrane of mammalian cells bears a negative charge [89]. Therefore, the electrostatic repulsion in principle prevents the attachment between a cell and negatively charged polyanion such as poly (methylacrylic acid) (PMAA) [90]. Otherwise,

bio-inspired zwitterionic polymers with neutral charge (a pair of opposite charges in pendant groups) are found to enrich the robust cell-inert systems. The mechanism of zwitterionic polymers for cell-inert effect also contributes to the strong surface hydration. However, different from PEG or POx, the hydration layer is produced by ion solvation effect. Additionally, it is found that the hydration effect of zwitterionic polymers is rather affected by their molecular structures, chain density, species and space of ions. The zwitterionic polymers can be classified by the pair of opposite charges, including phosphorylcholine [(PC): $PO_4^-$and $N^+(CH_3)_3$], sulfobetaine [(SB): $N^+(CH_3)_3$ and SO_3^-], carboxybetaine [(CB): $N^+(CH_3)_3$ and COO^-] and mixed-charge polymers.

For example, Pereira *et al.* [88] studied the cell repellent properties of various concentrated polymer brushes, including PHEMA, poly(ethylene glycol) methyl ether methacrylate (PMeOEGMA), and zwitterionic poly [(3-acryloylaminopropyl) -(2-carboxyethyl) dimethylammonium] (PCBAA) brushes respectively, and found the platelet aggregation and the thrombus formation were largely reduced on these polymer surfaces, suggesting that cell-inert polymer brushes could be of service in biomedical applications requiring extensive blood-material surface contact (Figure 2.4b andc). Chen *et al.* [91] designed a PEG-block-PEMA-block-poly (2-methacryloyloxyethyl phosphorylcholine) (PEG-b-PHEMA-b-PMPC) triblock copolymer. Compared with PEG-b-PHEMA diblock copolymer, the cell-repellent effect of PEG-b-PHEMA-b-PMPC was much enhanced by the synergistic effect of PEG, PHEMA and zwitterionic PMPC.

2.4 Cell-Adhesive Polymer brushes for Controlling Cell Behaviors

ECM provides structural and chemical integrity surrounding the cells and subsequently determine the fate of cells [92]. By fabricating various polymer brushes that mimic natural ECM with different chemical, mechanical, and topographical cues, the interactions between cells and polymer brushes can be influenced to control cell behaviors. In this section, various cell-adhesive polymer brushes designed with the

three major cues aiming for controlling cell behaviors are discussed.

2.4.1 Cell-Adhesive Chemical cues with Functional Polymer Brushes

The chemical cues of polymer brushes to control cell behaviors include biological molecule modification, physicochemical properties (wettability, electrostatic, van der Waals forces, surface energy, etc.), stimulating responsibility, and so on.

2.4.1.1 Biological Molecules

Various proteins and peptides, i.e. biological molecules, such as the cytokines, growth factors, adhesion molecules and even the hormones presenting in the surrounding ECM provide one kind of chemical cues to cell behaviors. During adhesion process, as mentioned in 2.2, cell adhering onto a biocompatible polymer brushes surface is mediated by a protein layer. Once modified with such proteins, polymer brushes will become much easier to be attached to cells. This kind of proteins and peptides can bind to transmembrane receptors, including Arg-Gly-Asp (RGD), fibronectin, gelatin, and collagen, etc.

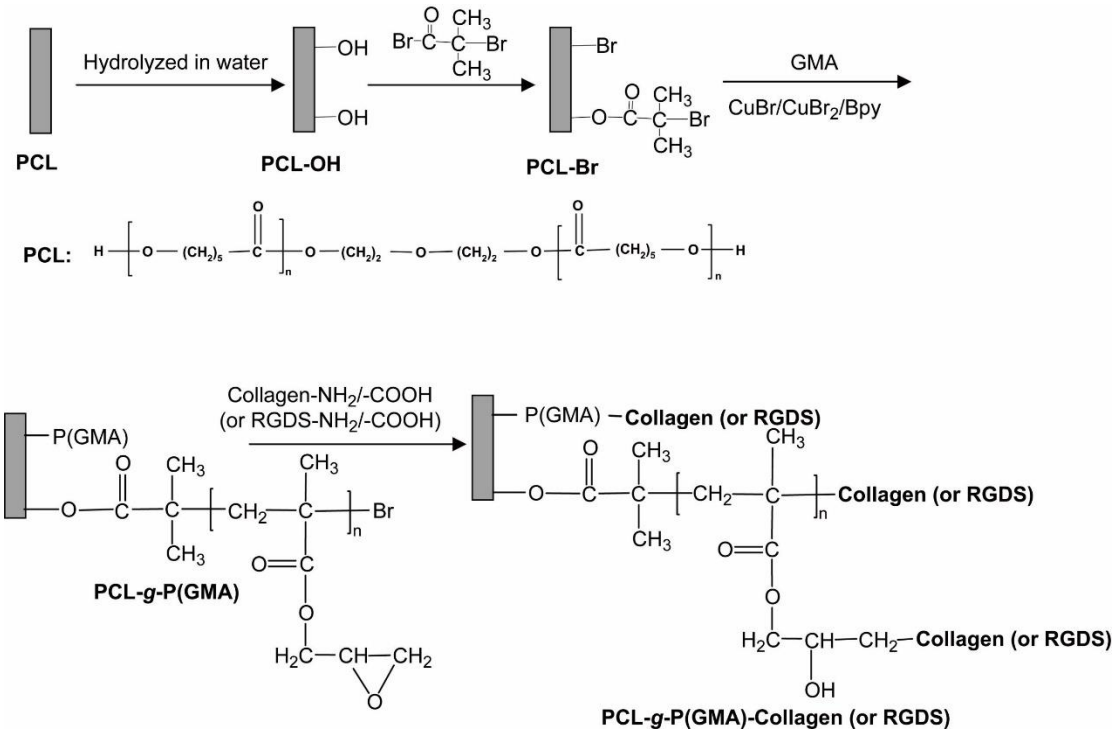

Figure 2.5. Schematic diagram illustrating the reaction of hydroxyl groups on the

hydrolyzed PCL surface with 2-bromoisobutyrate bromide to produce the PLC-Br surface, SI-ATRP of GMA from the PCL-Br surface to produce the PCL-g-PGMA surface, and collagen (or RGDS) immobilization on the PCL-g-PGMA surface to produce the PCL-g-PGMA-Collagen (or PCL-g-PGMA-RGDS) surface [93].

Poly (glycidyl methacrylate) (PGMA) brushes is one of the most widely used polymer brushes to be modified with such proteins via its epoxy groups which readily react with the amino or carboxyl groups of proteins [93-94]. For example, Xu and his co-workers [93] modified polycaprolactone (PCL) surfaces with PGMA brushes, and then fixed RGD and collagen on the surfaces via PGMA brushes to promote the adhesion of 3T3 fibroblast cells.

2.4.1.2 Wettability

Recent reports show that water wettability of a polymer brushes surface (hydrophobicity and hydrophilicity) is known to be one key factor to influence cell-polymer brushes interaction and the subsequent cell behaviors. Wettability of a surface can be seriously affected by surface functional groups and roughness [2], etc. To influence cell behaviors, it is worth noting that wettability can control essential protein adsorption on the polymer brushes surface and subsequent effect cell activities [95-99]. Water contact angle measurement is typically used to provide the information to quantify the wettability of a polymer brushes surface. Normally, most of the animal cells prefer a surface of moderate hydrophilicity for adhesion and growth, whereas polymer brushes of superhydrophilicity (contact angle below 5˚) and superhydrophobicity (contact angle above 150˚) are not favorable to cells attachment and growth [100-104]. However, some researchers show antipodal results. Wei *et al.* [105] grafted poly (hexamethyldisiloxane) (PHMDSO) brushes on a substrate and precisely decorated PHMDSO with different surface wettability (from hydrophobic to superhydrophilic) by altering the duration of oxygen-plasma treatment without changing the polymer surface morphology. It is found that the more hydrophilic of the

polymer surface, more fibroblasts can adhere and spread widely on the surface (Figure 2.6a).

Although there are many kinds of literature reporting on regulating cell behaviors by using various polymer brushes with different wettability, the mechanisms are not yet fully understood. Other parameters such as cell lines, roughness, chemical components of the polymer brushes and the complex ECM and metabolism of cells may be involved in controlling cell behaviors, in which the knowledge is out beyond the state-of-art.

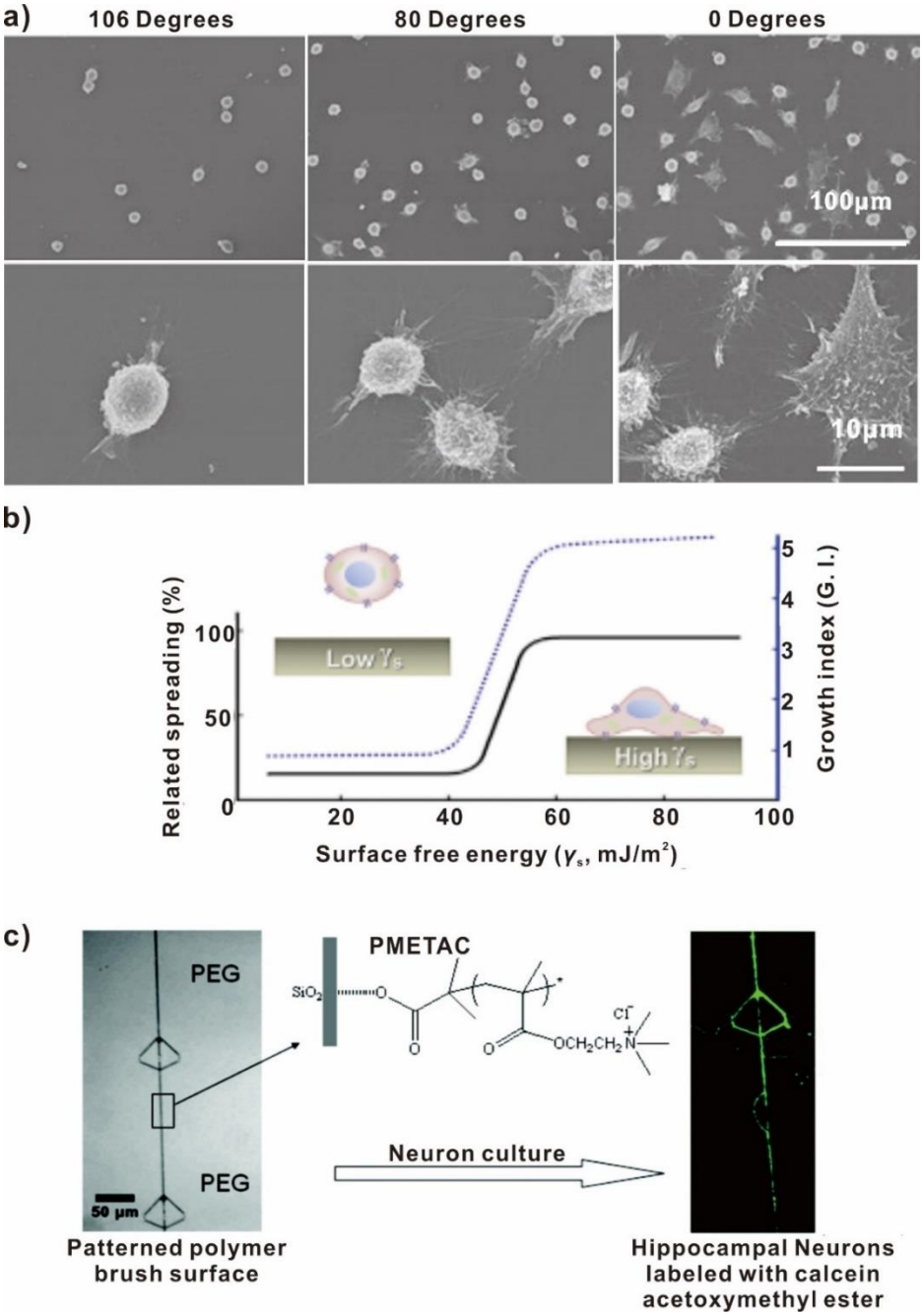

Figure 2.6. a) SEM of L929 attached to surfaces with different wettability in 24 hr in

low magnification (original: ×500) and high magnification (original: ×3000) [105]. b) Schematic image of cell adhesion behavior controlled by surface free energy [78]. c) Hippocampal neurons adhered on PMETAC patterns [106].

2.4.1.3 Surface Free Energy and Electrostatic Force

Surface free energy is another important chemical cue on polymer brushes. It can be regarded as a measure of unsaturated bond energy resulting from dangling bonds of surface material [107]. When touching with a polymer brushes surface, all activities of cells, such as protein adsorption and cell attachment, depend on the energy of the polymer brushes surface (Figure 2.6b). Researchers have studied the relationship between cell adhesion and substratum surface free energy on the polymer brushes surface [108-112]. In general, polymer brushes with high surface free energy can improve cell adhesion and spread, while polymer brushes surface of low surface free energy can suppress cell behaviors [113-114], no matter if the polymer brushes surface is modified with or without protein [108, 115]. The surface energy of the polymer brushes surface can be tailored by using plasma treatment. When the surface free energy of different plasma-treated polymer brushes surfaces is almost equal, a higher value for the polar component of the surface free energy will induce a higher degree of cell adhesion and proliferation on the surface [116-117].

On the other hand, as an electrostatic force for polymer brushes, the polymer chains with a positive charge can be used to be adhered to cells in case of cell membrane containing negative charge. For example, cationic poly [(2-(methacryloyloxy) ethyl) trimethylammonium chloride] (PMETAC) brushes was found to be a cell-adhesive polymer to excellently guide the growth of rat hippocampal neurons [106] (Figure 2.6c)

2.4.1.4 Switchable Responsiveness of Polymer Brushes

Surfaces capable of reversibly switching between cell-inert and cell-active surfaces for direct cell attachment and detachment are called switchable surfaces. These surfaces are usually achieved by surface grafting of responsive polymer brushes which

exhibit reversible conformational changes under distinctive external stimuli (such as temperature, pH, ionic strength, electrical field, etc.). Taking the advantages of these switchable surfaces that exhibited changes in surface properties dramatically upon the application of the external stimulus, they can be utilized to control cell behaviors, especially in the cell detachment from the culturing surface [118-119].

Conventionally, cell detachment from the culturing surfaces can be achieved by either trypsinization or mechanically scraping. However, in trypsinization, the excess trypsin will be internalized which damages intracellular proteins. Moreover, the exposure time of trypsinization ranging from a few minutes to tens of minutes depends on different cell types, which requires skillful control or otherwise cell viability will be lost. In scrapping, severe damages will be resulted not only in the ECM but also in the cell culture. However, with the switchable surfaces enabled by facile and harmless external stimulus, the cell can be detached easily from the culturing surface without damaging the ECM. These kinds of switchable surfaces are therefore attractive to regulate cell behaviors for better regenerative medicine applications.

Among different responsive polymers, thermoresponsive polymers are frequently used to fabricate surfaces with on/off switch to manipulate cell adhesion [120]. A typical thermoresponsive polymer such as PNIPAm responses depending on the ambient temperature. When the temperature is below lower critical solution temperature (LCST), PNIPAm is water-soluble and swollen; yet dehydrated and aggregated when the ambient temperature is above LCST. PNIPAm brushes with a thickness of several nanometers have been proven to be one of the excellent thermoresponsive polymers, thanks to the LCST window that lies within the ranges where cells can survive (around 32 °C in water) [121]. Okano's group have conducted extensive studies about switchable PNIPAm brushes surfaces for controlling cell attachment/detachment. In their experiment, PNIPAm brushes-modified tissue culture dishes are used to prepare cell sheets (Figure 2.7a) [122]. Various types of cells can adhere and proliferate on the modified dishes at 37 °C and detach when the temperature is below 32 °C. Base on the invention of PNIPAm brushes-modified tissue culture dishes, they even developed a cell sheet engineering which was a scaffold-free tissue reconstruction technology [123]

and successfully used this technology in clinical applications, including curing the severe disorders of the cornea (Figure 2.7b), periodontal regeneration, repairing impaired myocardium, the treatment of esophageal ulcerations in a canine model and so on.

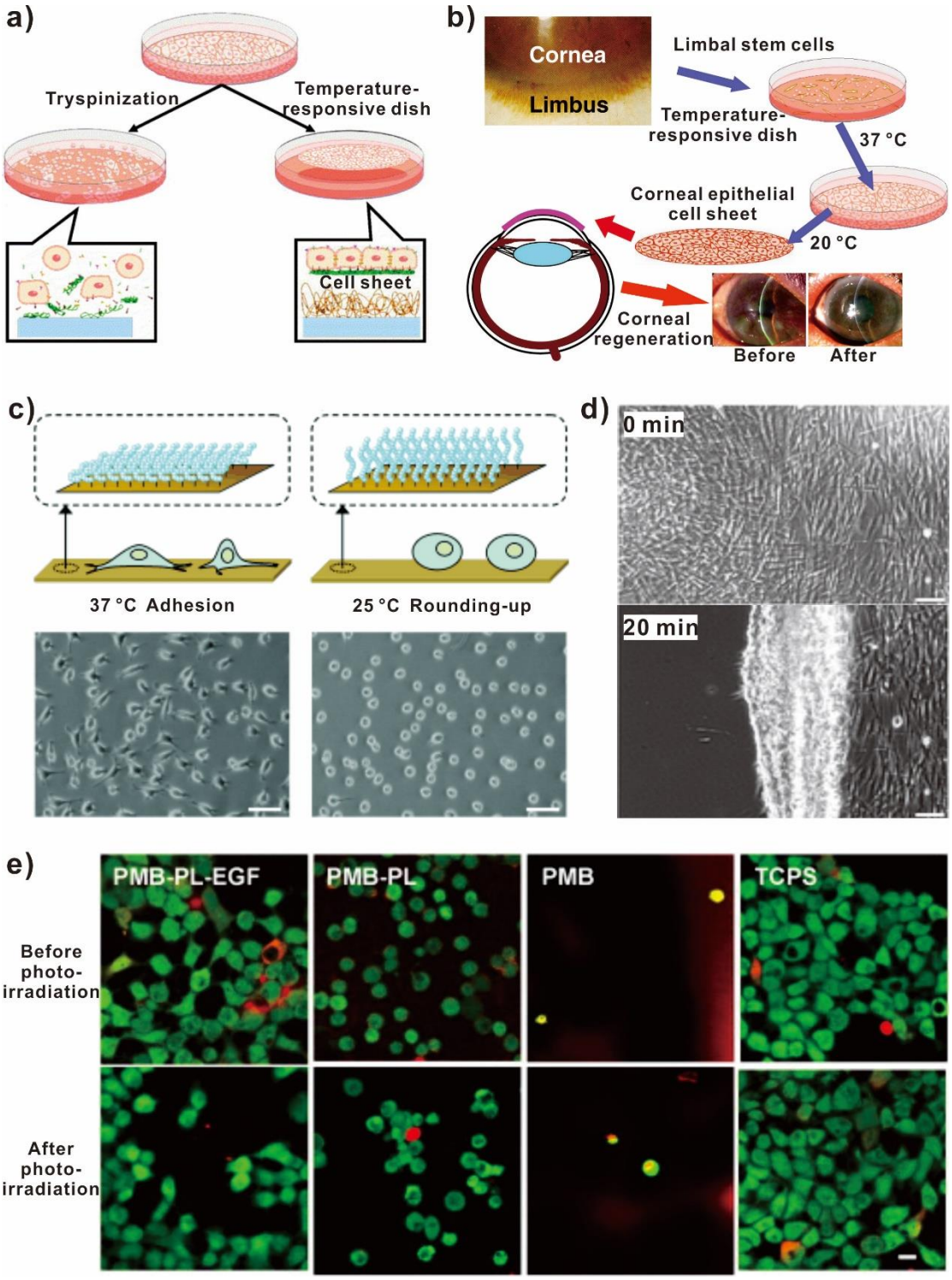

Figure 2.7. a) Schematic presentation of cells harvested from typical trypsinization and temperature-responsive culture dishes, respectively [122]. b) Corneal epithelial cell sheet

transplantation and corneal regeneration [123]. Limbal stem cells are isolated from a small limbal tissue biopsy and cultured on temperature-responsive culture dishes at 37 °C. Transplantable corneal epithelial cell sheets are harvested by reducing the temperature to 20 °C and grafted onto a damaged cornea of a patient suffering from Saltzman syndrome. Photographs were taken before and after the surgical operation. c) Cell adhesion and detachment on thermal-responsive P (OEGMA-co-MEO_2MA) modified gold substrates [124]. The scale bars are 100 μm. d) Images of human fibroblasts detached from P(TEGMA-EE) modified substrates at 17.5 °C [125]. Scale bar: 100 μm. e) Representative fluorescence microscopic images of Live/Dead viability staining adhered cells on different surfaces following photoirradiation [126]. The green fluorescent cells indicate living cells and the red fluorescent cells indicate cell death. Scale bar: 20 μm.

Apart from PNIPAm, other thermoresponsive polymers are also exploited for preparing switchable surfaces, such as poly [oligo (ethylene glycol) methacrylates] (POEGMA) derivatives. The main advantage of using thermoresponsive POEGMA derivatives over PNIPAm is the good reversibility of the stimulate-response process, as PNIPAm exhibits hysteresis during heating and cooling. POEGMA remarkably possesses the hydrophobic methacrylate backbone and hydrophilic oligo (ethylene glycol) (OEG) as side chains which lead to high thermosensitivity. Moreover, the LCST of POEGMA derivatives in aqueous solution can be precisely tuned over a wide range of temperatures (20-90 °C) by changing the length of OEG side chains or adjusting the composition of co-monomers [127], which cannot be achieved by using PNIPAm. For example, Wischerhoff *et al.* [124] precisely adjusted the comonomer composition and successfully grafted the copolymer brushes consisting of 2-(2-methoxyethoxy) ethyl methacrylate (MEO_2MA) and OEGMA with an LCST of around 35 °C in water. As such, fibroblasts could adhere to the brushes surface at 37 °C and detach without trypsinization at 25 °C (Figure 2.7c). Dworak *et al.* [125] successfully synthesized thermosensitive poly(tri(ethylene glycol) monoethyl ether methacrylate) [P(TEGMA-EE)] brushes onto glass and silicon wafers by SI-ATRP and studied smart

attachment/detachment on the polymer surfaces. Changing the temperature from 37 °C to 17.5 °C allowed the properties of the P(TEGMA-EE) surfaces to switch from cell-adhesive (hydrophobic) to cell-inert (hydrophilic) (Figure 2.7d). Thus, the P(TEGMA-EE) polymer layers were successfully applied to create and detach confluent fibroblasts sheets without requiring mechanical or enzymatic methods for cell detachment.

However, switchable surfaces prepared by thermoresponsive polymers cannot be directly applied to control cell behaviors of the individual cell because the temperature stimulus always affects the entire cell culture where controlling cell behaviors in localized areas cannot be achieved. To overcome this problem, photoresponsive switchable polymer surfaces which only respond to certain wavelength and intensity of light (harmless to living cells) can be applied. Photoresponsive polymers containing functional groups (such as azobenzene, 2-nitrobenzyl and nitrospiropyran groups) can be induced by irradiation. Ishihara's group [126] spun coating synthetic poly (2-methacryloyloxyethyl phosphorylcholine (MPC)-*co*-n-butyl methacrylate (BMA)-*co*-4-[4-(1-hydroxyethyl)-2-methoxy-5-nitrophenoxy] butyric acid (HMNBA)) (PMB-HMNBA) on a glass slide to prepare photoswitchable polymer surface. The photocleavable HMNBA linker can couple with the cell adhesive epidermal growth factors (EGF) on the polymer surface to improve cell adhesion. With external irradiation of light of certain wavelength, the HMNBA unit cleaved into two parts leading to a successful cell detachment from the photoswitchable polymer surfaces both with and without immobilized EGF (Figure 2.7e). Sumaru, Yoshimi and their co-workers [128] prepared PNIPAm-based copolymer P(NSp-NIPAm) containing acrylamide monomer with reversible photoresponsive nitrospiropyran (NSp) residue, which combined thermoresponse and photoresponse for regulating cell attachment/detachment. With the copolymer, they successfully fabricated micrometer-scale living cell pattern by regional photostimulation with the low-temperature washing.

2.4.2 Cell-Adhesive Mechanical cues with Functional Polymer Brushes

The mechanical properties of ECM play an important role in manipulating cell

behaviors. In nature, most tissue cells such as soft brain tissues and hard bone tissues adhere on fibrous ECM of various degrees of stiffness and elasticity [129]. It is known that stiffness of ECM *in vivo* ranges from around 0.1 KPa (brain tissues) to around 100 GPa (bone tissues) [130]. Stiffness and elasticity of fibrous ECM are greatly determined by, and proportionally related to the amount of collagen and elastin present in the fibrous ECM, leading to various distinctive mechanical properties exhibited in ECM. Naturally surrounded by ECM, living cells can not only sense these mechanical properties of ECM by applying force and testing the resulted backlash but also respond to the ECM by adjusting focal adhesion structure, cytoskeleton organization and the overall state [92, 131-132].

Preparing biocompatible polymer surface to mimic ECM with optimized stiffness, therefore, becomes critical in controlling cell behaviors. For example, mesenchymal stem cells (MSCs) differentiate into neurons, myoblasts, and osteoblasts as the stiffness of the substrate increased. The soft substrate that resembles brain tissue prefers MSCs to differentiate into neurons while the stiffer substrate is beneficial MSCs to differentiate into myoblasts. Then finally MSCs differentiate into osteoblasts on a rigid substrate that mimicked collagenous bone. An anisotropic model polymer brushes surface with different stiffness without changing other surface properties can be controlled by the SI-ATRP process [15, 133]. In detail, the density of initiator can be manipulated by mixing with a chemical substance which has a similar structure with that to the initiator, leading to the alteration of the surface stiffness [134]. Over the past decades, some reports have studied on the stiffness of polymer brushes substrates for directing cell behaviors, especially for regulating cell spreading, migration and differentiation.

For example, Nam *et al.* [133] prepared poly [poly (ethylene glycol) methacrylate] (PPEGMA) brushes on Si wafer with different grafted density by controlling the imitator density (100%, 1%, and 0.1% respectively, so the corresponding polymer brushes were named cP100, cP1, and cP01) of SI-ATRP, and then immobilized collagen onto the polymer brushes to observe the change of the cell behaviors of MSCs because the alteration in the grafted density lead to the altered surface elasticity. The static

contact angle remained approximately 44° for the cP100 and cP1, indicating other physical, chemical, or geographical parameters of the polymer brushes did not influence by the changed density. The cell culture experiments showed that the adhered MSCs numbers on various polymer brushes surfaces increased with the decrease of the surface stiffness of the polymer brushes.

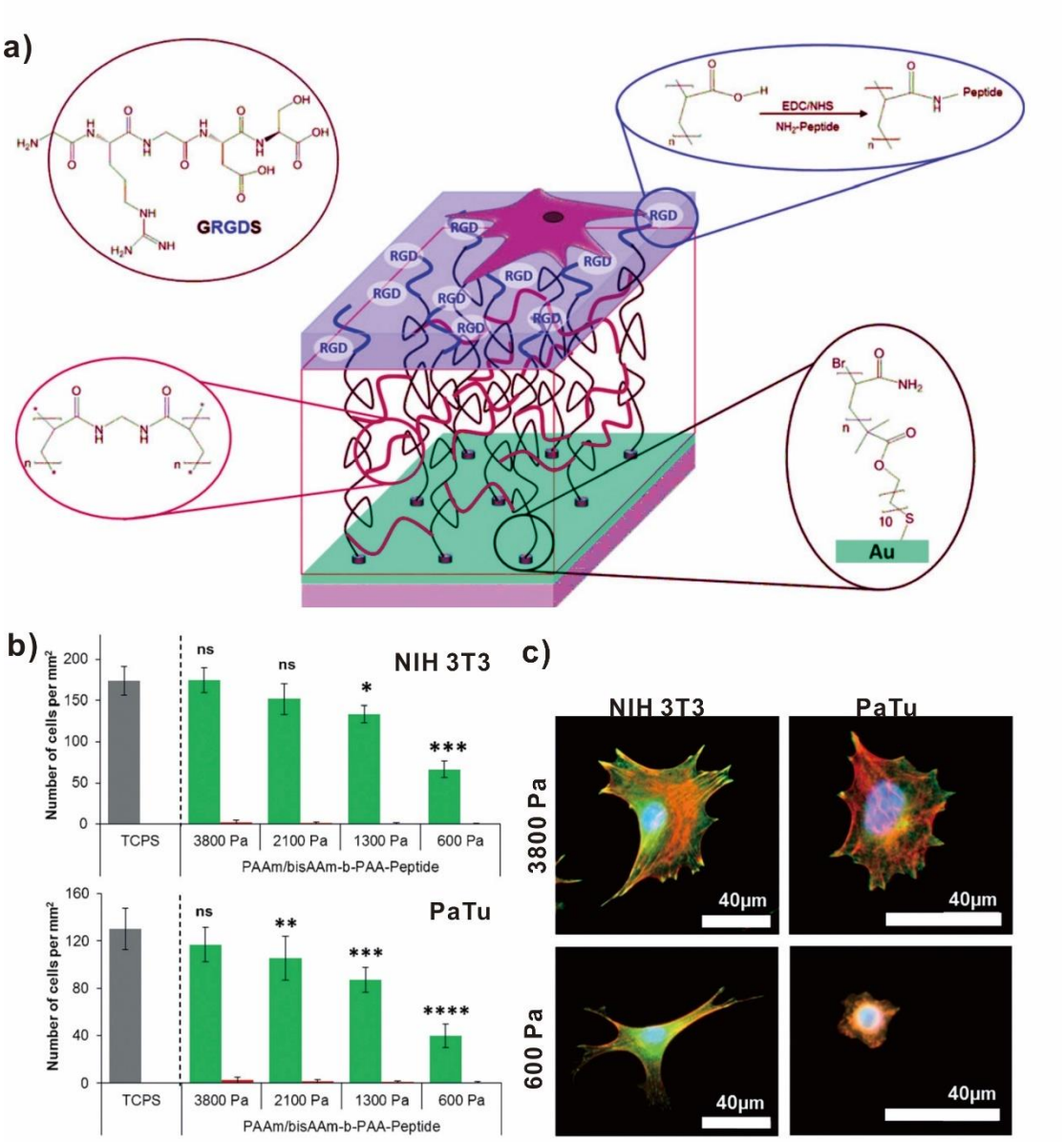

Figure 2.8. a) The biofunctional block-copolymer brushes (PAAm/bisAAm-bPAA) architecture. The crosslinking is implemented in the initially polymerized PAAm block, while the adhesion peptide RGD, conjugated to the subsequently polymerized PAA block, affords the signaling. b) Number of cells per mm^2 (NIH-3T3 cells, and PaTu 8988t cells) on peptide-functionalized polymer brushes (green RGD, red RAD)

compared to cells attached to a tissue culture poly styrene (TCPS) dish after 24 hours of culture. c) Fluorescence microscopy images of NIH-3T3 and PaTu 8988t cells on PAAm-b-PAA-RGD brushes with different moduli of the PAAm block. The immunostaining method is included in the Supporting Information [135].

Lilge and Schçnherr designed a biofunctional block-copolymer brushes polyacrylamide (PAAm) block with defined cross-linking followed by a second poly (acrylic acid) (PAA) block, which could be conjugated with a selective adhesion RGD architecture (PAAm-b-PAA-RGD) (Figure 2.8a) [135]. The change of the stiffness of the initially polymerized PAAm block was manipulated by maintaining a constant concentration of AAm while varying the concentration of the cross-linker bis-AAm (bisAAm) in the polymerization solution for each sample. The stiffness of PAAm/bisAAm brushes varied from 3800 Pa for stiff substrates (prepared with 100% bisAAm) and 600 Pa for soft substrates (0% bisAAm). Subsequently, a short PAA block polymerized to extend the PAAm block for conjugating RGD peptide (GRGDS) via NHS/EDC chemistry to the block-copolymer brushes. The adhesion and spreading behaviors of NIH-3T3 fibroblasts and pancreatic tumor cells (PaTu 8988t) were clearly controlled by the stiffness of the PAAm-b-PAA-RGD brushes. The cells interacted with the brushes by altering their cytoskeleton organization and focal adhesion formation, leading to the change of adhered cell densities and morphologies. Stiffer PAAm-b-PAA-RGD brushes facilitated cell attachment and spreading (Figure 2.8b and c).

2.4.3 Cell-Adhesive Topographical Cues with Functional Polymer Brushes

Other than those above chemical and mechanical cues, topographical cues on material surfaces also can significantly influence the interaction between cells and the substrates [136]. Normally, the topography of one material surface can be divided into the random surface topography and regular surface topography (patterned surface). Random surface topography including porosity [137], roughness [114, 116, 138] and pore size

[139] can significantly affect protein adsorption thus cell response toward material surfaces. By designing random surface topography with suitable topographic parameters that mimic nano- and microtopographic milieus, material surfaces can provide directional guidance for cells to adhere and grow.

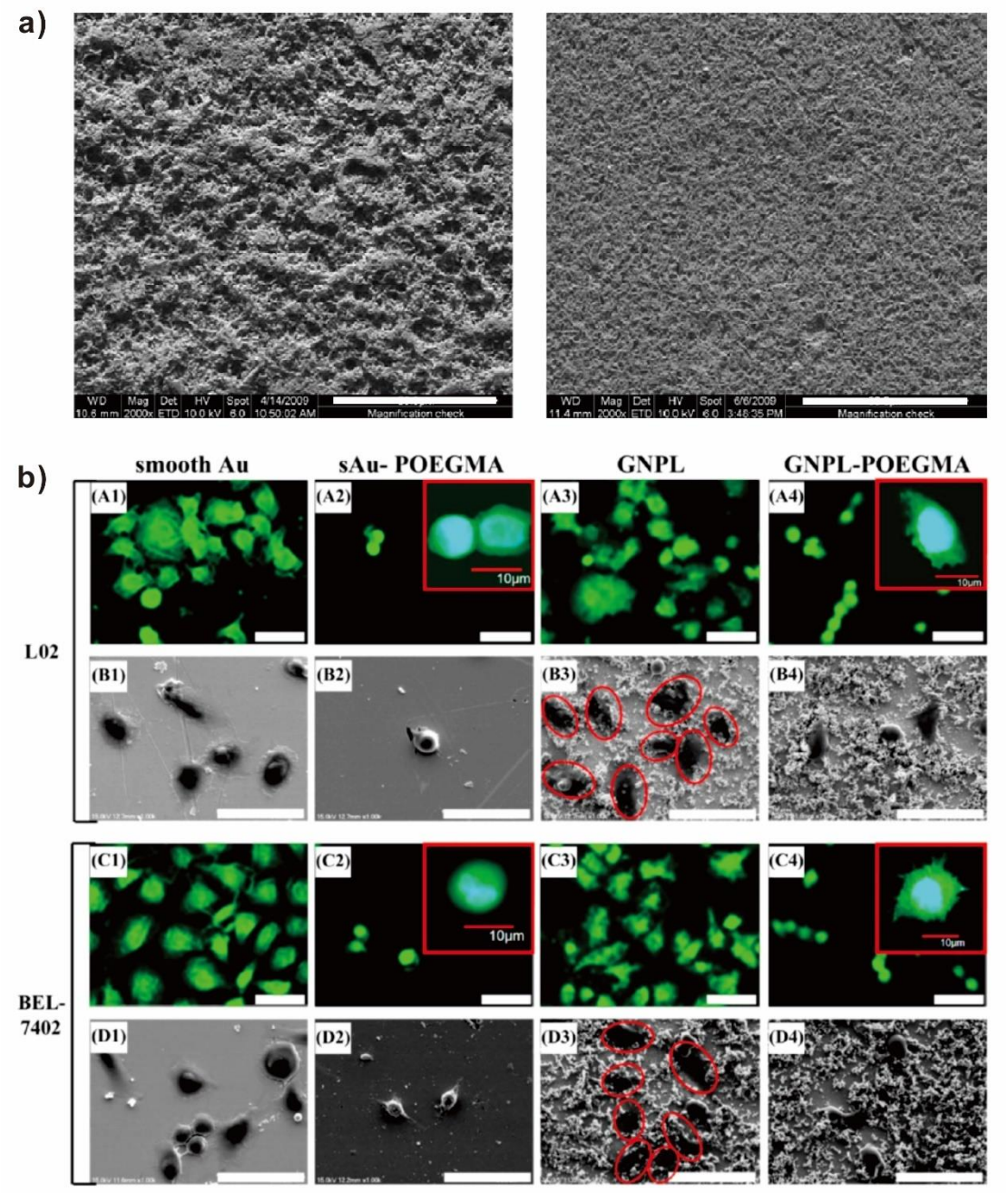

Figure 2.9. a) Surface SEM images for (left) the unmodified PVDF membrane and (right) PHEMA modified PVDF membrane [140]. Scale bar: 50 μm. b) Fluorescence and SEM images of L02 and BEL-7402 cells on surfaces [141]. Spreading cells on the GNPL surface are marked by red ovals in B3 and D3. Scale bar: 50 μm. The shape and

filopodia of the cells on POEGMA-modified surfaces were observed by confocal microscopy and are shown as insets in A2, A4, C2, and C4 (scale bar: 10 μm).

To control topographical cues on material surfaces, the irregular surface architecture of the material should first be precisely designed. A common method to prepare polymer brushes surface with random topography is that growing polymer brushes on a texturized substrate. For instance, Meng *et al.* [140] grew poly (2-(N, N-dimethylamino) ethyl methacrylate) (PDMAEMA), poly (2-oligo (ethylene glycol) monomethyl ether methacrylate) (POEGMA) and PHEMA brushes on polyvinylidene difluoride (PVDF) microporous membrane via surface-initiated electron transfer atom transfer radical polymerization (SI-AGET ATRP), and successfully obtained porous polymer brushes surfaces (Figure 2.9a). Shi *et al.* [141] modified Au nanoparticle layer (GNPL) (prepared by chemical gold plating) and smooth Au surfaces with protein-resistant POEGMA brushes using SI-ATRP to study the respective roles of topography on the adhesion and spreading of human hepatocytes and hepatocellular carcinoma cells. They found that both two kinds of cells adherent onto texturized POEGMA brushes surfaces were more stably attached and thus were more durable compared to those on smooth surfaces (Figure 2.9b). Therefore, topography plays a more important role for cell adhesion on a protein-resistant surface.

2.4.4 Cell-Adhesive Functional Polymer brushes with Multiple Cues

Apart from using a single type of cue to control cell behaviors, researchers have been showing increasing interest in the rational design of polymer brushes systems with a combination of different cues, which is believed to show a synergistic effect and enables better manipulation of cell behaviors for cell biology study, regeneration medicine and other cell-based applications.

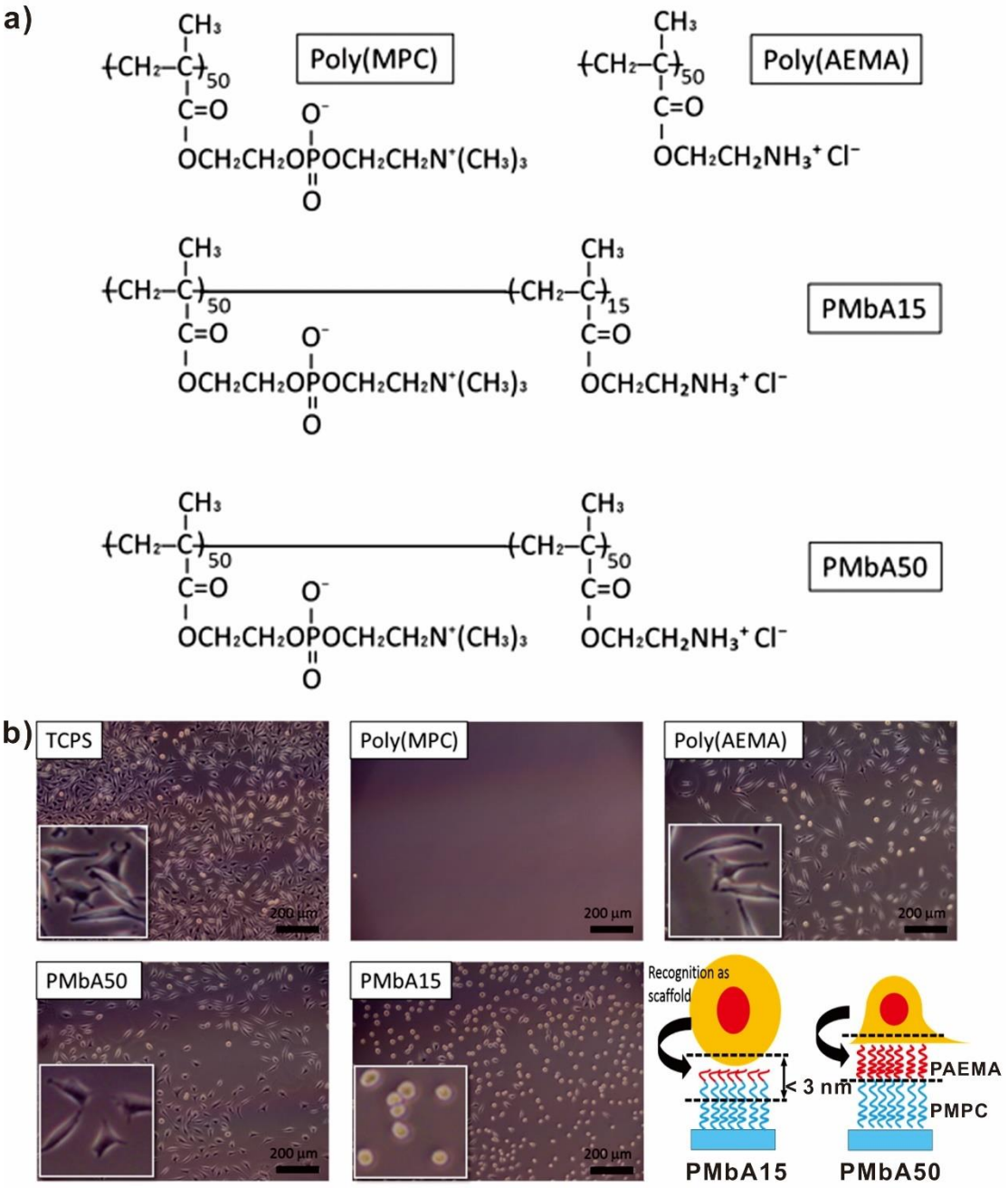

Figure 2.10. a) Chemical structures of polymers prepared. b) schematic image (lower right) of cellular response to non-contacting nanoscale sublayer, and microscopic images of adhered L929 on TCPS (upper left), poly(MPC) (upper middle), poly(AEMA) (upper right), PMbA50 (lower left), and PMbA15 (lower middle) after 72 h from seeding [142].

For example, some researchers have combined the chemical and mechanical cues to prepared polymer brushes substrates for controlling cell behaviors. Azuma et al. [142]

fabricated a well-defined diblock polymer brushes system (named PMbA15 and PMbA50, Figure 2.10a) composed of 2-methacryloyloxyethyl phosphorylcholine (MPC) acting as highly viscous part (mechanical cues) and cell-adhesive cationic 2-aminoethyl methacrylate (AEMA) (chemical cues). The static contact angles (SCA) of air bubbles in water on the PMPC, PAEMA, PMbA15 and PMbA50 brushes surfaces were 168 ± 2, 131 ± 4, 129 ± 6 and 138 ± 7 respectively. The approximate SCA results indicated the physical, chemical or geographical parameters of PAEMA, PMbA15 and PMbA50 brushes were similar. Then they used such diblock polymer brushes to culture L929 mouse fibroblasts and examined the influence of the non-contacting underlying PMPC layer on the cell adhesion. They found that the viscoelasticity of the non-contacting lower PMPC layer of PMbA15 containing shorter PAEMA chains could influence the cell adhesion and spread. Although the top PAEMA layer of PMbA15 was cell-adhesive resulting in cell adhesion, cells could response the mechanical property of the underlying PMPC layer and keep rounded morphology during adhesion process (Figure 2.10b).

Some literature also studied the combined action of chemical and topographical cues, mechanical and topographical cues, and even the chemical, mechanical and topographical cues of polymer surfaces for manipulating cell behaviors. More examples and discussion will be introduced in section 2.5.

2.5 Fabrication of Patterned Polymer Brushes for Controlling Cell Behaviors

With the rapid development of various surface patterning techniques at micro- and nanoscales, patterned polymer brushes with different chemistries and mechanical properties provide precise control of and new insights into cell behaviors. Polymer brushes are usually patterned with regular surface topographies such as ordered nanofibers, nanolines, nano- or microgrooves, squares and grids which can be used in cell orientation, osteogenic differentiation and neuron differentiation via contact guidance [143-144]. Focusing on materials, there are two designe philosophies to prepare

patterned polymer brushes substrate for contronlling cell behaviors. One is to pattern either cell-adhesive or cell-inert polymer brushes with a topographical guidance for cell behavior control. Another is to create patterned polymer brushes with the combination of both cell-inert and cell-adhesion polymers.

Otherwise, in the past decade, the patterning techniques for patterned polymer brushes have been witnessed dramatic progress. According to the pattern processes of polymer brushes, these techniques can be divided into two approaches, including 1) direct patterning that polymer brushes are directly written on a substrate or the preformed polymer brushes films are selectively removed by locally confined mechanical force or irradiation ("top-down"), and 2) indirect patterning that the surface-bound initiators are patterned onto a substrate in one-dimensional (1D) or two-dimensional (2D) arrays by various lithography techniques and then the initiator patterns serve as templates to graft polymer brushes via SIP ("bottom-up") [145]. In the indirect patterning process, the initiator patterns can be ether generated in situ by UV or X-ray irradiation of a substrate, or directly written onto a substrate, or removed/degraded selectively from pre-fabricated surface-immobilized initiator layer, or immobilized onto previously patterned surfaces using selective chemistry [145].

Various lithography techniques are applied to direct and indirect patterning for controlling cell behaviors [146], including photolithography (PL), electron-beam lithography (EBL), mechanical contact lithography [scanning probe lithography (SPL), soft lithography (SL) and nanoimprinting lithography (NIL)] and lithography techniques based on surface forces [capillary force lithography (CFL) and colloidal lithography], etc.

2.5.1 Photolithography

PL which is also named as optical lithography or ultraviolet lithography is considered as the most established lithography technique for fabricating precise and complex patterned polymer brushes surfaces with resolution down to several hundred nanometers [144, 147].Typically, the traditional process of PL includes steps of 1) patterns

transfer from designed photomasks to light-sensitive photoresist on the substrates by , 2) a series of chemical treatments to leave the exposure patterns into the surfaces underneath the photoresist, or to deposit new materials (such as protein and initiator) in the desired pattern upon the surfaces (Figure 2.11a). Takahashi *et al.* [148] developed a stripe-like surface with micropatterned thermoresponsive copolymer brushes of equal stripe and space width using PL and indirect patterning method. The stripe-like polymer brushes surface consisting of both the cell-adhesive PNIPAm brushes domain as well as the cell-inert PNIPAm-b-poly(N-acryloylmorpholine) (PNIPAm-PAcM) brushes domain allowed normal human dermal fibroblasts to be aligned on the polymer surfaces. Then the ambient temperature was below the LCST of PNIPAm, it was found that the aligned cells on stripes with a moderate width (50 μm) could be oriented as cell sheets (Figure 2.11b).

Otherwise, the interference photolithography (IPL) is another facile and high-throughput photolithography technique to fabricate periodic nano- and micropatterns of polymer brushes for controlling cell behaviors. In prototypical IPL process (Figure 2.11c), a coherent laser beam is split into two equal parts, which were then guided by the mirror and focused to superpose on the pre-fabricated polymer brushes surface to form a sinusoidal light intensity distribution (i.e., interference pattern). Polymer brushes lying on the maximum energy peaks will be most ablated, while polymer brushes under the energy minimum will be remained to form the ridge of the periodic patterns [149]. Yu *et al*. [150] prepared patterned PNIPAm brushes (~80 nm) surfaces containing both micro- and nanopatterns using a combination of IPL technique and SI-ATRP (Figure 2.11d and e). The patterned PNIPAm brushes surfaces were comprised of two part: 1) the striped micro-scale areas with unpatterned PNIPAm brushes, and 2) the square microscale areas containing nanopatterned PNIPAm. As we mentioned above, thin PNIPAm brushes (several nanometers) above LCST is cell-active, whereas thick PNIPAm brushes, such as an 80-nm thickness in Yu's work, is cell-inert. However, interestingly, this limitation of thick PNIPAm brushes for cell culture applications is circumvented by introducing nanopatterns to grafted PNIPAm brushes. They found that fibroblasts exclusively and precisely adhered onto microsized square areas which were

consisted of nanopatterned PNIPAm brushes at 37 °C (above LCST), and cell micropatterning was obtained after 72 hours (Figure 2.11f). Nanopatterned PNIPAm brushes at 37 °C collapsed and exposed the underlying substrate, which led to the improvement of protein adsorption of the polymer-free areas so that cells could attach onto the nanopatterned regions. Moreover, the thermoresponsive of nanopatterned PNIPAm brushes was kept, and cells detached from the nanopatterned PNIPAm brushes at 25 °C (below LCST) without influence from different periodic nanopatterns. This approach of cell micropatterning and cell sheet harvesting provide a potential for preparing unique cell sheet sizes for biological applications.

On the other hand, some polymer brushes with functional groups can be photocleaved and thus used in direct patterning method for preparing patterned polymer brushes. For instance, Kamada *et al.* [151] grew zwitterionic poly (carboxymethylbetaine) (PCMB) brushes which is cell-inert polymer brushes mentioned above onto a Si wafer by SI-RAFT. With a surface-confined aromatic RAFT agent at the bottom of polymer chains, the PCMB brushes can be cleaved under UV irradiation due to photodecomposition of the phenyl group. Therefore, PCMB brushes grid was fabricated by PL with a photomask. The cell culture experiments showed that 3T3 fibroblast cells adsorbed on and adhered to the UV irradiation-induced hollow areas. These results indicated that the surface-confined aromatic RAFT agent can be a useful tool for fabricating patterned polymer brushes with directing patterning method via PL technique.

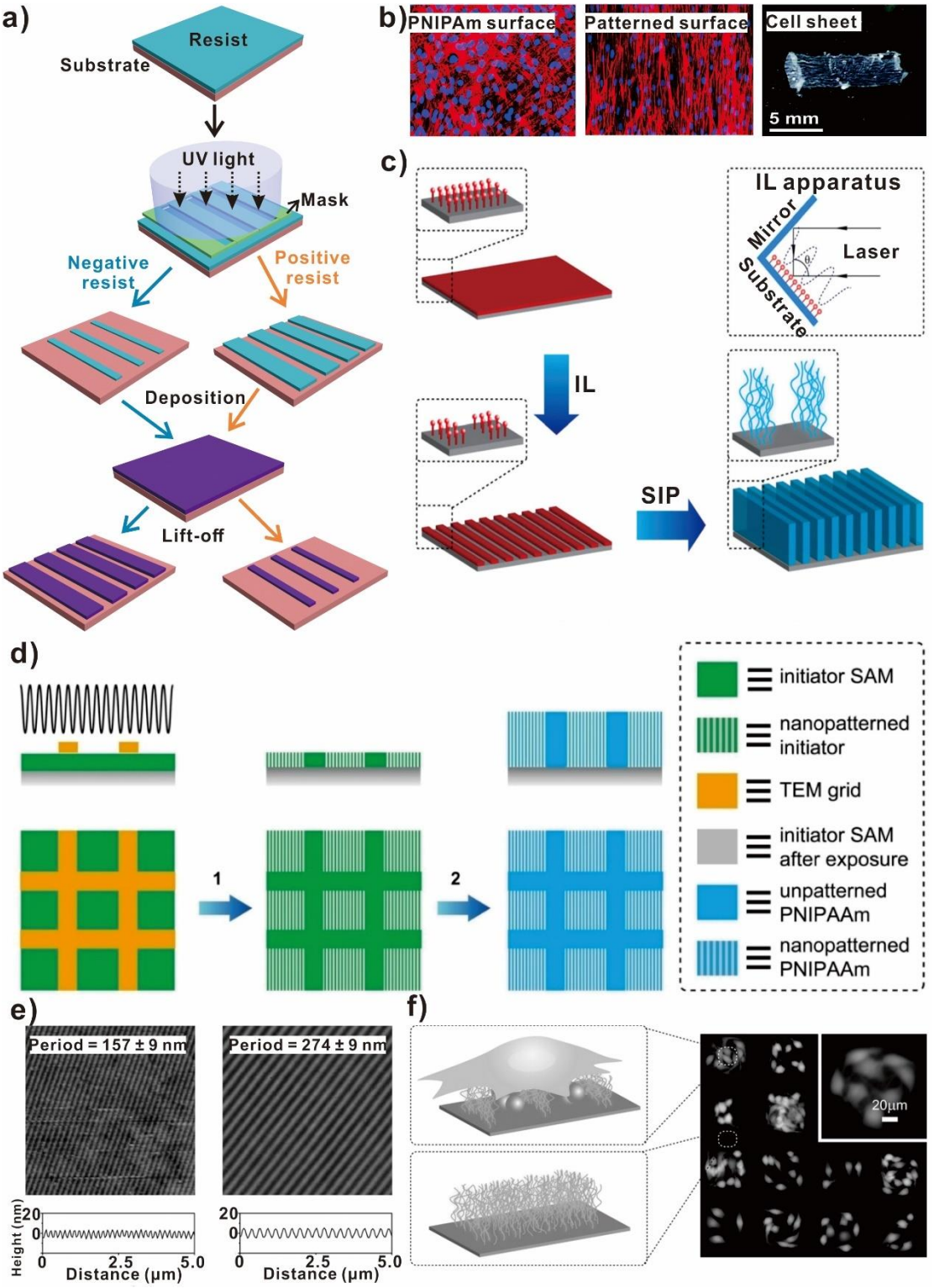

Figure 2.11. a) Schematic presentation of PL process. b) The fluorescence images of adherent fibroblasts on nonpatterned PNIPAm and patterned copolymer brushes surfaces (Actin: red and nuclei: blue. Scale bar: 100 μm), and the photograph of a cell sheet harvested from patterned surfaces showing orientation [148]. c) Schematic of preparation of nanopatterned brushes by IL and SIP [152]. First, nanopatterns of ATRP

initiators are fabricated via IL. Second, brushes (e.g., PNIPAAm) are grafted from the nanopatterns of ATRP initiators. d) Procedure for preparing PNIPAAm surfaces with both micropatterns and nanopatterns [150]. e) Contact-mode AFM height images obtained in air of nanopatterned PNIPAAm surfaces generated at a constant polymerization time (6 min, corresponding to tPNIPAAm = 78.8 ± 3.5 nm). f) The fluorescence images of viable NIH-3T3 fibroblasts located exclusively on the nanopatterned regions after 72 h. Cells were treated with LIVE/DEAD stain prior to imaging.

2.5.2 Electron-Beam Lithography

EBL is another mature lithography technique which can be used to prepare large-area biocompatible polymer patterns for biological applications, but more advantageous to PL in producing ultrahigh-resolution nanofeatures under sub 5 nm [153]. The light wavelength limits the resolution of PL. However, one major difference of EBL from PL is that EBL utilizes focused electron beam of much shorter wavelength as the energy source exposing to the lithographic resist so as to reduce interference.

EBL can be performed by scanning a focused electron beam to draw patterns (using a mask or directly writing) on an electron-sensitive film-coated substrate (Figure 2.12a). When using polymer brushes to act as the electron-sensitive film in EBL process, it requires the polymer should be e-beam scissile, such as poly (methacrylate) (PMMA). On this occasion, patterned polymer brushes can be fabricated by direct patterning method. On the other hand, EBL also can be used in indirect patterning method. For example, Idota *et al.* [154] developed a facile one-step method to fabricate patterned polymer brushes surface by simultaneously controlling both the EBL and graft polymerization techniques from the monomer solution without using any photo-sensitive resists. To do so, the cell-inert PAA-grafted glass substrate was first prepared by free radical polymerization. The NIPAm monomer solution and Espacer 300 (a conductive water-soluble polymer) were then spin coated on the cell-inert PAA-grafted glass substrates for subsequent EBL process. Only in those electrons beam exposed

areas, NIPAm monomers were polymerized and grafted onto the PAA-modified surfaces. To investigate the cell interaction on such a polymer brushes-modified surface, endothelial cells were used. It was observed that endothelial cells adhered and spread along the orientation of PNIPAm stripes when the ambient temperature was above LCST but detached when the ambient temperature was below LCST.

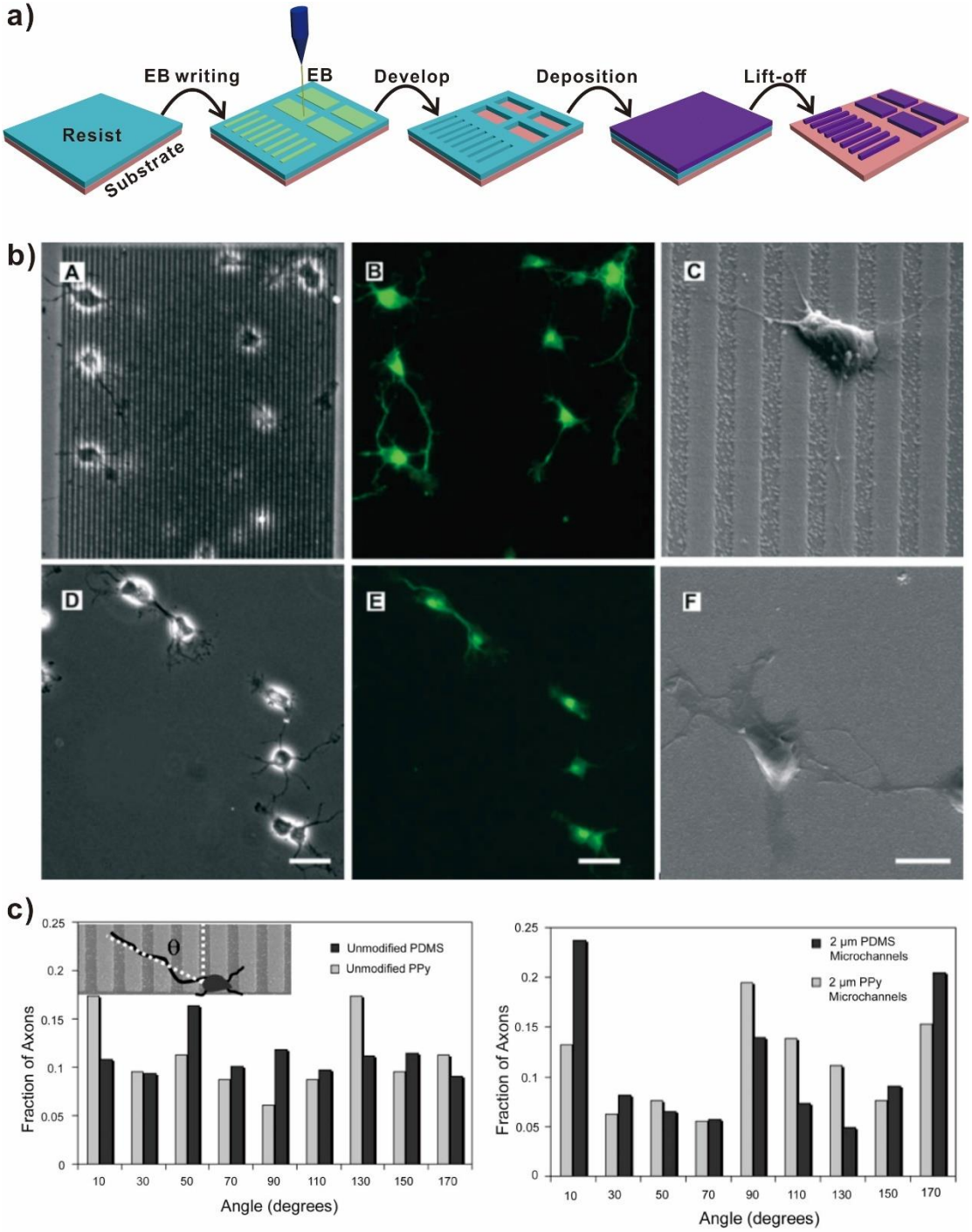

Figure 2.12. a) Schematic presentation of EBL process. b) From left to right: phase-contrast, fluorescence, and SEM microscopy images, of hippocampal neurons on PPy.

A-C) Cells cultured on 2 μm wide and 200 nm deep PPy microchannels; D-F) cells cultured on unmodified PPy. The green labeling (Alexa 488) corresponds to Tau-1 (axonal marker) immunostaining. Cells polarized more readily on microchannels than on unmodified PPy. The scale bar is 20 μm (A, B, D, E) and 5 μm (C, F). c) A quantitative analysis of the axon angle. Histograms for axon angle distribution on unmodified PPy/PDMS substrates (left) and 2 μm PPy/PDMS microchannels (right).

Gomez *et al.* [155] prepared electrically conducting polypyrrole (PPy) brushes microchannel on ITO-coated slides by EBL and electropolymerization for controlling neuron behaviors (Figure 2.12b). A lot of neurons cultured on PPy microchannel for studying the influence of microstructure PPy on neuron polarization, axon length, and orientation. They found that neurons cultured on patterned PPy were much easier to be polarized than that on unpatterned PPy substrates. The microchannel was a benefit to the formation of cell axons (Figure 2.12c).

2.5.3 Soft Lithography

SL is one of the microfabrication techniques based on printing using elastomeric stamps. These stamps are usually made with polydimethylsiloxane (PDMS) particularly due to its biocompatibility, durability, gas permeability and the ease of fabrication. To fabricate PDMS stamps, PDMS prepolymers are first casted onto a patterned mould fabricated by PL or EBL. After curing, PDMS stamps as a replica can be peeled off from the mould. The surface of these stamps of protruding nano- or microreliefs is capable of carrying materials as inks which are subsequently transferred onto the substrate surface. For bio-related applications, PDMS stamp adopted in SL technique can pattern complex materials such as SIP initiators, polymers and proteins [156-157], where a resolution of about 10 nm can be achieved. As a technique to fabricate patterned polymer brushes surface to control cell behaviors, SL is facile, high-throughput and inexpensive. Therefore, it is highly desirable for mass production of patterned polymer surface when compared with PL and EBL.

There are two major patterning techniques in SL [144]. One is called the microfluidic patterning, which can be used for fabricating patterned polymer brushes with direct patterning method. In this method, PDMS mould is used to print micro-sized channels on pre-grafted polymer brushes surface for manipulating cell behaviors in dynamic conditions (Figure 2.13). A major type of SL technique to fabricate polymer brushes is called the microcontact printing (μCP), which is always used to form patterned polymer brushes with indirect patterning method. The *μcp* technique is based on self-assembly of printed molecules in which inked PDMS stamp with relief patterns can transfer ink patterns on a substrate through conformal contact. Typical μCP using PDMS stamp can result in patterns of 1-μm surface features. Lately, further development of nanocontact printing (nCP) can even produce much smaller surface features of nanoscale [158]. In order to exploit patterned polymer brushes that mimics cell microenvironment to control cell behaviors, the polymer brushes are always patterned by μCP with the aid of PDMS stamps to result in both cell-inert and cell-active areas. Once the surfaces are patterned with certain cell-inert materials, the non-patterned areas can then be coated with cell-active materials, and *vice versa*.

In particular, thiols and trichlorosilane are the most widely used functional materials in μCP to respectively modify gold and glass substrate surface for SIP to prepare patterned polymer brushes for cell culture study. For example, Huck's group had patterned polymer grafted-substrates by using μCP for controlling cell behaviors [159-160]. Taking advantage of extreme protein resistance offered by POEGMA, they specially synthesized POEGMA brushes patterns under optimized conditions to achieve high-quality ECM patterns for single cell spreading and polarization control (Figure 2.13b). Based on these results, they further prepared polymer brushes-based single cell micropatterns to direct the fate of epidermal stem cells and gave evidence for a cross-talk between geometrical and chemical cues on fate decision. Such micropatterning (20 and 40 μm-diameter discs, 40 μm-diameter rings, arc shaped patterns) is made possible by the protein resistance displayed by several types of brushes, including POEGMA, poly (3-sulfopropylmethacrylate) (PSPMA), poly (2-(methacryloyloxy)-ethyl-trimethyl-ammonium chloride)-r-(3-sulfopropylmethacrylate) (COPO) and poly (2-

(methacryloyloxy) ethyl-dimethyl-(3-sulfopropyl)-ammonium hydroxide) (PMEDSAH). This method provides a platform to probe simultaneously multiple parameters to precisely control the cell behavior.

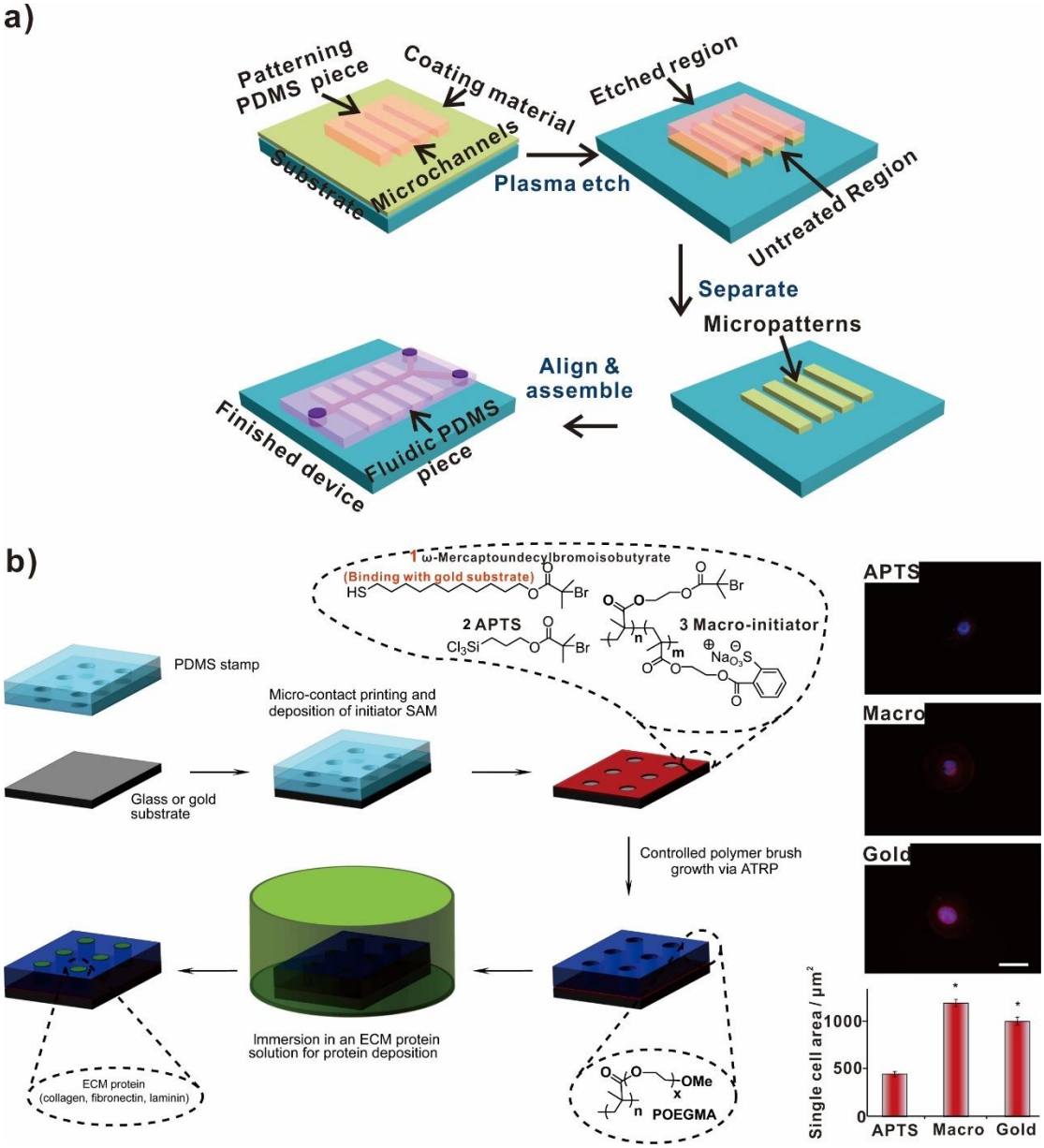

Figure 2.13. a) Schematic presentation of the procedure for micropatterning cells inside a microfluidic device using cell-adhesive or non-adhesive substrates. b) Schematic presentation of the formation of ECM protein/POEGMA patterns on glass or gold substrates by μCP and SI-ATRP, and fluorescence microscope images of single cells (scale bar: 30 μm) spreading on 50 μm islands after 3 hr (F-actin: red and nucleus: blue) and the corresponding projected single cell area measured from F-actin staining images

(*P < 0.01). The substrates used were APTS-coated glass (APTS), LBL-coated glass with macro-initiator printing (Macro) and gold (Gold).

2.5.4 Scanning Probe Microscopy-Based Lithography

Scanning probe microscopy-based lithography (SPL) such as atomic force microscopy (AFM), dip-pen nanolithography (DPN), polymer pen lithography (PPL), and dip-pen nanodisplacement lithography (DNL) can create high-resolution polymer brushes patterns with indirect patterning methods, serving as a crucial fabrication tool for controlling cell behaviors [161]. SPL makes use of a sharp scanning tip to create patterns on a surface with nanoscale resolution, combining with organic transformations to induce redox, nucleophilic, metal-catalyzed, enzyme-catalyzed, and other reactions [162].

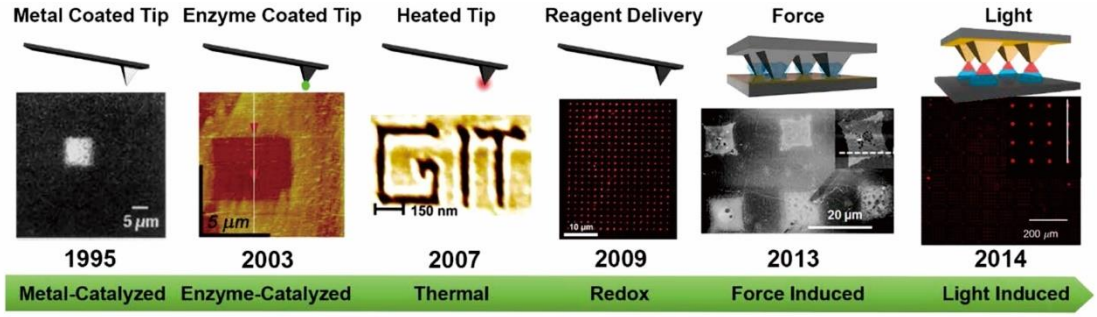

Figure 2.14. Evolution of SPL-directed organic transformations involving metal catalyzed, enzyme catalyzed, thermal, redox, force, and light induced reactions [162].

Among these lithography methods, DPN is widely applied in preparing patterned polymer brushes for many bio-related applications [163-165]. In this method, an AFM tip inked with SIP initiators is scanned along a surface of solid substrates to deposit initiators onto the surface directly. The lateral dimensions of the patterned surface features can range from 10 nm to micrometer scale. Laing *et al.* [165] fabricated thermoresponsive hydrogel microspot arrays based on thermoresponsive N, N-diethylacrylamide (DEAAm) and bifunctional Jeffamine ED-600 by DPN and photopolymerization, and studied the cell response to the thermally controlled switchable microspot arrays. It was found that the Jeffamine part acted as carrier matrix

which allowed a reduction in the evaporation of DEAAm molecules with high volatility so as to improve ink transfer from tip to the substrate. AFM and Raman spectroscopy were used to observe the thermally induced change in height and hydration state of the thermoresponsive behavior of polymer arrays. The endothelial cells cultured on the polymer arrays show that protein expression and cell-substrate interaction changed with the temperature change.

To improve the throughput and lower the cost of DPN, Huo *et al.* developed a low-cost and high-throughput lithography method namely PPL. In this method, instead of using AFM cantilever as a tip, a cantilever-free and elastomeric pyramidal tip array are used to deliver inks to a surface. Compared with DPN, feature size produced by PPL can range from nano- to microscopic scale using one single tip array. For example, Zhuang *et al.* [166] used PPL techniques and SI-ATRP to prepare massively parallel PGMA brushes patterns and successfully grafted proteins on the PGMA patterns.

2.6 Conclusions and Summary for Research Gaps

The development of patterned polymer brushes with rational designs in chemical, topographical and mechanical cues for directing cell behaviors is one emerging trend for cell biology study, regeneration medicine, tissue engineering and many other biological applications. The above has introduced different fabrication methods of patterned polymer brushes for controlling cell behavior, with a detailed discussion of the underlying mechanisms and ample examples of biomimetic studies. It should be noted that, up to date, the exact cell behaviors on ECM is still largely unclear, due to the complicated ECM environments as well as the vast diversity of properties of different cell types. Therefore, it requires significant continuous exploration and study of biomimetic patterned polymer brushes in the future. Nevertheless, the lack of a user-friendly method to fabricate a versatile patterned polymer brushes-based artificial ECM with well-designed topography, and abundant chemical properties has significantly limited the developed in this field.

Apart from the fundamental materials preparation and the underlying mechanism

study, most works over the past decades have been focused on one-component, one-seized uniform patterns of polymer brushes substrates for cell culture. Otherwise, among cell behaviors, cell adhesion and orientation have been studied most often. However, controlling other cell behaviors, such as cell differentiation and migration, are landmark work for understanding the mystery of life and prolong the life of human beings. Therefore, it is highly desirable that more advanced responsive, multi-component and multiscale patterned polymer brushes which can better mimic the real ECM should be developed for successfully manipulating complex cell behaviors (e.g. directional differentiation). Furthermore, for a wider range of practical application, it is also anticipated that remarkable development will be achieved in the areas of the flexible and stretchable substrate that patterned polymer brushes is tethered onto.

CHAPTER 3 METHODOLOGY

In this chapter, the general methodology for this thesis is introduced. The project involves fabricating patterned polymer brushes which biomimic ECM via DNL, μCP, and SI-ATRP for controlling cell behaviors. Methods for surface modification of substrates will be introduced, and then the detail lithography processes of DNL and μCP will be elaborated. Next, the cell culture experiments will be described. Finally, the instruments for various characterization will be illustrated.

3.1 Materials of Substrates

3.1.1 Substrates

Silicon (Si) wafers (4", <100>, resistivity 1-10 Ω·cm) with 500 nm silicon dioxide (SiO_2) on one side and glass wafers were purchased from Semiconductor Wafer, Inc. DuPont Teijin Films supplied poly (ethylene terephthalate) (PET) substrates. Au substrates were prepared by thermal or electron-beam evaporation of Cr/Au thin films on Si, glass wafers and PET films (named Au-Si, Au-glass, and Au-PET).

3.1.2 Surface Modification of Substrates

Before patterning, Au substrate surfaces could be modified by SAMs or surface-grafted polymer brushes which are grown from initiator SAMs modified Au surfaces.

Herein, thiols were chosen as model molecules to form SAMs of protecting layer and SAMs of initiators due to they are very easy to react with Au by Au-S bond spontaneously. In this thesis, two typical thiol inks were used, 1) 16-mercaptohexadecanoic acid (MHA) for forming protecting SAMs, and 2) ATRP initiator ω-mercaptoundecyl bromoisobutyrate (MUDBr, synthesized from 11-mercapto-1-undecanol and 2-bromo-2-methylpropionyl bromide according to the

reference [167]) to prepare initiator SAMs for growing polymer brushes by *in-suit* ATRP.

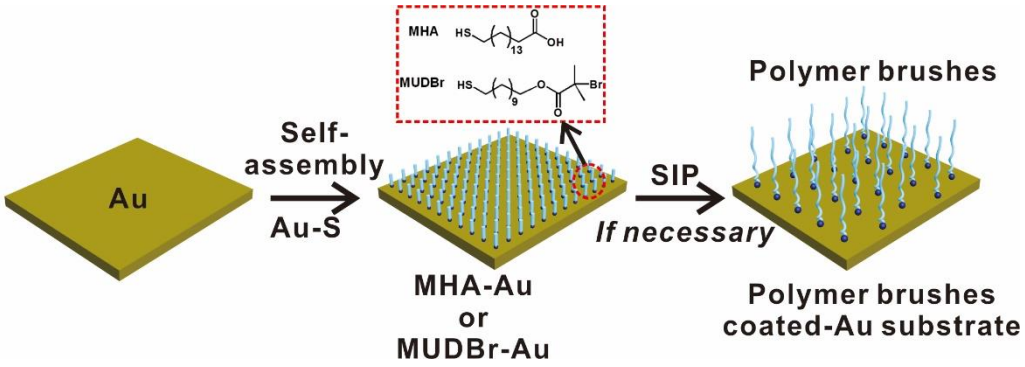

Figure 3.1. Scheme for the formation of thiol SAMs and polymer brushes modified Au substrates.

Before surface modification, Au-Si, Au-glass, and Au-PET wafer were pre-treated by ultrasonic cleaning with deionized water (DI water), acetone and isopropanol in sequence (30 min in each solution). Then thiol SAMs were prepared by solution deposition, and next, the surface-grafted polymer brushes could be grown by ARGET SI-ATRP if necessary. The detailed procedures are as follows.

Solution deposition for SAMs preparation: The cleaned Au substrates were simply immersed into ethanol solutions of thiols (2.5 mg/mL) at room temperature for 24 hrs to form SAMs. The obtained SAMs modified Au substrates were rinsed with ethanol and dried via nitrogen stream.

Surface grafting of polymer brushes: MUDBr modified Au substrates and ARGET SI-ATRP were employed to graft functional polymer brushes onto the substrate surfaces. Generally, the MUDBr-Au substrates were placed in centrifuge tubes with reaction solutions which were prepared according to the polymerization recipes as below.

1) *The preparation of PGMA brushes*: GMA (7.8 g), methanol (4.8 g), DI water (1.5 mL), and ascorbic acid (150 mg) were mixed in a 50-mL centrifuge tube, followed by dissolving copper (I) bromide (CuBr, 78 mg), and 2, 2'-bipyridyl (bpy, 210 mg). Then the MUDBr-Au substrate was placed into the resulting dark brown mixed solution to start the polymerization. After 2 hrs of polymerization at ~37 °C, the substrate was taken out and rinsed with methanol and water, and then successively washed with dichloromethane and methanol, followed by drying with compressed air.

2) *The preparation of PMMA brushes*: MMA (5 g), methanol (3.2 g), DI water (1.5 mL), and ascorbic acid (150 mg) were mixed in a 50-mL centrifuge tube, followed by dissolving CuBr (71 mg), and bpy (156 mg). Then the MUDBr-Au substrate was put into the resulting dark brown mixed solution to start the polymerization. After 3 hrs of polymerization at ~37 °C, the substrate was taken out and rinsed with methanol and water, and then successively washed with acetone and toluene, followed by drying with compressed air.

3) *The preparation of PMETAC brushes*: METAC (6.9 g, Mw 207.7, 80 wt. % in H_2O), methanol (5.6 g), DI water (2 mL), and ascorbic acid (200 mg) were mixed in a 50-mL centrifuge tube, followed by dissolving CuBr (135 mg), and bpy (260 mg). Then the MUDBr modified Au substrate was put into the resulting dark brown mixed solution to start the polymerization. After 4 hrs of polymerization at ~37 °C, the substrate was taken out and rinsed with methanol and water, and then successively washed with acetone, followed by drying with compressed air.

4) *The preparation of POEGMA brushes*: OEGMA (4 g, Mw 300), methanol (4.8 g), DI water (1.5 mL), and ascorbic acid (150 mg) were mixed in a 50-mL centrifuge tube, followed by dissolving CuBr (70 mg), and bpy (156 mg). Then the MUDBr modified Au substrate was put into the resulting dark brown mixed solution to start the polymerization. After 2 hrs of polymerization at ~37 °C, the substrate was taken out and rinsed with methanol and water, and then washed with toluene and methanol, followed by drying with compressed air.

5) *The preparation of PHEMA brushes*: HEMA (5 g), methanol (2 g), DI water (2.5 mL), and ascorbic acid (150 mg) were mixed in a 50-mL centrifuge tube, followed by dissolving CuBr (147 mg), and bpy (400 mg). Then the MUDBr-Au substrate was put into the resulting dark brown mixed solution to start the polymerization. After 2 hrs of polymerization at ~37 °C, the substrate was taken out and rinsed with methanol and water, and then successively washed with toluene and methanol, followed by drying with compressed air.

6) *The preparation of PNIPAm brushes*: NIPAm (1.5 g), methanol (12 g), DI water (15 mL), and ascorbic acid (300 mg) were mixed in a 50-mL centrifuge tube, followed

by dissolving CuBr (48 mg), and N, N, N', N'', N''-pentamethyldiethylenetriamine (PMDETA, 165 μL). Then the MUDBr-Au substrate was put into the resulting dark brown mixed solution to start the polymerization. After 3 min of polymerization at 40 °C, the substrate was taken out and rinsed with methanol, water, and acetone, followed by drying with compressed air.

7) *The preparation of poly (3-sulfopropyl methacrylate) potassium salt (PSPMAK) brushes*: SPMAK (6.9 g), methanol (6.4 g), DI water (4 mL), and ascorbic acid (150 mg) were mixed in a 50-mL centrifuge tube, followed by dissolving CuBr (66 mg), and bpy (260 mg). Then the MUDBr-Au substrate was placed into the resulting dark brown mixed solution to start the polymerization. After 3 hrs of polymerization at ~37 °C, the substrate was taken out and rinsed with methanol and water, and then successively washed with toluene and methanol, followed by drying with compressed air.

8) *The preparation of poly (methacrylic acid, sodium salt) (PMANa) brushes*: NaMA (4.5 g), DI water (15 mL), and ascorbic acid (150 mg) were mixed in a 50-mL centrifuge tube, followed by dissolving CuBr (144 mg), and bpy (310 mg). Then the MUDBr-Au substrate was put into the resulting dark brown mixed solution to start the polymerization. After 50 min of polymerization at ~60 °C, the substrate was taken out and rinsed with methanol and water, and then successively washed with toluene and methanol, followed by drying with compressed air.

3.2 Lithography Processes

3.2.1 Dip-Pen Nanodisplacement Lithography

Our group [168] recently developed the DNL method which uses a SAM as resist layer to limit the initiator diffusion. The DNL process is schematically illustrated in Figure 3.2a. A contact mode AFM tip inked with initiator molecules, e.g. MUDBr, was brought to touch with the surface modified Au substrates. With a suitable load (>10 nN), the molecules on the substrate surface would be mechanically cleaved away by the tip, and the volatile ink simultaneously self-assembled to the bare areas, which achieved

the nanodisplacement process. The surface modification of SAMs or polymer brushes protects the bare Au surface from ink contamination so that the feature size will equal to the cleaving area. The nanostructured MUDBr nanodots can be small to 25 nm (Figure 3.2b). Finally, polymer brushes were then grown from initiator pre-patterned areas by SIP.

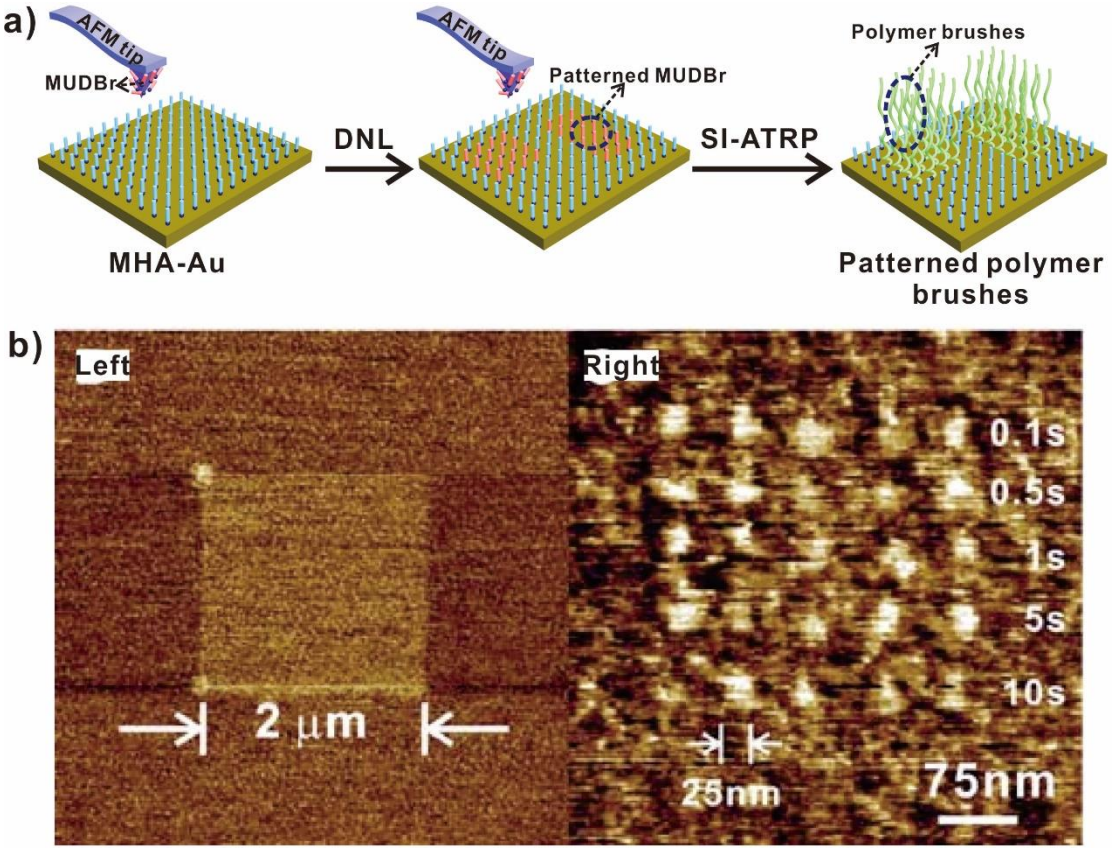

Figure 3.2. a) Schematic illustration of fabricating patterned polymer brushes on MHA-Au substrate by DNL and SI-ATRP. b) Left: Lateral force microscopy (LFM) image of an MUDBr square written by DNL. Right: MUDBr nanodots made by DNL at constant tip-substrate contact force (1000 nN), but different tip-substrate contact time. Each dot was made by indenting the tip onto the MHA-Au one at a time [168].

The main instrument for DNL is the AFM (XE-100, Pask Systems, Figure 3.3), which is consisted of the scanning tunneling microscope (STM) and the stylus profilometer [169]. The AFM scans a surface at nanometer resolution in *x*-*y*-*z* directions via a sharp tip which is placed at the end of a conducting cantilever and made of silicon or silicon nitride with curvature radius less than 10 nm. A special design of the XE-100

AFM is the independent *x*-*y*- and *z*-piezo scanners, allowing the separate movements of *x*-*y* plane and the *z*-piezo scanner. Therefore, the XE-100 AFM can be used for lithography. With precise control of piezoelectric elements, the tip moved up and down in the *z*-direction with precisely regulated contact force or *z*-piezo extension, and the sample stage moved with nano-size positioning in *x* and *y* directions at the same time. After positioning and approaching, the cooperated software XEP was used to program the movements of the tip, the *z*-piezo extension, dwell time and designed patterns to perform the lithography process.

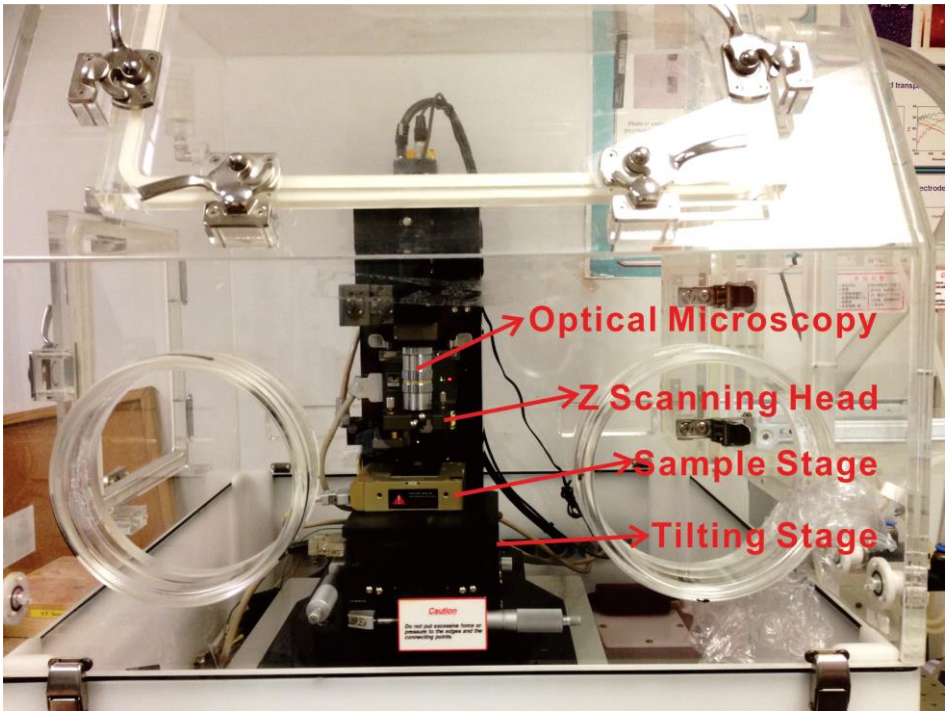

Figure 3.3 An XE-100 AFM encased in a humidity-controlled box on the vibration isolation table.

Importantly, the XE-100 AFM has a tiltable sample stage which is able to be adjusted to lead the sample paralleling with tip array. Therefore, to improve the writing efficiency, our group continually reported a parallel DNL (p-DNL) [170-171] for high-resolution, large-area, and serial fabrication of complex polymer brushes structures. The p-DNL is a multi-cantilever version of single-tip DNL mentioned above. The only difference of lithography process of single-tip DNL and p-DNL is the leveling, i.e. the

sample stage should be adjusted to parallel with the tip array before patterning. Via tilting the sample stage angle in the *x*-direction, the multi-cantilever tip array in the p-DNL process could be deemed to be paralleled with the substrate surface when all tips of the tip array showed similar reflection upon contacting (Figure 3.4b).

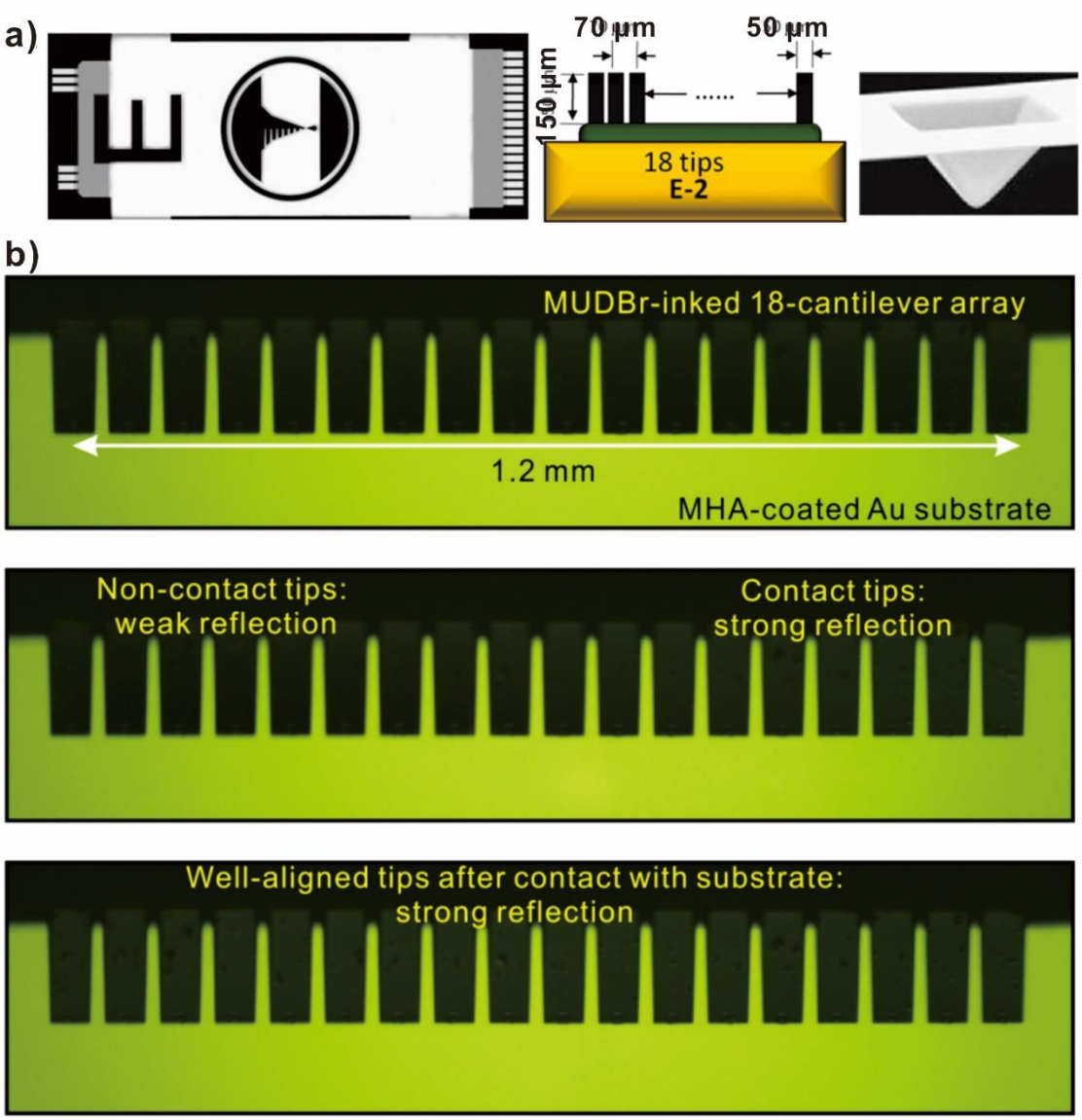

Figure 3.4. a) E-type 1D cantilever array with square-shaped cantilevers and 18 tips. Copy from NanoInk. Inc. b) Optical micrographs of the MUDBr-inked, 18-cantilever tip array before (top) and after (middle and down) contacting with the MHA-Au substrate, where the 18 tips are partially aligned (middle) or fully-aligned (down) as confirmed by monitoring the differences of optical reflections of the cantilevers [170].

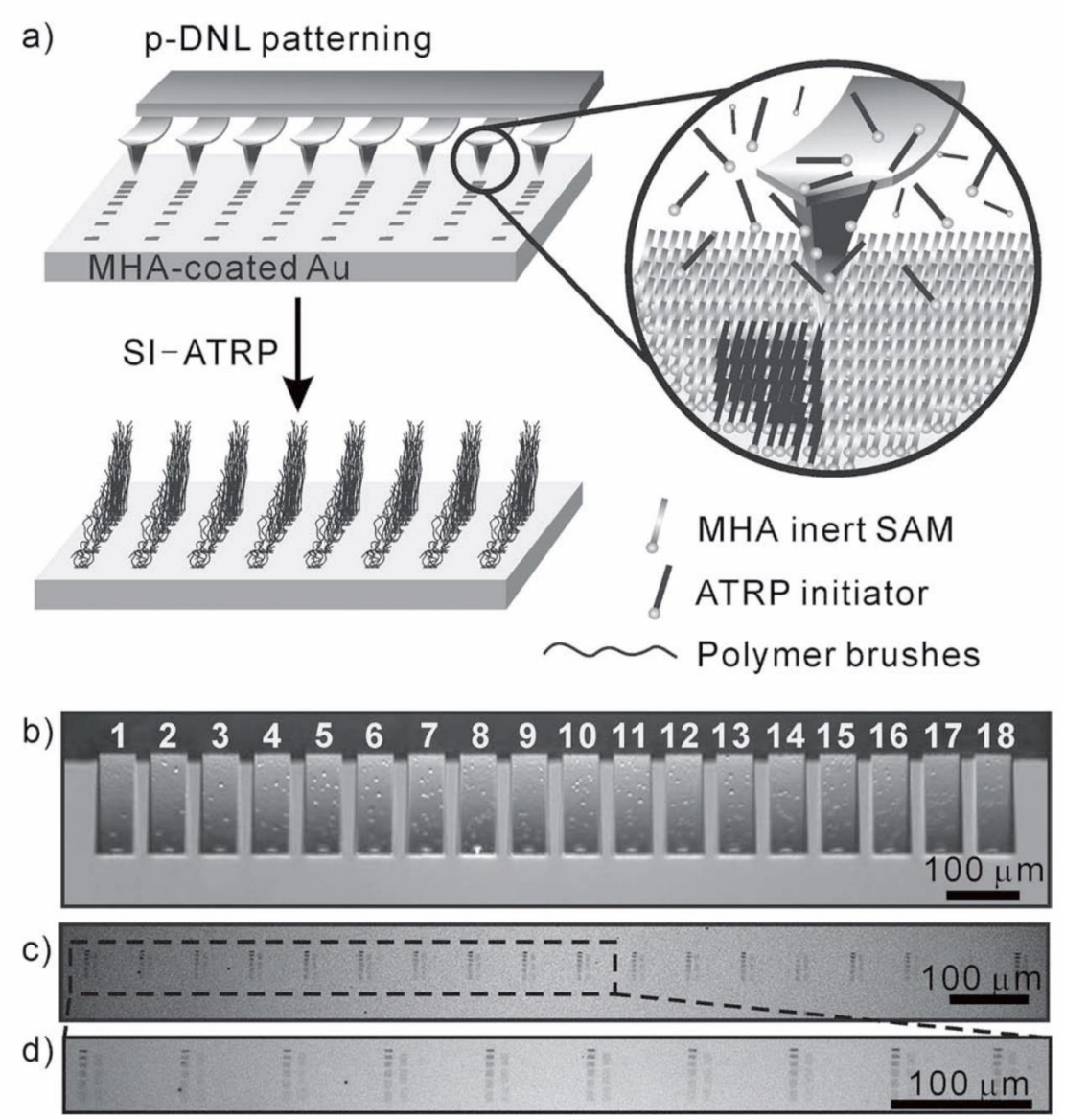

Figure 3.5. (a) Schematic illustration of the large-area, parallel fabrication of 3D polymer brushes by p-DNL and SI-ATRP [170]. (b-d) Optical micrographs [170] of (b) the 18-tip cantilever array used for p-DNL, (c) the PMMA brushes fabricated by the 18 tips via p-DNL and SI-ATRP, and (d) the zoom-in PMMA brush structures made by tip no.1 to 10.

A cantilever array of 18 AFM tips (Figure 3.4a, Nanoink. Inc.) simultaneously displaced the inert SAM molecules or polymer chains on the Au surface with MUDBr molecules pre-inked on the tips. Compared with single-tip DNL, the outcome of the p-DNL was an array with 18 columns, as the number of the tips array (Figure 3.5b-d). To

solve the uniformity of parallel fabrication, the feature density method (Figure 3.6) was applied in the p-DNL process. With feature density method, the morphology of polymer brushes was constructed by appropriate control of the lateral space between identical nanobrushes [172]. A white/black bitmap should be used as guide map in feature density method, and be transferred to an initiator ‘‘bitmap’’ consisted of initiator nanodots by DNL process. The lateral space of the initiator nanodots was controlled by the pixel density of the bitmap. So finally, various polymer brushes gradient structures would be obtained.

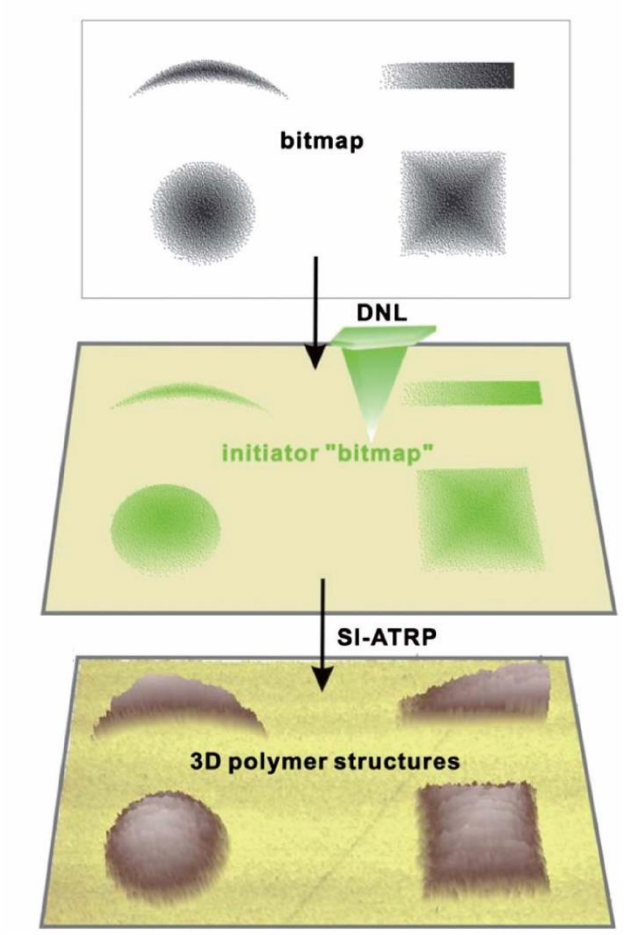

Figure 3.6. Programming the 3D structures with polymer nanobrushes by the feature density method [172]. A black-white bitmap image is first transferred into an initiator ‘‘bitmap’’ via the DNL, from which 3D structures of polymer nanobrushes, i.e. slide, conic, new moon, and pyramidal shapes, are grown via SI-ATRP.

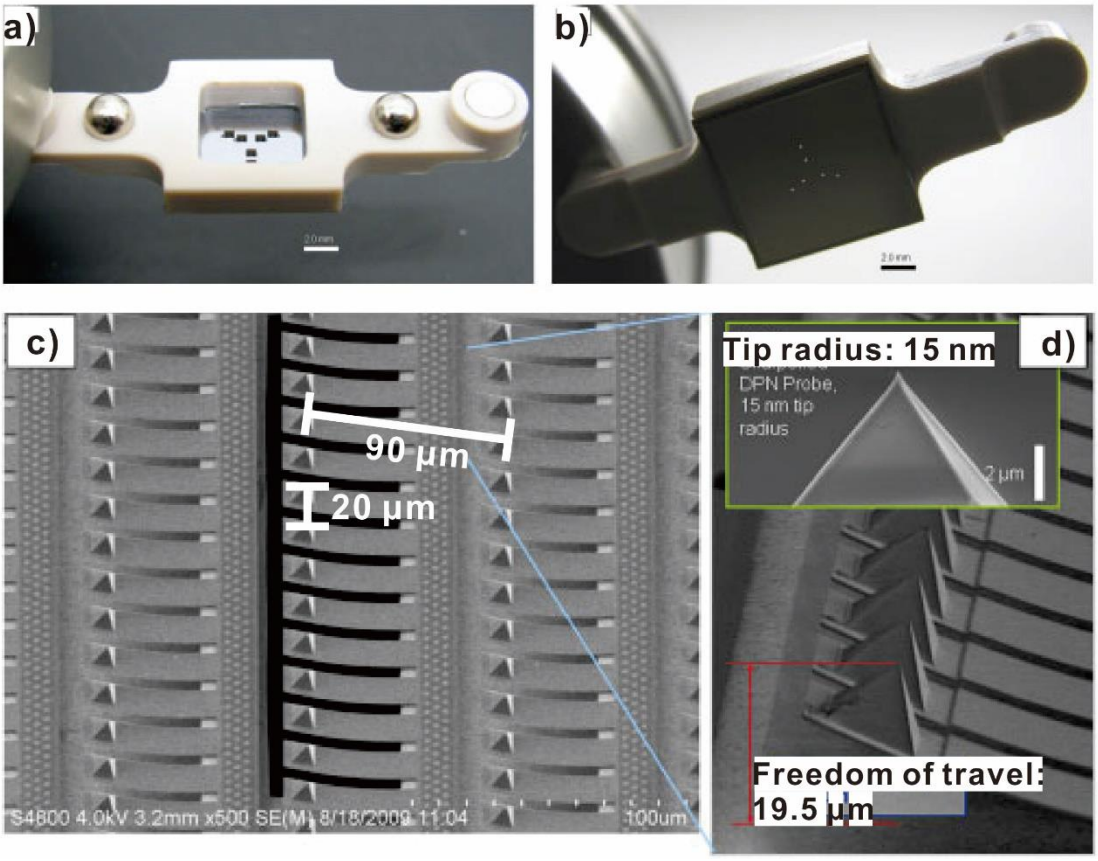

Figure 3.7. a) Top view of the 2D 55,000-tip cantilever array mounted to the *z*-piezo scanner. Scale bar: 20 mm. b) Bottom view of the 2D 55,000-tip cantilever array. Scale bar: 20 mm. (c) Zoomed SEM image of the cantilevers in front of a viewport. (d) SEM image of the cantilever's freedom of travel [173].

From single-tip to 18-tip cantilever array, the patterned areas enlarge from square micrometer to square millimeter size. However, the patterned areas are not enough for cell activity study. Hence, a 2D 55,000-tip cantilever array (NanoInk. Inc.) were employed to fabricate larger patterned areas. Each writing tip of the array occupies a surface area of 90 µm × 20 µm, leading to the patterned areas range to square centimeter size (1 cm × 1 cm). Importantly, before writing, the tip array should be paralleled with the substrate. The leveling method is different with 18-tip cantilever array. There are six etched viewports on the back of the 2D 55,000-tip cantilever array Figure 3.7a). Through the six viewports, the planarity offsets at three different points can be monitored. In detailed, before leveling, the inked 2D 55,000-tip cantilever array was put onto the *z*-piezo scanner with a 1 × 1 cm^2 aperture (Figure 3.7b). Then, the sample

stage was multiple adjusted in both *x* and *y* directions by monitoring the optical reflections of tip array. When all tips of the three different points showed similar reflection upon contacting at the same time, the leveling came to an end. After making parallel of the 2D 55,000-tip cantilever array and the substrate, the subsequent lithography procedures were as with the p-DNL process of 18-tip cantilever array.

3.2.2 Microcontact Printing

The μCP process includes the preparation of PDMS stamp and ink transfer. After ink patterns transferred onto the substrate, patterned polymer brushes will grow from the ink areas by SIP.

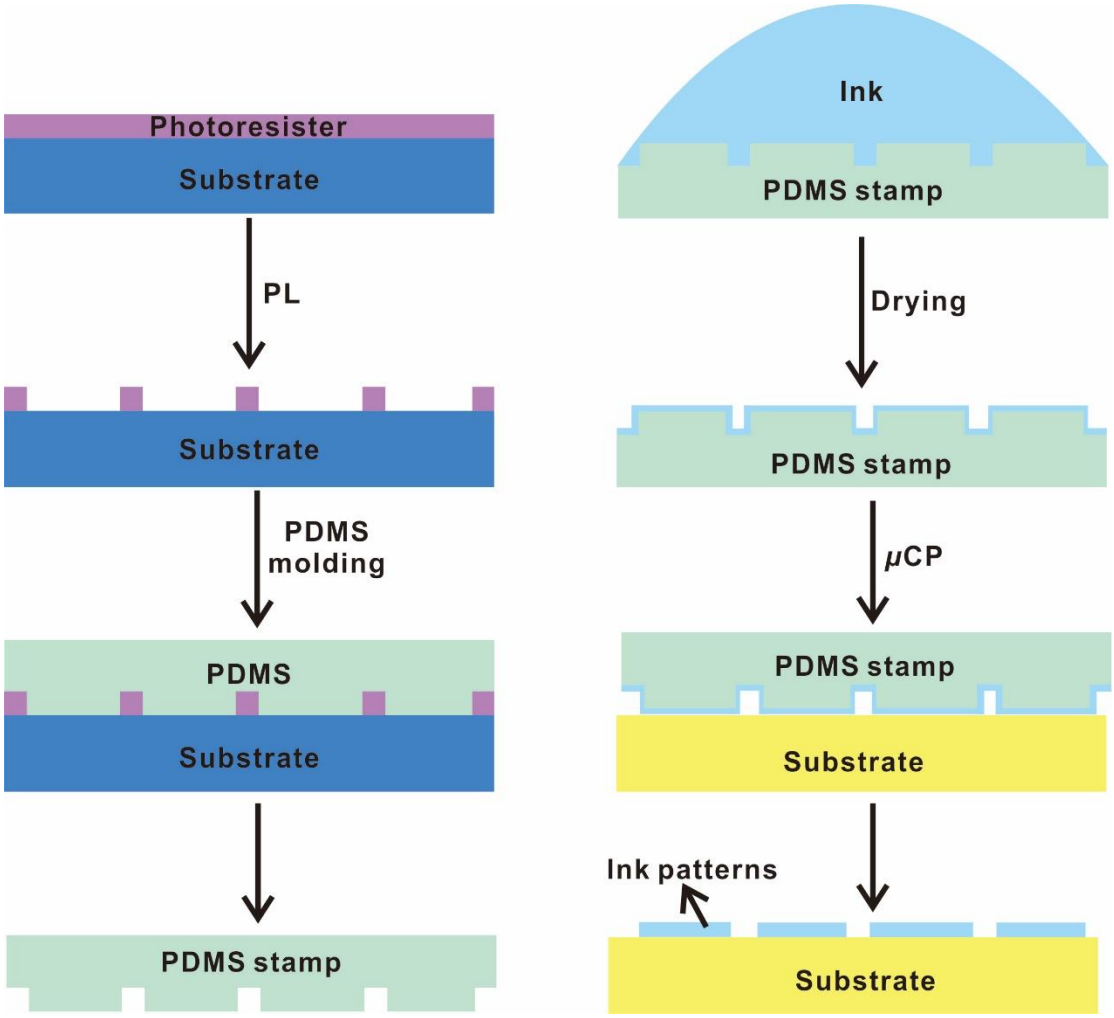

Figure 3.8. Schematic images for the μCP process.

PL for fabricating Si mold: A 5-30 μm thick of NR9-8000 negative photoresist layer was spin coated on a Si wafer with 500 nm silicon dioxide, followed by soft baking at 120 ˚C for 180 s. Then the resist coated wafer was exposed to UV light at 365 nm wavelength with the photomask we designed. The unexposed photoresist was then developed in resist developer RD6 at room temperature and washed with DI water, and followed by hard baking at 100 ˚C.

Surface fluorination by vapor deposition: The prepared mold by PL was treated by O_2 plasma for better fluridizer adsorption, and then put into a close chamber. The 1H,1H,2H,2H-perfluorooctyltrichlorosilane (PFOTS) (10 μL) was used to modify Si mould with hydrophobicity for making the PDMS easy to be peeled off. The chamber was kept in vacuum for PFOTS evaporation and vapor deposition for overnight.

Fabrication of PDMS stamp: SYLGARD 184 silicone elastomer kit was applied to prepare PDMS stamp. The base and curing agent were mixed in a 10 (base):1 (curing agent) ratio by weight for manual mixing. Then the mixture was degassed under vacuum, and placed onto the top of the fluorinated Si mould. After being cured at 80˚C for overnight, and the solidified PDMS stamp was carefully peeled off from the Si mould, and washed with ethanol followed by drying with compressed air.

Ink transfer: 2.5 mM ethanol solution of MUDBr was coated onto the surface of PDMS stamp by cotton swab. After drying, the PDMS stamp was pressed on the polymer brushes modified Au substrate (passivation of the terminal Br of polymer brushes-coated Au substrate was carried out in 0.1 M DMF solution of NaN_3 at 50 °C for more than 6 h) for 60 s, and then peeled off removed. The MUDBr pattern was transferred to the surface of the polymer brushes modified Au substrate in the pressing process, and this sample was called MUDBr@polymer brushes-coated Au wafer. Finally, patterned binary polymer brushes structure was obtained after SI-ATRP reaction on the MUDBr@polymer brushes-coated Au wafer.

3.3 Cell Culture

Mouse embryonic fibroblast (NIH-3T3) and human cervical carcinoma (HeLa)

cells were chosen for the cell culture experiments. The cells were incubated on tissue culture polystyrene (TCPS) dishes in high glucose of Dulbecco's modified eagle medium (DMEM) with 5 % fetal bovine serum (FBS) and 1 % penicillin-streptomycin and then placed in an incubator with 75 % humidity and 5 % CO_2 at 37 °C for incubation.

3.4 Characterization

3.4.1 Optical Microscopy

The optical microscopies were widely used in these experiments to preliminary check the patterned polymer brushes, including bright-field microscopy, fluorescent microscopy and confocal laser scanning microscopy (CLSM).

There were two kinds of bright-field microscopy used here. The first one was metallographic microscope (Nikon Eclipse 80i) with reflecting illumination, which was employed to observe the patterned polymer brushes on the non-transparent Au-Si substrate. Importantly, the metallographic microscope also could be used to observe transparent samples, such as patterned polymer brushes on Au-PET and Au-glass substrate. The second one was biological microscope with transmission illumination, which was used to study cell morphology.

On the other hand, fluorescent dyes are useful tools for cell behavior study. Herein, red fluorescent rhodamine-phalloidin (Rhod-phalloidin) and blue fluorescent 4', 6-Diamidine-2'-phenylindole dihydrochloride (DAPI, Sigma) were applied to stain cytoskeleton and nuclei respectively. Therefore, fluorescent microscopy (Nikon Eclipse 80i) and CLSM (Leica TCS SPE) was used to observe the red cytoskeleton and blue nuclei of cells. Briefly, dyed cells were exposed to the corresponding excitation light to lead fluorescence emission.

3.4.2 AFM

Except being applied in the lithography process, AFM was also used for characterization of surface topography via a sharp AFM tip. The information of surface

topography is collected by the tip which can scan the surface, and a cantilever deflection is triggered. The deflection is measured by an optical deflection sensor which is made up of a laser beam reflected by the backside of the cantilever, and a position-sensitive photodetector for receiving the laser signal. Being compared with STM, the imaging mode of AFM is based on Van der Waals force between the tip and the sample (Figure 3.9b), which is divided into contact mode, non-contact mode, and tapping mode. The force changes with the distance variations between the tip and sample. The relation curve of Van der Waals force and distance is shown in (Figure 3.9c).

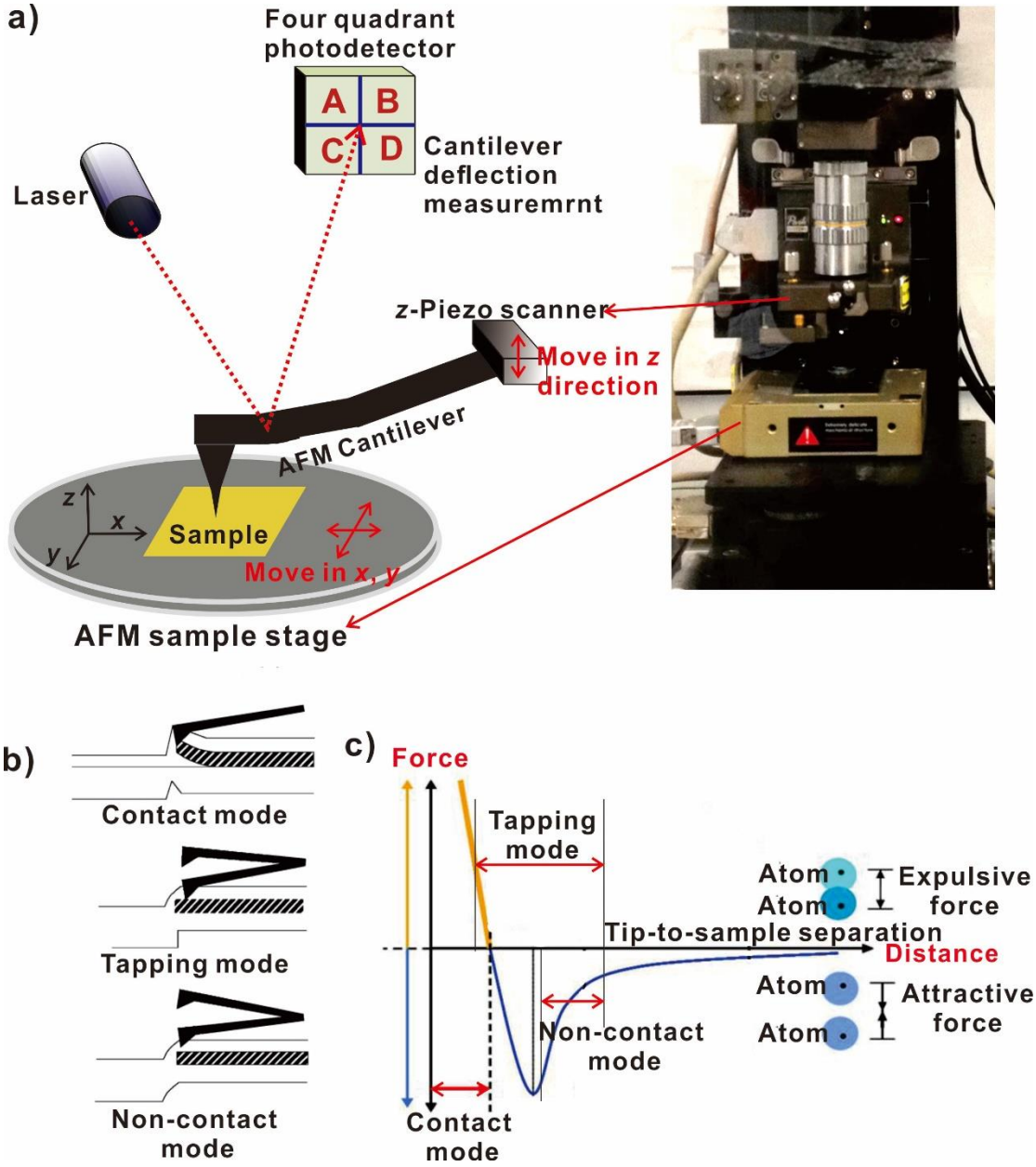

Figure 3.9. a) AFM schematic. b) Sketches of contact mode, tapping mode and non-contact mode. c) The Van der Waals force variation versus tip-to-sample distance

between AFM tip and sample.

When the AFM is working in contact mode, the tip always contacts the surface of the sample under a certain force. The interactions between the tip and the sample are repulsive, and the cantilever produces vertically (mapping to topography images) and lateral (corresponding to lateral force microscopy) deflections. For AFM working in non-contact mode, the Van der Waals force transfers to attraction with increasing distance, so the tip is vibrating near the surface of the sample. The system can adjust the tip-to-sample distance to fix the oscillation amplitude (less than 10 nm) or frequency. Scanning software can record the topography image of the sample surface according to the measuring the tip-to-sample distance.

Furthermore, there is another imaging mode called tapping mode for AFM. In tapping mode, the cantilever is driven to vibrate up and down by a piezoelectric element fixed to the AFM tip holder. The frequency of the cantilever is very close to its resonant frequency. The amplitude is set as 100 to 200 nm and will decrease in value when the tip comes closer to the surface of the sample. For keeping the amplitude stable, the *z*-piezo electric scanner is used to control the driving voltage. Therefore, the tapping AFM image is generated by imaging with the changes of driving voltage.

3.4.3 Attenuated Total Reflectance Fourier Transform Infrared Spectroscopy (ATR-FTIR)

The surface chemical composition of surface modified samples was analyzed by the ATR-FTIR (PerkinElmer Spectrum 100) spectrometer.

The FTIR is an important tool to character the chemical composition of materials. But traditional FTIR with transmission method using tablet or coating for the measure has great insufficient on the samples which are indissolvable, or hard and solid, or refractory. To overcome these deficiencies, the ATR accessory of FTIR has been developed since1980s. The ATR-FTIR obtains the surface chemical information from the signals of internally reflected IR beam which meets the sample surface. It has

become a powerful tool for analyzing of the surface chemical constitution in many fields.

3.4.4 Water Contact Angle

Contact angle here refers to the angle θ_c of the tangent line of gas-liquid interface and the boundary line of solid-liquid interface, qualifying the water wettability of a surface. It is well known that water wettability of a surface is a key issue to control cell behaviors. The water wettability of patterned polymer brushes was tested by the drop shape analyzer (EasyDrop, Krüss). If the θ_c was below 90°, then the surface of patterned polymer brushes was hydrophilic, i.e. the surface was easy to be wetted by an aqueous solution. On the other hand, while the θ_c was above 90°, the polymer brushes surface was hydrophobic and hard to be wetted.

3.4.5 X-Ray Photoelectron Spectrometer (XPS)

XPS is also a surface chemical analysis technique. It can be used to detect the composition of surface chemical elements of materials. The XPS analysis of these experiments was carried out with a Sengyang SKL-12 spectrometer. When a beam of X-ray was irradiated onto a polymer brushes surface, the electrons of elements from the top 0 to 10 nm of the polymer brushes escaped. By measuring the kinetic energy and number of escaped electrons, the XPS spectra were obtained.

CHAPTER 4 PREPARATION OF WELL-DEFINED PATTERNED POLYMER BRUSHES BY DNL

4.1 Introduction

Controlling cell behaviors *in vivo* and *in vitro* are the critical point in fundamental cell biology research, advanced biomedical engineering, regenerative medicine, tissue engineering, and cell-based bioassay and drug screening. Cell behaviors can be manipulated by the three cues (i.e. chemical, topographical, and mechanical properties) of artificial ECM. Among the materials of artificial ECM, polymer brush has excellent advantages due to the vertically aligned and covalently bonded polymer chains with various functional groups applying remarkable spatially distributed chemical and mechanical properties. Hence, creating high-throughput 2D and 3D patterned polymer brushes on the micro- and nanoscale with abundant chemical properties and suitable mechanical properties is emerging as a powerful platform for biomedical applications.

Current lithography techniques, such as serial patterning lithography (EBL [174-177] and DPN [178-182]), and mask or mold-based lithography (PL [183-185], imprint lithography (IL) [186-187], colloidal lithography (CL) [188] and SL [189-192]), are able to fabricate 2D and 3D patterned polymer brushes on nano- and microscale. However, they all have their limitation. For example, even though PL and EBL are mature industrial techniques that can construct precise and complex patterns, they require expensive equipment and clean room environment and are less compatible with biological materials. Other patterning technique such as SL also suffers from deformation of the elastic stamp (e.g. roof collapse), while SPL is typical of very low throughput. Serious ink diffusion limits the pattern resolution of DPN. To realize large-area 2D and 3D patterned polymer brushes in a facial, rapid, and low-cost lithography manner remains to be a key technical problem.

Herein, the DNL technique, based on SPL, was developed to prepare patterned polymer brushes. It is cost-effective, high resolution and registration, and offered large-area throughput when using AFM tip arrays. Complex nanopatterned polymer brushes can be prepared by DNL containing flexible and controllable chemistry, topography, mechanical properties, and multiplexing for controlling cell behaviors. Generally, in the DNL process, an AFM tip or tip array inked with imitator molecules was brought into contact with SAMs modified Au substrate. The small molecules of SAMs were cleaved away by the tip with certain force (>10 nN). Notably, the initiators on the tip simultaneously self-assembled onto the cleaved areas to realize the nanodisplacement. The SAMs here were used to protect the unpatterned areas from ink diffusion. As a result, the feature size of initiator patterns was equal to the cleaved area. Finally, patterned polymer brushes were grown from the initiated areas by SIP.

4.2 Materials

ATRP initiator MUDBr was kindly provided by Prof. Hongwei Ma, Suzhou Institute of Nano-Tech and Nano-Bionics. All other chemicals were obtained from Sigma-Aldrich and used as received. Au substrates were prepared by thermal evaporation of 25 nm Au/5 nm Cr on <100> Si wafers with 500 nm SiO_2 on one side, and 50 nm Au/5 nm Cr on the glass wafer. The contact mode AFM tip and non-contact mode AFM tip was purchased from NanoSensor Inc. The 1D 18-tip cantilever array and 2D 55,000-tip cantilever array were obtained from NanoInk. Inc.

4.3 Experimental

4.3.1 Substrate Modification

The MHA SAMs modified Au substrate (MHA-Au) was prepared by the process mentioned in section 3.1.2 at room temperature and dried via nitrogen stream for next experiments.

4.3.2 Fabrication of Patterned Polymer Brushes by DNL Technique

The procedures of single-tip DNL experiments: An AFM tip in contact mode was firstly inked with MUDBr by being immersed in an MUDBr ethanol solution (2.5 Mm) for 40 s and drying in the air. The MUDBr-inked tip was then loaded onto the *z*-piezo scanner of the XE-100 AFM and approached to an MHA-Au substrate under contact mode at ambient conditions. By scanning with high load, the MHA molecules were mechanically scratched away by the AFM tip, and the MUDBr molecules simultaneously self-assembled onto the scratched areas to realize the nanodisplacement process. The MUDBr patterns were then obtained. After patterning, the substrate was brought down for SI-ATRP reaction.

The procedures of 1D p-DNL experiments: A cantilever array including of 18 AFM tips was inked with MUDBr by being immersed into an ethanol solution of MUDBr (0.1 mM) and drying in the air for 30 min to avoid diffusion, and then was loaded to the *z*-piezo scanner of the XE-100 AFM. The 18-tip cantilever array was subsequently paralleled to the MHA-Au substrate by tilting sample stage in the *x* direction. Under contact mode, once the AFM tip was in contact with the surface of the MHA-Au substrate, the optical reflections of the cantilever could become lighter. Hence, by monitoring the optical reflections of the cantilever array, i.e. tilting sample stage, we could make sure all the 18 tips were contacted with the substrate at a time. Then a white-black bitmap as pattern template was downloaded to the XEP lithography software. With precisely controlling the movements of the *z*- and *x*, *y*-piezo scanners and the feature density method (a pixel of the bitmap could be regarded as a feature), the gradient MUDBr initiator patterns were obtained. Finally, the substrate was brought down for SI-ATRP reaction after lithography.

The procedures of 2D p-DNL experiments: A 2D 55,000-tip cantilever array was inked with MUDBr by immersing it in MUDBr solution (0.1 mM) for 10 s and drying in air for at least one hr. Then it was loaded to the *z*-piezo scanner of the XE-100 AFM.

The pre-made MHA-Au substrate was placed onto the sample stage. Then the 2D tip array should be levelled with the substrate due to the 2 key operating conditions of fabricating uniform and homogenous 3D patterned polymer brushes: (1) all of the *z*-position of the 2D 55,000-tip cantilever array should be carefully controlled with respect to the substrate; (2) the variation in cantilever deflection must be as minimized as possible [173]. The leveling was realized via the six etched viewports on the back of the cantilever array. By tilting sample stage in *x* and *y* directions to monitor the optical reflections of the cantilever array which were able to be observed from the viewports, the 2D cantilever array could be parallel with the substrate. After finishing leveling, the remaining procedures of lithography were as with the 1D p-DNL. Finally, the substrate was brought down for the SI-ATRP reaction after finishing lithography.

4.3.3 SI-ATRP for Patterned PMMA Brushes

The patterned PMMA brushes were grown from the pre-patterned MUDBr areas prepared by DNL technique via SI-ATRP. The reaction proceeded as the receipt mentioned in section 3.1.2. After finishing the reaction, the samples were dried via nitrogen stream for characterization

4.3.4 Characterization

ATR-FTIR was used to detected the surface chemistry of MHA-Au. Optical microscope with the bright field was employed to observe the patterns of PMMA brushes. AFM topography was measured by XE-100 AFM with the non-contact mode at ambient conditions.

4.4 Results and Discussions

4.4.1 Fabrication of Patterned PMMA Brushes by Single-Tip DNL

DNL is a simple, versatile and low-cost scanning probe nanolithography method for fabrication high-resolution, large-area, and uniform 2D and 3D patterned polymer brushes. The typical procedures of fabricating patterned polymer brushes with DNL include three steps: firstly, the preparation of modified substrate, such as MHA-Au substrate; secondly, the construction of ATRP-initiator (MUDBr) patterns on the substrate via DNL with control of feature density; finally, the growth of polymer brushes from patterned initiators with SI-ATRP.

The MHA-Au substrate was prepared as the procedures mentioned in chapter 3. Then ATR-FTIR was used for confirming the existence of MHA molecule on Au surface. As shown in Figure 4.1, a clear peak of C=O stretching of the carboxyl group at 1734 cm^{-1} was detected, indicating the successful self-assembled MHA on Au surface.

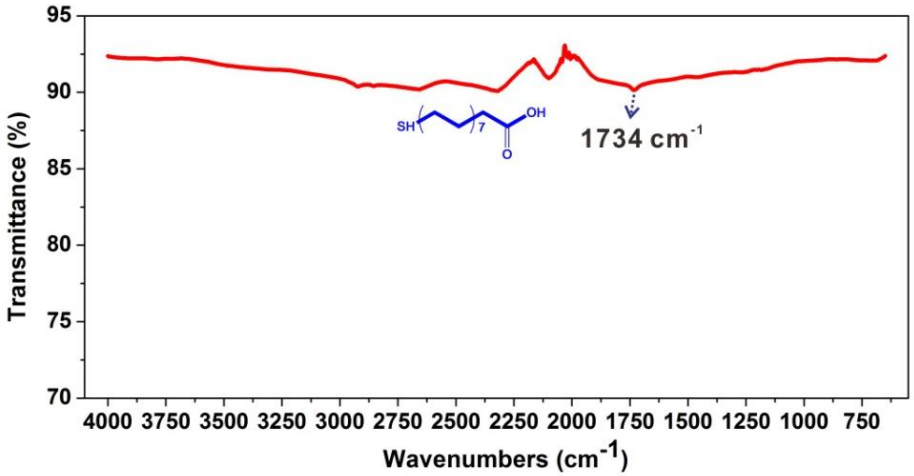

Figure 4.1. The ATR-FTIR spectrum of MHA-Au substrate.

Then in the single-tip DNL experiments, an MUDBr-inked tip was loaded onto the XE-100 AFM and brought into contact with an MHA-Au substrate to start lithography. A typical six-step MUDBr pyramid (1 μm × 1 μm, 2 μm × 2 μm, 3 μm × 3 μm, 4 μm ×

4 μm, 5 μm × 5 μm and 6 μm × 6 μm) was written by scanning the same area at high tip-substrate contact force (3500 nN, 4 s^{-1}). The MHA molecules were mechanically scratched away by the AFM tip, and the MUDBr molecules simultaneously self-assembled onto the scratched areas to form MUDBr patterns. To prepare the pyramid, a 1 μm × 1 μm MUDBr square was firstly written, then a 2 μm × 2 μm MUDBr square was secondly written by scanning in the same coordinate origin. And so on, for each of the remaining four steps. The gradual change of the pyramid could be readily achieved by converting line density. Then the PMMA brushes were grown from the MUDBr pre-patterns by SI-ATRP, and the pyramid of PMMA brushes on MHA-Au substrate was obtained.

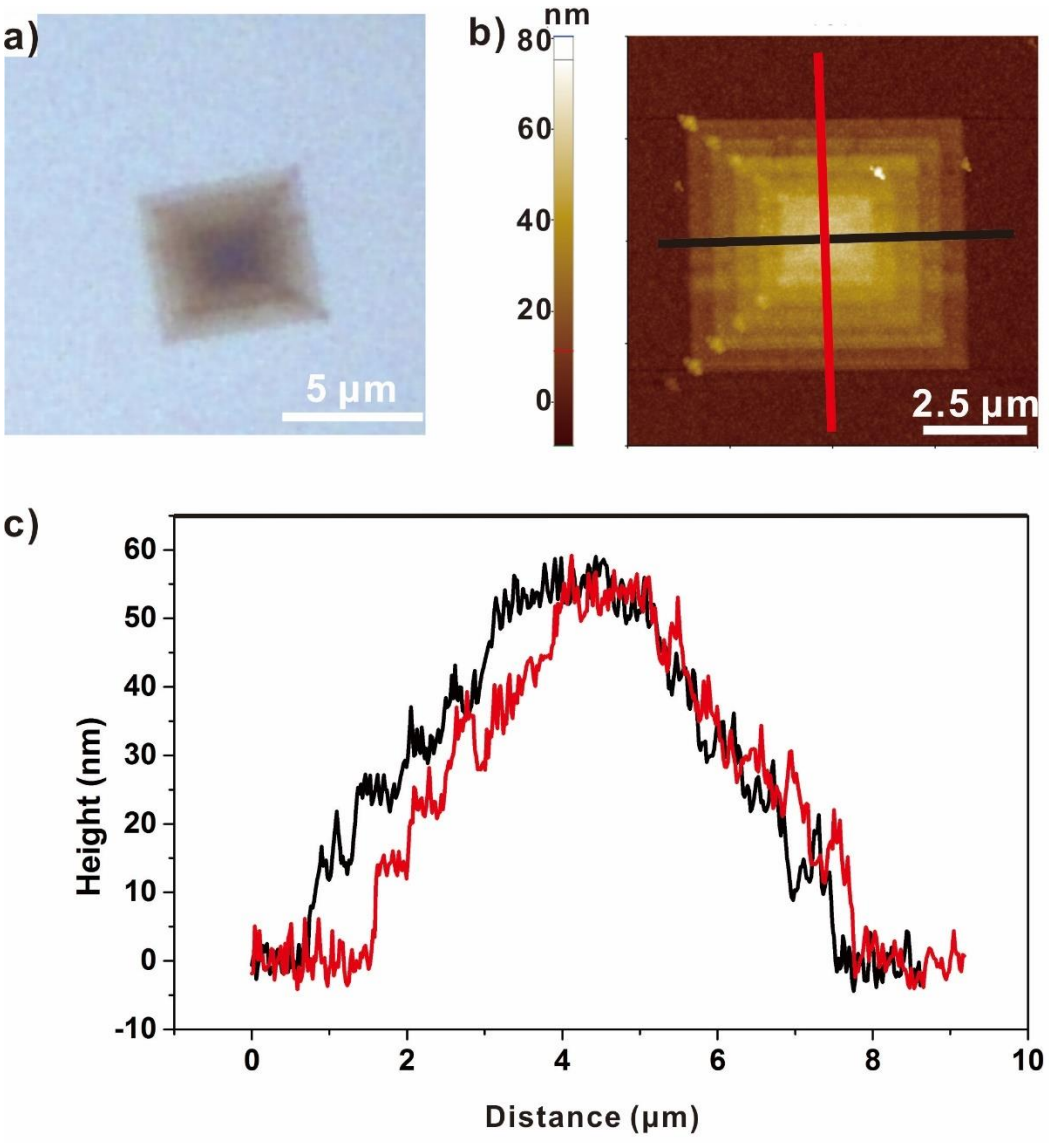

Figure 4.2. a) Optical micrograph of the six-step pyramid of PMMA brushes fabricated

by single-tip DNL and SI-ATRP. b) AFM topographic view and c) cross-sectional profiles of the six-step pyramid.

To study the details of the PMMA pyramid, the optical microscopy was applied to observe the obtained samples (Figure 4.2a). Under the optical microscope, there was a polymer pyramid on the substrate, indicating the single-tip DNL and SI-ATRP was a successful completion. The AFM under non-contact mode was used to further detect details of the PMMA pyramid (Figure 4.2b). The height control of each step was achieved by adjusting the line density during the single-tip DNL process. As shown in the Figure 4.2c, the heights of the six steps of the PMMA pyramid increase from 13 nm at low line density to 55 nm at high line density. As the designed width of the steps was too small (only 1 μm), the height control of the first step and the second step by line density was less effective, leading the unclear height difference of the first step and the second step.

4.4.2 Fabrication of Patterned PMMA Brushes by P-DNL

As previously stated, we successfully prepared a six-step PMMA pyramid by single-tip DNL. However, the low fabrication throughput of single-tip DNL [170, 193] becomes a serious flaw. The demonstrated patterning areas of a single-tip DNL process are limited to 90 μm. It is too small for cell culture experiments and even some characterizations (such as AIR-FTIR and XPS). For the cell culture study and many other applications, the large-area patterned polymer brushes are required in order to collect enough and statistical results. Therefore, our group developed p-DNL to address the challenge. The p-DNL is a multi-cantilever version of single-tip DNL. It not only can duplicate a large number of patterned polymer brushes in the same time but also can maintain the high resolution of the polymer brush nanostructures. According to the tip array used, the p-DNL includes 1D p-DNL and 2D p-DNL.

In the 1D p-DNL process, an 18-tip cantilever array and an MHA-Au substrate were used to perform the experiments. Different with single-tip DNL, 18 patterns could

be prepared at one time. Therefore, the pattern areas were large from micrometer scale of single-tip DNL to millimeter scale of 1D p-DNL.

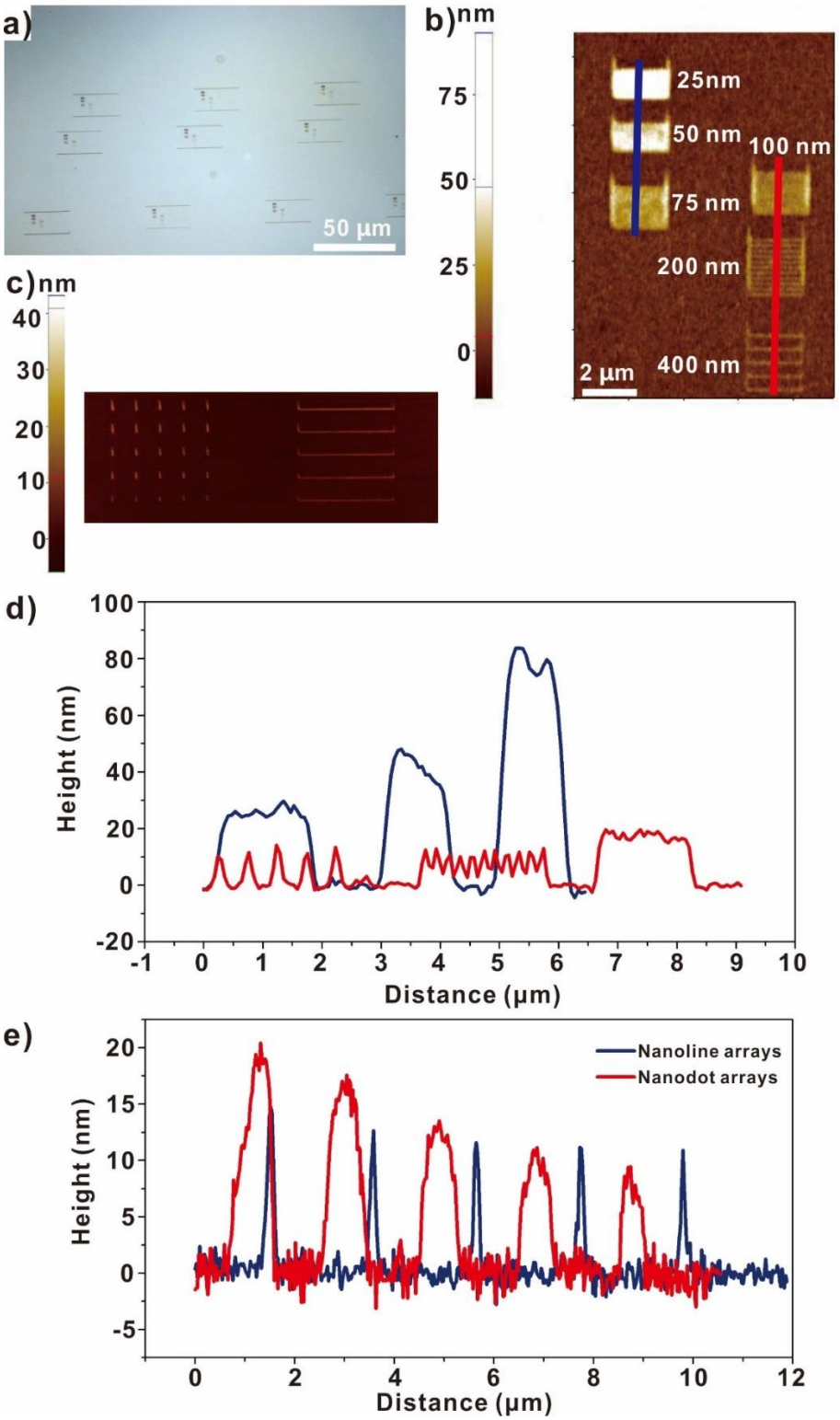

Figure 4.3. a) Optical micrograph of PMMA nanodot and nanoline arrays fabricated by 1D p-DNL and SI-ATRP. b) AFM topographic view and d) cross-sectional profiles of

the PMMA nanoline arrays. c) AFM topographic view and e) cross-sectional profiles of the PMMA nanodot and nanoline arrays with different *z* extension.

The optical microscopy and the AFM characterization results of the fabricated PMMA structures by 1D p-DNL were shown in Figure 4.3. Nanolines and nanodots are basic compositions of 3D patterned polymer brushes constructed by DNL with feature density method [172] which solves the fatal uniformity challenge in parallel fabrication. Therefore, polymer brush nanolines and nanodots should be studied first. From our group's previous studies, it is known that the instrument parameters during the lithography process, including *z* extension, dwell time, and drawing speed, influence the pattern size, shape, and quality. However, notably, the *z* extension is a fatal parameter. Hence, in the following experiments, we would focus on the effects of different *z* extension on the patterned polymer brushes.

In Figure 4.3b, the PMMA nanoline arrays were prepared with different line-to-line spacing with fixed *z* extension (2 μm). Because of the nanoconfinement effect of polymer brushes [194-195], the ambient PMMA brushes spread laterally onto the substrate while the central PMMA brushes collapsed with the expanded space resulting from the ambient spreading. Therefore, the structures of the PMMA nanolines were from isolation to the merger with the decreasing line-to-line spacing (400 nm to 25 nm). As a result, the heights of the PMMA brushes significant increased from 15 nm to 80 nm.

For the PMMA nanodot and nanoline arrays in Figure 4.3c, they were fabricated with different *z* extension but fixed line space and dot space. With the increase of the *z* extension (1.2 to 2.4 μm), the heights of the nanodots and nanolines increased from 10.8 nm to 20.8 nm, and 9.7 nm to 13.2 nm respectively. These increased heights were attributed to the larger *z* extension lead more effective nanodisplacement, which was similar to our previous report [196]. Otherwise, it was clearly observed that there were two tails appeared at both ends of the PMMA nanolines, and the nanodots were not circular but turn to short line segments with different aspect ratios. The phenomenon was consistent with our group's previous study [171]. In the nanodisplacement process, the AFM tip went down vertically to contact with the substrate. While the tip was

further pushed in the vertical direction by the increased *z* extension, the cantilever would bend to allow the *z* extension reach the preset depth, resulting in the horizontal movement of the tip. After a certain dwell time, although the cantilever was back to the initial state (i.e. straight state), the horizontal movement of the tip had already occurred beyond repair. Therefore, to precisely prepare patterned polymer brushes, the *z* extension is a crucial adjective point, which not only affects the height of polymer brushes but also has a significant influence on the shapes of polymer nanolines and nanodots.

Various PMMA gradient patterns had been fabricated subsequently by the 1D p-DNL with the feature density method. To fabricate the PMMA gradients, the dot-to-dot spacing between generated nanobrush arrays changes gradually. A white-black bitmap with gray-scale gradients, and defined pixel number and pixel distance were used as a guide map for the DNL experiments. In the DNL experiments, only the black pixels were identified as 'writing' dots. In Figure 4.4b, the PMMA gradients were prepared by different *z* extension (left to right: 3, 2.5, 2, and 1 μm) at 50 nm of pixel distance. From the cross-sectional profile of the PMMA gradients, the perfect gradient was obtained when the *z* extension was 1 μm. The heights of the peak of the PMMA gradients increased from 40 nm to nearly 80 nm with the increase of the *z* extension. For the PolyU logo of PMMA brushes (Figure 4.4c), a bitmap of PolyU logo was used as the guide map. And the pattern was constructed with 2 μm of z extension and 500 nm of pixel distance. Due to the large pixel distance, the nanobrushes distinctly separated and then collapsed. Therefore, the height of the PMMA PolyU logo was only about 9 nm.

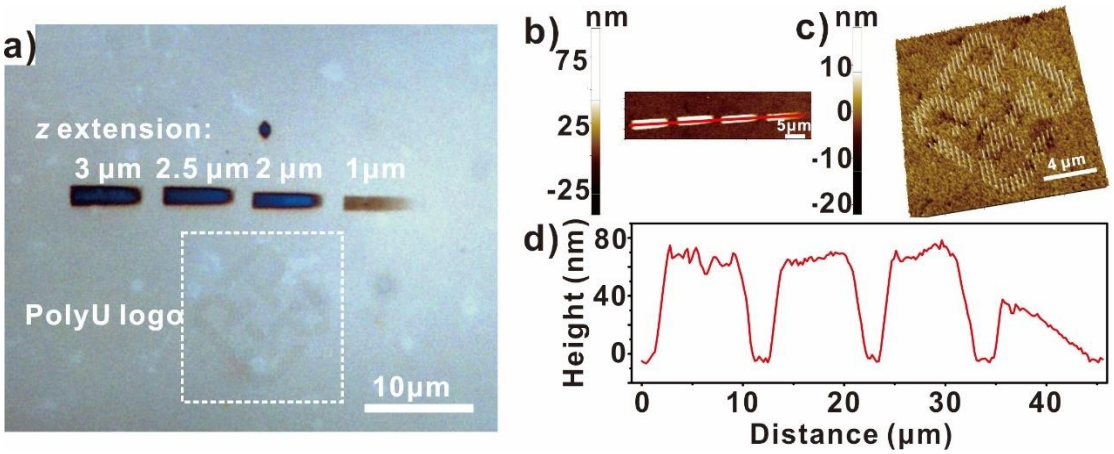

Figure 4.4. a) Optical micrograph of the PMMA gradients and PolyU logo fabricated by 1D p-DNL and SI-ATRP. b) AFM topographic view and d) cross-sectional profile of the PMMA gradients. c) AFM topographic view of the PMMA PolyU logo.

In the 2D p-DNL process, a 2D 55,000-tip cantilever array was used to perform the experiments. With the 2D 55,000-tip cantilever array, massively parallel patterned polymer brush could be simultaneously fabricated. Hence, the pattern areas were large to square centimeter. Same as 1D p-DNL, the leveling is very important to obtain well-defined patterned polymer brushes in 2D p-DNL. To study the fundamental of 2D p-DNL, the PMMA nanodot and nanoline arrays were prepared under different *z* extension (from 1.2 to 5.4, Figure 4.5a). As expected, the increased *z* extension led the shapes of the nanodots changing from elliptical dots to short line segments (Figure 4.5c-e). However, due to the variation in 55,000-tips cantilever deflection, the nanodot and nanoline arrays were misaligned, especially for the nanoline arrays, which were very different with the nanodot and nanoline arrays prepared by 1D p-DNL. Therefore, it concluded that the 2D 55,000-tip cantilever array was not suitable for directly lineation, but suitable for patterning dots (i.e. pixel of a bitmap) to form patterns. Otherwise, the changed *z* extension didn't induce distinct height difference of the nanodots and nanolines, indicating that the *z* extension did not affect the resulted patterns of 2D p-DNL a lot. The same conclusion was summarized in fabricating PMMA gradient (Figure 4.5f and g). So, we could arbitrary select any *z* extension (less than the tip's free travel distance: 19.5 μm) for patterning complex structures. But higher *z* extension

was suggested due to higher *z* extension improve the efficiency of nanodisplacement.

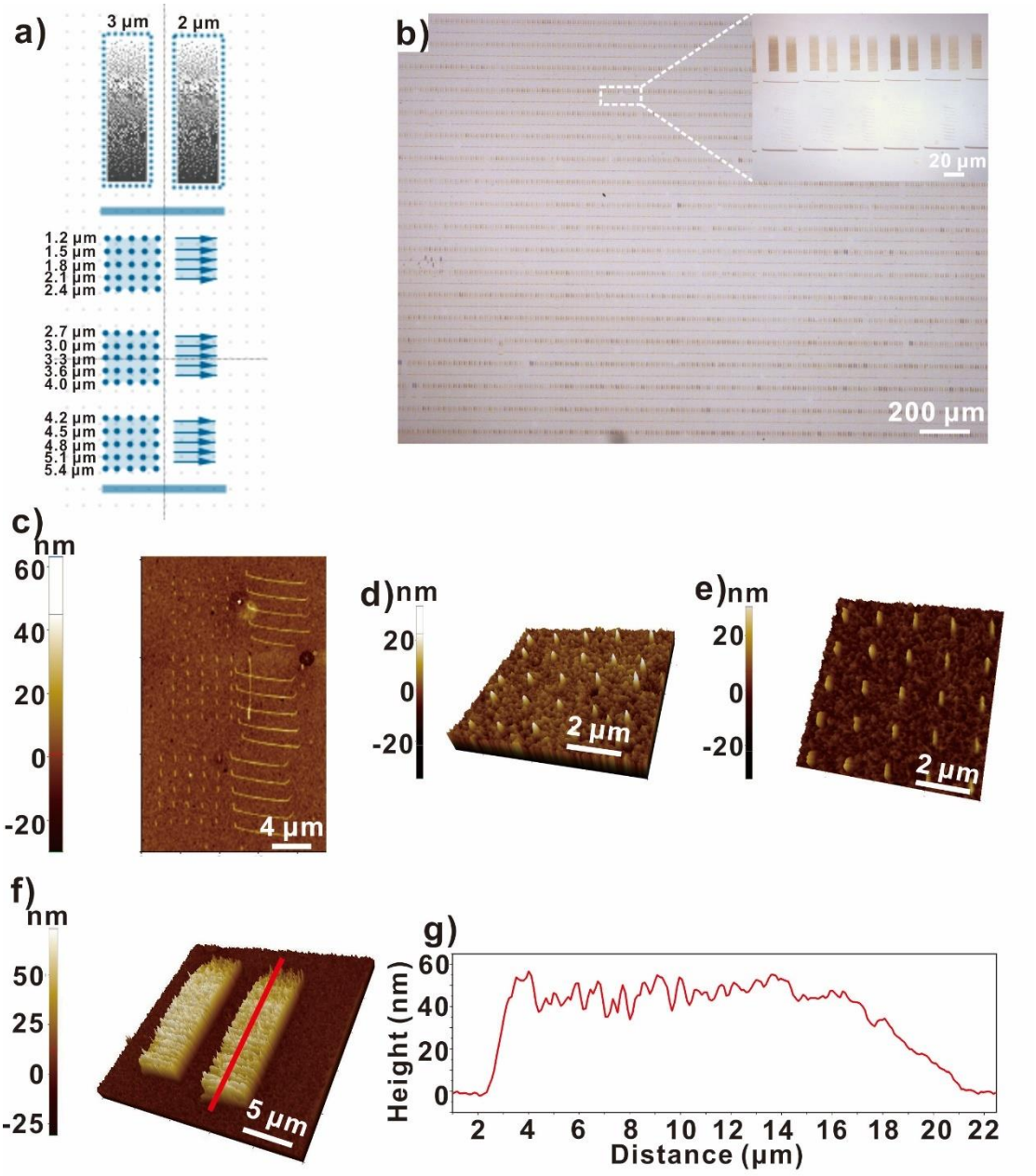

Figure 4.5. a) Designed z extension for patterning nanodot and nanoline arrays, and gradient structures. b) Optical images of the large-area PMMA nanodot and nanoline arrays, and gradient structures. c) AFM topography of the resulted PMMA nanodot and nanoline arrays. d) AFM topography of the low *z* extension resulted in PMMA nanodot arrays. e) AFM topography of the high *z* extension resulted in PMMA nanodot arrays. f) AFM topography and the cross-sectional profile of the PMMA gradients.

Hence, we chose 5 μm of *z* extension to prepare large-area and crossed PMMA

rings on the Au-glass substrate (50 nm Au/5 nm Cr on glass). The designed bitmap was showed in Figure 4.6a. Each of the 35-μm ring structure was composed of 5704 dots. With the observation of optical microscopy, uniform crossed PMMA rings were found (Figure 4.6b), indicating the successful fabrication. The AFM topography showed the full width at half maximum (FWHM) of the PMMA brush rings were about 570 nm. To illustrate how narrow nanoline we could fabricate by 2D p-DNL, we used the 570 nm-width PMMA brushes as etching resister to generate Au nanoline. The large-area and crossed PMMA rings were treated by O_2 plasma for 1 min and then immersed in commercial Au etching solution and Cr etching solution respectively. By AFM characterization, when the PMMA brushes uncoated Au was etched, the FWHM of the remaining PMMA brushes coated-Au ring was about 350 nm. After completely removing the PMMA brushes, the remaining Au nano-ring was only about 220 nm in FWHM. The narrow 220 nm-width Au nanostructures could be widely used in many areas, such as transparent electrodes, protein or DNA sensor, and surface plasmon resonance.

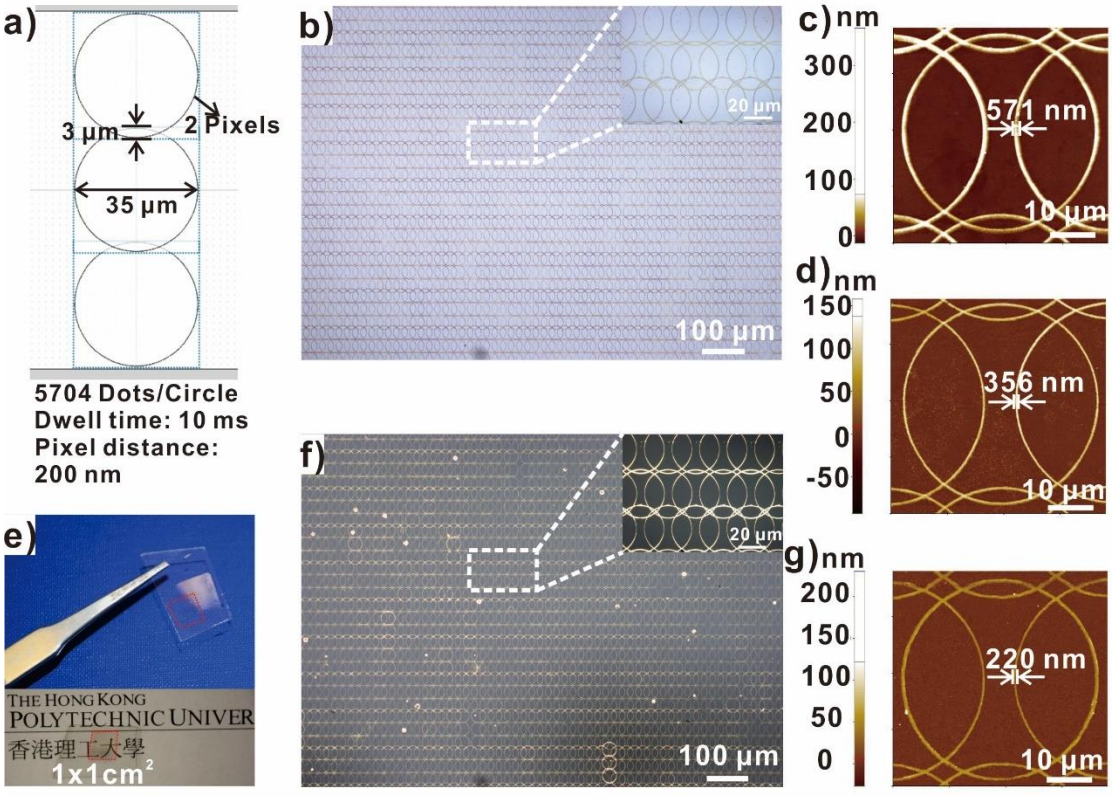

Figure 4.6. a) Designed patterning parameters for ring mesh Au nanostructures. b)

Optical image of the large-area ring mesh PMMA nanostructures. c) AFM topography of the resulted PMMA nanostructures. The thickness of the resulted PMMA nanostructures was 59 nm. d) AFM topography of resulted PMMA on Au nanostructures after Au and Cr etching solution treatment in b). The thickness of the resulted PMMA on Au nanostructures was 113 nm. e) Pictures of resulted Au nanostructures after 5 min of plasma treatment in d). f) Optical image of the large-area ring mesh Au nanostructures in e). g) AFM topography of the Au nanostructures in e). The thickness and transmittance of the resulted Au nanostructures were 52 nm and 81.3% respectively.

4.5 Conclusions

In this chapter, the DNL technique for fabricating 2D and 3D patterned polymer brushes was introduced, including single-tip DNL and p-DNL. By using DNL and SI-ATRP, the high-resolution, large-area, uniform and serial fabrication of various patterned PMMA brushes on MHA-Au substrates were successfully obtained. The DNL technique is diffusion-limited due to the MHA SAMs acted resist layer prevents the gold surface from undesirable volatile initiator diffusion. So, the resolution of DNL technique is highly depended by the radius curvature of the AFM tips. Based on our group's previous work, the resolution is about 25 nm when the radius curvature of the AFM is 20 nm [168]. The pattern areas were large from square micrometer of single-tip DNL to a square centimeter of 2D p-DNL. During the lithography process, the *z* extension was found to be the important critical parameter which not only influences the height of patterned polymer brushes but also affect the pattern shape and quality. Moreover, due to the large pattern area, uniform and high-resolution of resulted polymer brushes (570 nm-FWHM) and Au nanopatterns (220 nm-FWHM), the 2D p-DNL has great potential for preparing nano-size polymer brush patterns to a range amount of applications, such as controlling cell behaviors, a transparent electrode, *etc*.

CHAPTER 5 FABRICATION OF BINARY 3D POLYMER BRUSH STRUCTURES BY P-DNL

5.1 Introduction

Polymer brushes are employed as a robust material for surface modification with excellent mechanical, topographical, and chemical properties [197-199]. Notably, binary polymer brush patterns acted model surfaces have a wide range of applications in interfacial phenomena study (e.g. cell adhesion) [200-201] due to binary structures can better utilize the chemical advantages of polymer brushes. There are many reports have been studied on preparing binary polymer brush patterns. Among them, two common methods have been developed.

The first method is initial forming a homogenous polymer brush layer on a substrate by SIP which is continually exposed to light irradiation to create the second-layer polymer brushes with patterns. For example, Hawker *et al.* [202] prepared ordered binary polymer brush micropatterns by a combination of SIP and PL technique. The well-defined poly (tert-butyl acrylate) (PTBA) brushes were patterned by using PL, and the laterally patterned PAA brushes were then grown from the PTBA-uncoated areas. Takahashi and coworkers [148] developed a microstripe-like PAcM brush on thermoresponsive PNIPAm brush surface by patterning living terminal group on the PNIPAm chains via PL technique and the subsequent selective SIP. Zhou *et al.* [203] fabricated a binary polymer brush micropatterns by two-step SIP. The initiators for the second SIP were bonded to the substrate through the exposed areas produced via UV radiation on the first homogeneous polymer brush layer. Another method is repeatedly using μCP and SIP to prepare binary and multi-component polymer brush patterns [204-205]. Zhou and coworkers [205] developed a multi-component polymer brush micropatterns by printing initiator patterns on the bare Au surfaces by PDMS stamps for SIP. However, all of the binary or multi-component polymer brush patterns prepared

by the above methods were 2D structures.

Herein, a new method combining p-DNL and two-step SI-ATRP was developed to generate binary 3D polymer brush structures. In detail, an 18-tips cantilever array was chosen to proceed the p-DNL process. The 3D PMMA brushes acted first-layer of the binary system were grafted to an Au substrate by p-DNL and SI-ATRP. Then during the *in-suit* p-DNL process, the PMMA chains were scratched by the tips, and meanwhile, the initiator patterns were formed. The *in-suit* p-DNL is very important which can precisely prepare second-layer 3D polymer brush structures on the first-layer 3D PMMA brushes. Therefore, the second-layer polymer brushes were grown from the pre-patterned initiators by the second-step of SI-ATRP. By directly printing initiator molecules on 3D PMMA brush and subsequently growing second-layer polymer brushes from the printed initiator patterns, the binary polymer brush patterns were obtained with high resolution and complex 3D structures.

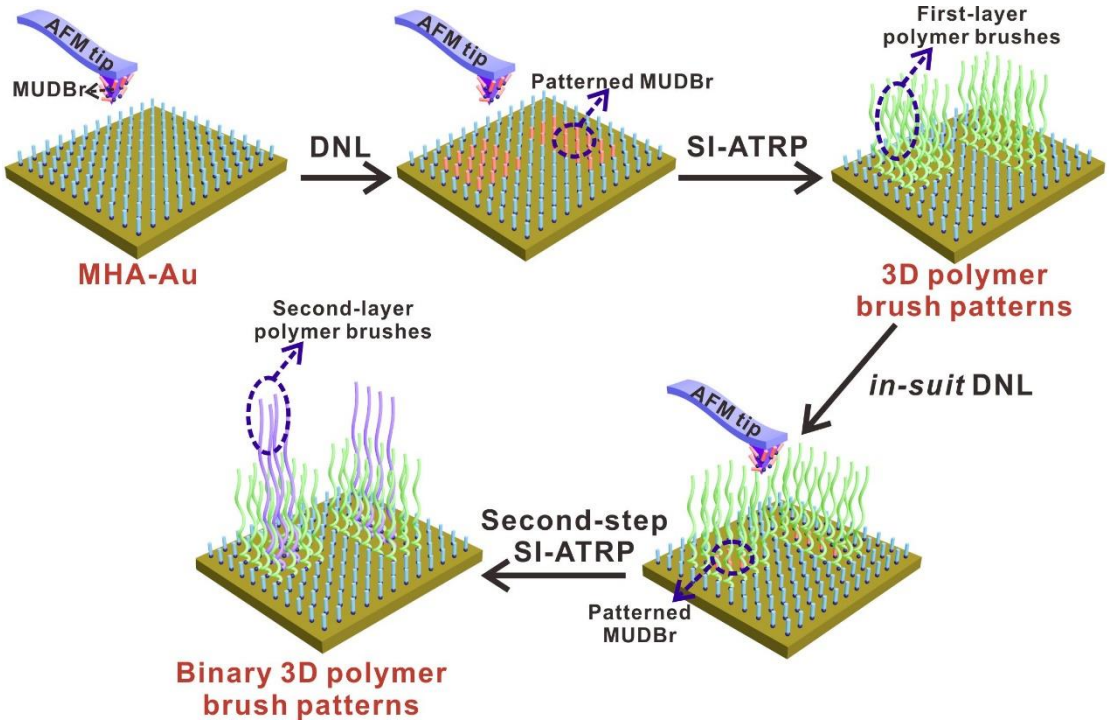

Figure 5.1. Schematic illustrations of the fabrication of binary 3D polymer brush structures by P-DNL and SI-ATRP.

5.2 Materials

ATRP initiator MUDBr was kindly provided by Prof. Hongwei Ma, Suzhou Institute of Nano-Tech and Nano-Bionics. All other chemicals were obtained from Sigma-Aldrich and used as received. Au substrates were prepared by thermal evaporation of 25 nm Au/5 nm Cr on <100> Si wafers with 500 nm SiO_2 on one side. The non-contact mode AFM tip was purchased from NanoSensors Inc. The 1D 18-tip cantilever array was obtained from NanoInk. Inc.

5.3 Experimental

5.3.1 Substrate Modification

The MUDBr SAMs modified Au substrate (MUDBr-Au) was prepared at room temperature and dried via nitrogen stream, and PMMA brushes were then grown from MUDBr-Au via SI-ATRP. The substrate was named PMMA brushes coated-Au substrate. Then the passivation of the terminal Br of PMMA brushes coated-Au substrate was carried out in 0.1 M DMF solution of NaN3 at 50 °C for more than 6 hrs.

The MHA SAMs modified Au substrate (MHA-Au) was prepared at room temperature and dried via nitrogen stream.

All the procedures above proceeded as the receipt mentioned in section 3.1.2.

5.3.2 Fabrication of Initiator Patterns by P-DNL Technique

A cantilever array including of 18 AFM tips was inked with MUDBr by being immersed into 0.1 mM of ethanol solution of MUDBr and dried in the air for 30 min to avoid ink diffusion. Then the inked cantilever array was loaded to the *z*-piezo scanner of the XE-100 AFM. The 18-tip cantilever array was subsequently parallel to the PMMA brushes coated-Au substrate (or MHA-Au substrate) by tilting sample stage in the *x* direction. Then a white-black bitmap was downloaded to the XEP lithography software for patterning. With precisely controlling the movements of the *z*- and *x*, *y*-

piezo scanners, the MUDBr initiator patterns were obtained. Finally, the substrate was treated with ultrasonic in toluene for 1 min to remove the scratched PMMA chains, and dried by nitrogen stream waiting for further experiments.

5.3.3 The Second-Step SI-ATRP of Binary Polymer Brush Patterns

The second-layer polymer brushes (PGMA or PMMA) of the binary polymer brush patterns were grown from the pre-patterned MUDBr areas prepared by p-DNL technique via SI-ATRP. The reaction proceeded as the procedures mentioned in section 3.1.2. After reaction, the samples were dried via nitrogen stream for characterization

5.3.4 Characterization

ATR-FTIR was used to detect the surface chemistry of PMMA brushes coated-Au and MHA-Au substrates. Optical microscope with the bright field was employed to observe the binary polymer brush patterns. The XE-100 AFM measured AFM topography with the non-contact mode at ambient conditions.

5.4 Results and Discussions

5.4.1 Fabrication of 3D polymer brush structures on Homogenous PMMA Brushes Coated-Au Substrate by P-DNL and SI-ATRP

The homogenous PMMA brushes (thickness: 16 nm) coated-Au substrate was prepared by SI-ATRP, and then placed onto the sample stage of the XE-100 AFM. An 18-tips cantilever array inked with MUDBr was loaded to the *z*-piezo scanner. After paralleling the cantilever array and the PMMA brushes coated-Au substrate, the XEP lithography software was used to precisely control the movements of the *z* and *x*, *y*-piezo scanners to fabricate various MUDBr initiator patterns (dots array, lines array, gradients, and flowers). During the p-DNL process, the PMMA brushes containing old MUDBr molecules on the substrate were thoroughly scratched by the tips and the new

MUDBr molecules inked on the tips were self-assembled the starched areas simultaneously, as shown in Figure 5.2. The relevant second-layer polymer brushes (such as PGMA or PMMA brushes) were subsequently grown by the second-step SI-ATRP from the new MUDBr patterned areas.

Figure 5.2. Schematic illustrations of the fabrication of second-layer polymer brush patterns on homogenous PMMA brushes coated-Au substrate by p-DNL and SI-ATRP.

The basic compositions of 3D polymer brush structures are polymer nanolines and nanodots, which were fabricated and studied first. The optical microscope and the AFM characterization results of the fabricated PGMA nanodot and nanoline arrays on PMMA brushes coated-Au substrate were shown in Figure 5.3.

The PGMA nanodot and nanoline array could be clearly seen under the optical microscope with the bright field (Figure 5.3c). When the *z* extension increased from 1.2 μm to 2.4 μm, the height of the nanodot array and the nanoline array increased from 14.7 nm to 33.2 nm, and 10.5 nm to 21.5 nm respectively. The shapes of the dots also changed from bold dot to similarly short line segment. Compared with control experiments (fabricating PGMA nanodot and nanoline arrays on MHA-Au substrate with same lithographical conditions, Figure 5.3b), we found that the PGMA nanodots in MHA-Au (Figure 5.3f) had serious stretching effect (i.e. the horizontal movement of the tip mentioned in section 4.4.2), while the stretching effect of the PGMA nanodots on PMMA brushes coated-Au substrate (Figure 5.3g) was much weaker. The length of the PGMA nanodots on PMMA brushes coated-Au substrate was shorter than that on MHA-Au substrate (Table 5.1). It was contributed to the long chains of the PMMA

brush resists could make the laterally grown PGMA brushes more tightness and less collapse. Therefore, the height of the PGMA nanodots on PMMA brushes coated-Au substrate was higher (Table 5.1). Moreover, the 3D topography of PGMA dots on PMMA brushes coated-Au substrate looked like a perfect ‘mountain,' which would be a benefit to fabricating well-defined 3D structures. The PMMA chains of the substrate may make the tips move slower, and lead more effective nanodisplacement of the initiator on the tips, resulting wider full width at half maximum (FWHM) of the PGMA nanodots (Table 5.1) and nanolines (Figure 5.4).

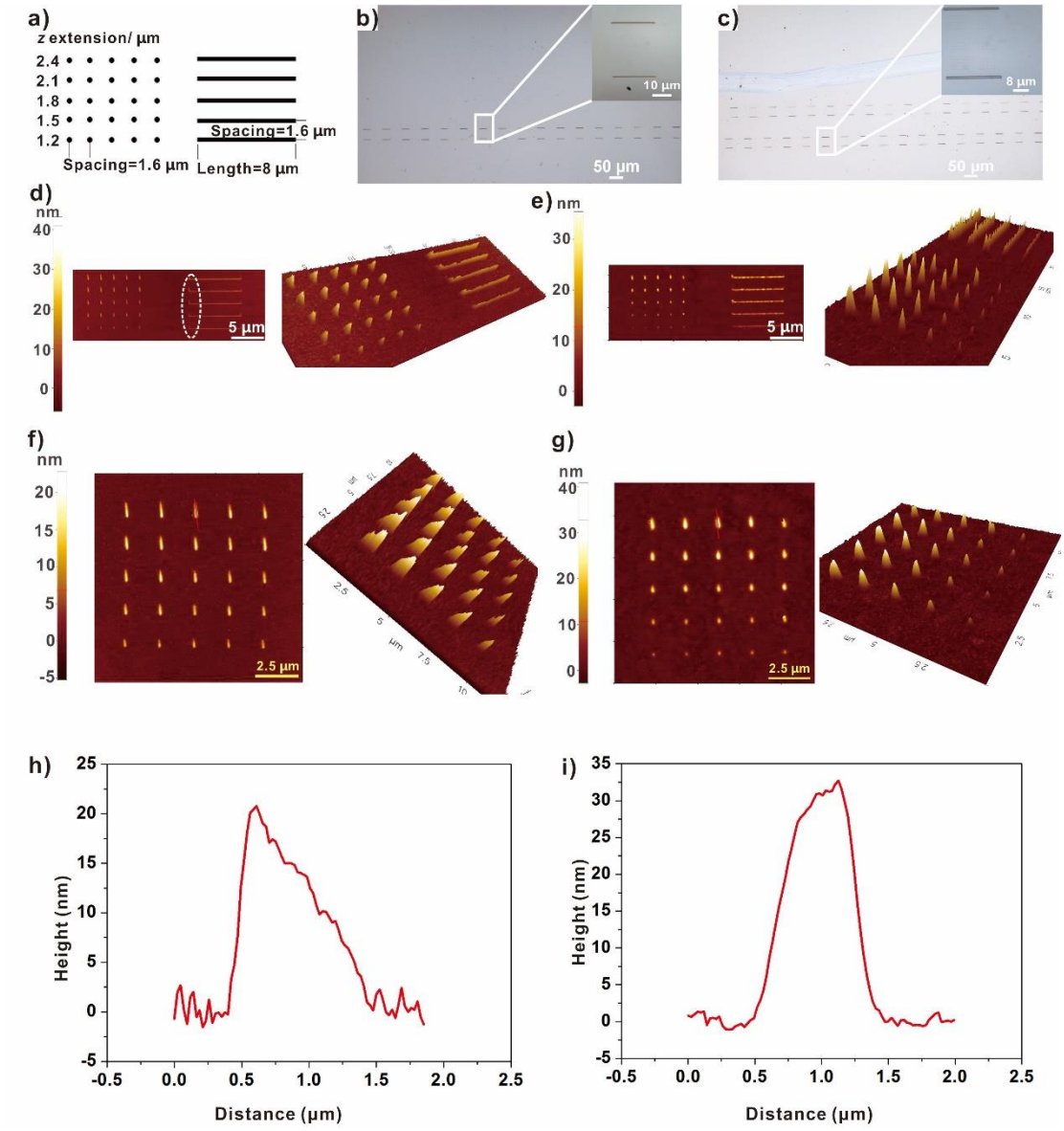

Figure 5.3. a) The designed parameters of dots and lines array. b-c) Optical microscopic images and d-e) AFM topographic views of PGMA nanodot and nanoline arrays on b,

d) MHA-Au and c, e) PMMA brushes coated-Au substrates. f-g) AFM topographic views and h-i) cross-sectional profiles of the PGMA nanodot array on f, h) MHA-Au and g, i) PMMA brushes coated-Au substrates.

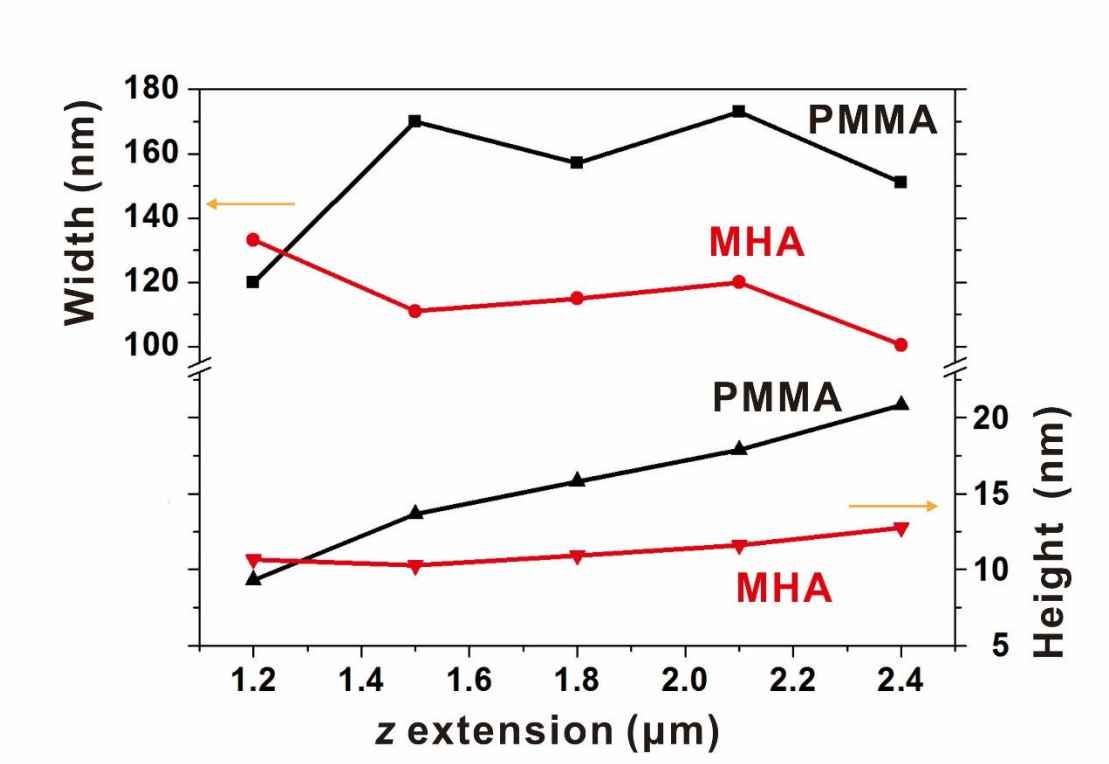

Figure 5.4. The width (FWHM) and the height of PGMA nanoline arrays on MHA-Au and PMMA brushes coated-Au substrates.

Table 5.1. The height, length (FWHM) and width (FWHM) of PGMA dot array on different substrates.

Z extend Height/ μm	MHA			PMMA		
	Height/ nm	Length/ nm	Width/ nm	Height/ nm	Length/ nm	Width/ nm
1.2	15.0	405.4	135.4	13.5	224.0	153.2
1.5	16.8	518.0	143.5	19.3	307.8	174.6
1.8	16.8	618.0	151.0	26.7	368.6	202.2
2.1	19.4	680.0	161.1	29.4	464.4	210.9
2.4	20.8	752.5	160.0	30.9	568.2	209.6

Also, the PMMA brushes on the substrate decreased the horizontal movement of AFM tips, leading shorter and fewer tails at the ends of the PGMA nanolines (Figure5.3e). Otherwise, the height of PGMA nanolines on PMMA brushes coated-Au substrate were from ~10 nm to ~21 nm with the increase of z extension, which was higher than PGMA nanolines on MHA-Au substrate at same z extension (from ~10 nm to ~13 nm). Compared with small MHA molecules, the PMMA chains of the PMMA brush-coated Au substrate not only protected the Au on the bottom from ink diffusion, but also made the PGMA nanodots and nanolines lower stretching effect, and more tightness and less collapse.

After the investigate of nanodots and nanolines, we further fabricated complex 3D PMMA structures on the PMMA brush coated-Au substrate. The AFM topographies and cross-sectional profiles of the fabricated 3D polymer gradients and flowers on PMMA brushes coated-Au substrate were shown in figure 5.5. The gradients were patterned with different pixel distance (10, 15, 20, 30, 50, 80 nm) of the bitmap and fixed 2 μm of *z* extension. It was found that when the pixel distance was 10 nm, the gradients became columnar structures and lost the slope structure. Only the pixel distance was extended to 80 nm we could obtain a real gradient PMMA with slope structure. Furthermore, at 80 nm of pixel distance (Figure 5.5f), the 3D PMMA flower was shown clear ups and downs. But at 50 nm of pixel distance (Figure 5.5i), the PMMA flower was flatter, which the 3D effect was not satisfactory enough. In the previous study of our group, the distance between neighboring pixels at 50 nm was high enough to get good gradient polymer structure under 2 μm of *z* extension on MHA-Au substrate [171]. It was very different with our results at this moment. Which could be explained by comparing with MHA (small molecule), the PMMA brushes of the PMMA brush-coated Au substrate acting as polymer resist layer extruded the brushes of second-step SI-ATRP, resulting in the 3D PMMA structures more tightness and less collapse. This phenomenon was similar to the preceding fabricated nanodot and nanoline array.

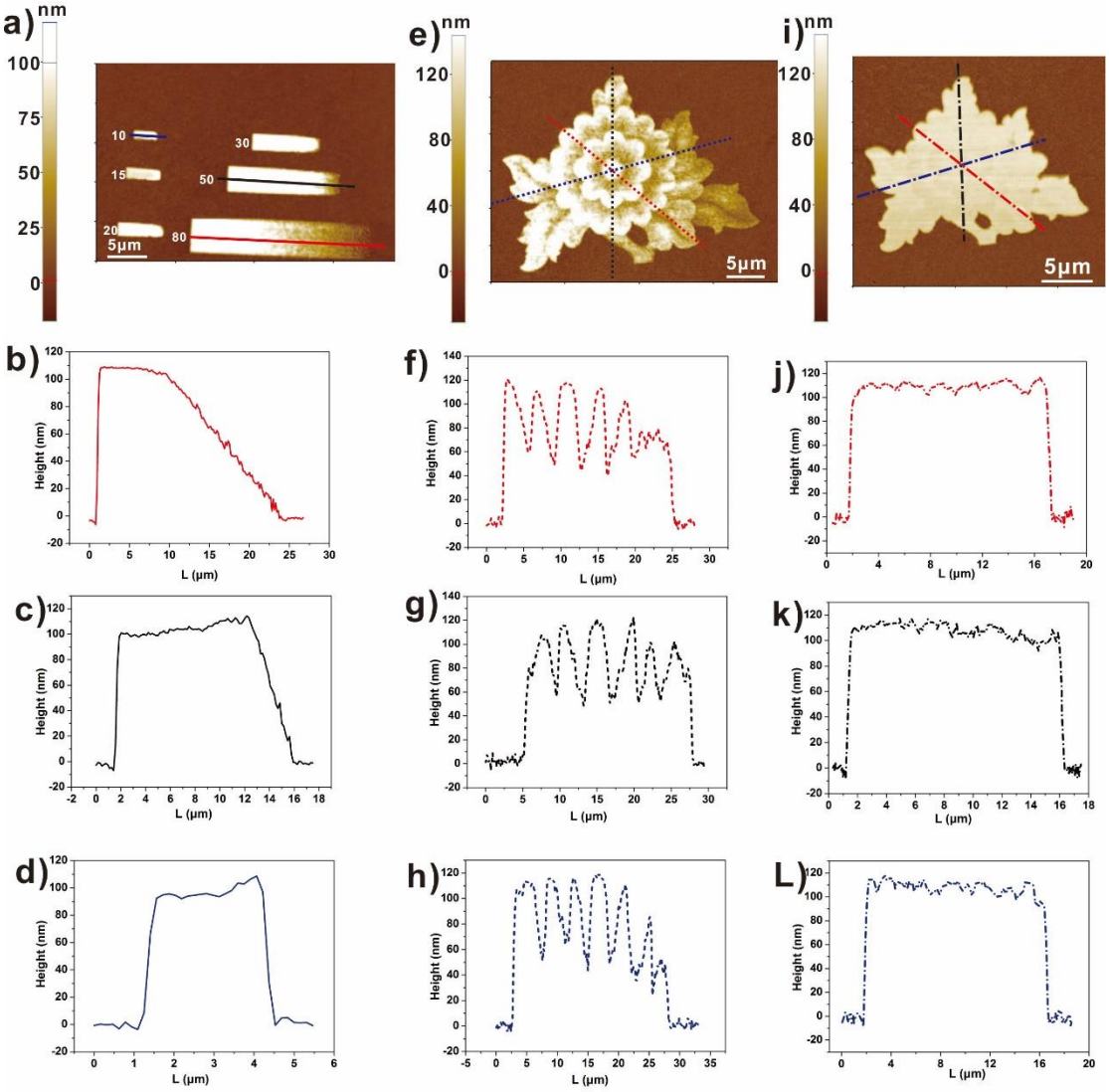

Figure 5.5. (a, e, i) AFM topographic views and (b, c, d, f, g, h, j, k, L) cross-sectional profiles of the PMMA gradient and flowers fabricated with different pixel distance on PMMA brushes coated-Au substrate.

5.4.2 Preparation of Binary 3D PGMA@PMMA Brush Patterns by *in-situ* Repeated P-DNL

In the last section, we have studied the details of 3D PMMA brush patterns fabricated on flat PMMA brushes coated-Au substrates. The results showed that according to our methods, we were easy to fabricate binary 3D polymer brush structures on a flat substrate. However, can we fabricate more well-defined complex structures, such as 3D polymer brush structures fabricated on a gradient polymer substrate? As the

proof of concept, cell behaviors are greatly affected by the chemical, topographical, mechanical properties of the substrate. A combination of 3D polymer brush structures and gradient polymer substrate can offer more topographical properties, chemistry gradient, and special mechanical properties, which may be used to control cell behaviors. Whereas, we tried to generate binary 3D PGMA@PMMA polymer brush patterns on PMMA gradient structures.

A series of PMMA gradients acted as substrate was constructed by 1D p-DNL on MHA-Au substrate (Figure 5.6a and b). The heights of the apex of the PMMA hemisphere and pyramid were about 40 nm. Then the second time p-DNL was proceeded based on the prepared PMMA gradient. Importantly, the 18-tips cantilever array of second-time p-DNL should be aligned with the prepared PMMA gradient array to realize the *in-suit* preparation. To achieve the cantilever array settling upon the PMMA gradient array, we used the contact mode of AFM characterization to scan the PMMA gradients time to time, and continual manual adjusted the sample stage in *x* and *y* directions. After successfully positioning, we used the XEP lithography mode to pattern the hemisphere, pyramid, and cuboids on the pre-fabricated PMMA hemispheres and pyramids. The PGMA brush hemispheres, pyramids (Figure 5.6c) and cuboids (Figure 5.7b) were grown from the areas by second-step SI-ATRP, and we finally obtained binary 3D PGMA@PMMA brush patterns.

From AFM characterization (Figure 5.6d)), the height of the peak of the PGMA hemisphere on the PMMA hemisphere was about 160 nm; the highest point of the PGMA pyramid on the PMMA pyramid was about 170 nm. As the tightness effect of the PMMA gradients, the gradient of the PGMA structures was not very clear but still showed with a narrow top and wide bottom structure. In Figure 5.6c, the heights of PGMA cuboids on PMMA hemisphere and pyramid were about 150 nm and 175 nm respectively, and maintain the same FWHM from top to bottom.

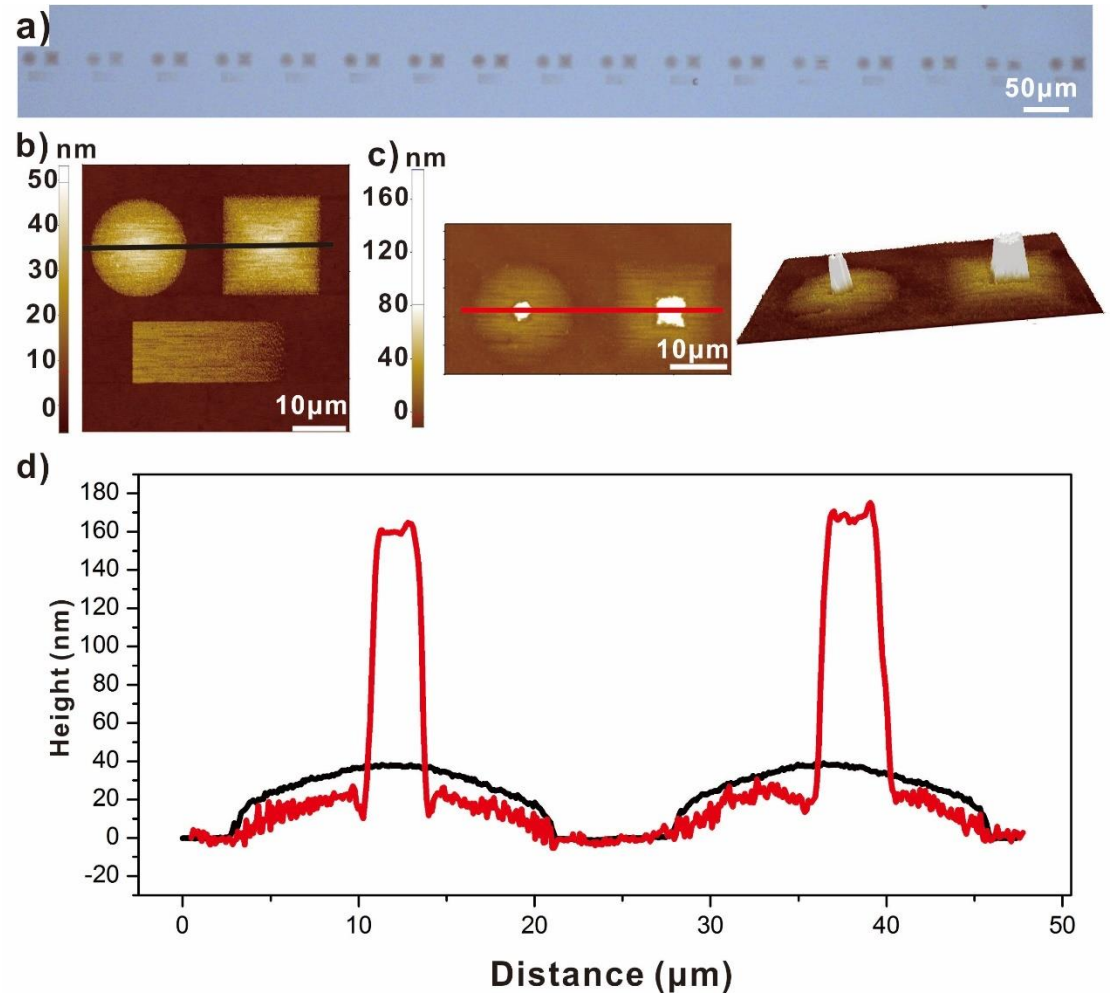

Figure 5.6. a) Optical microscopic image and b) AFM topographic views of PMMA gradient fabricated by 1D p-DNL on MHA-Au substrate. c) AFM topographic views and d) cross-sectional profiles of the PGMA hemisphere and pyramid fabricated by *in-situ* repeated 1D p-DNL on PMMA brushes coated-Au substrate.

Additionally, in Figure 5.6d and Figure 5.7c, we found that the heights of PMMA hemispheres and pyramids were lower after second-time p-DNL. The reason was that the PMMA chains were scratched off by the tips during positioning. So, it would be better to fabricate a reference object near the PMMA gradients to do the positioning in the future.

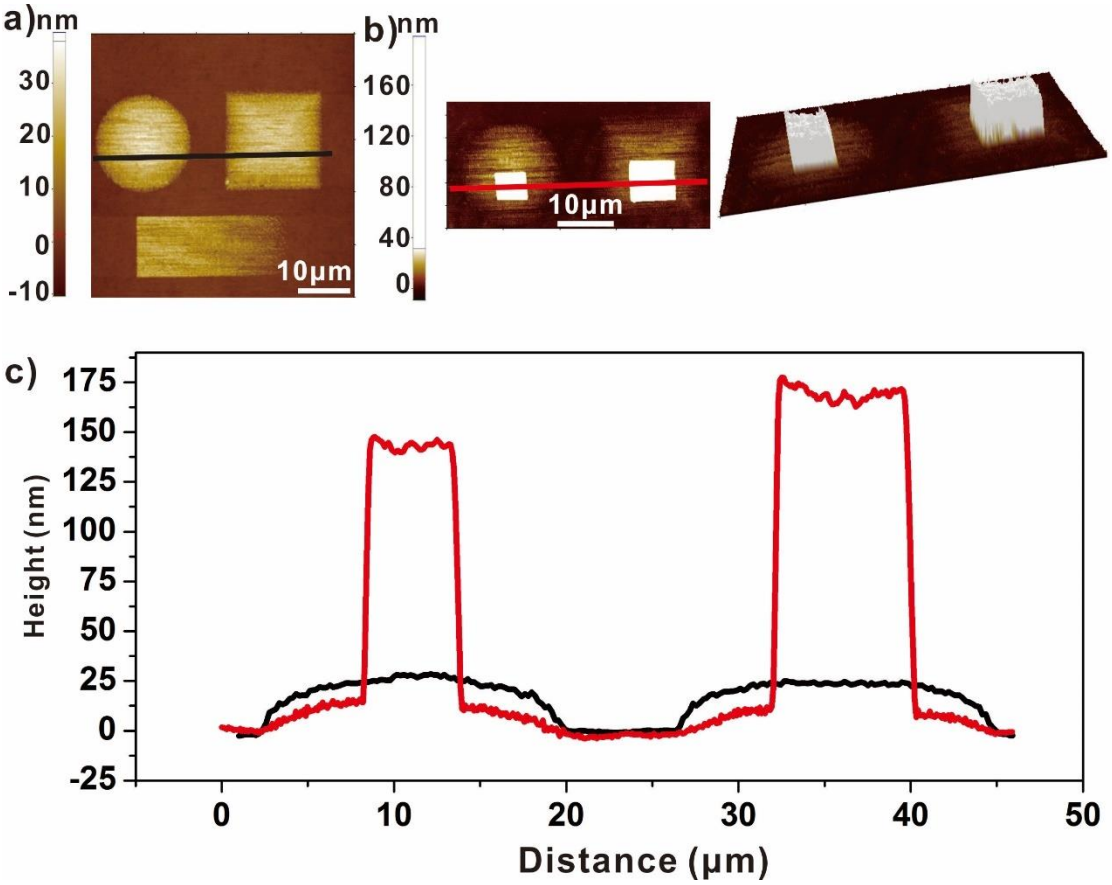

Figure 5.7. a) AFM topographic views of PMMA gradient fabricated by 1D array DNL on MHA-Au substrate. b) AFM topographic views and c) cross-sectional profiles of the PGMA cuboids fabricated by in situ repeated 1D p-DNL on PMMA brushes coated-Au substrate.

5.5 Conclusions

By integrating p-DNL technique and SI-ATRP, binary 3D polymer brush structures were successfully generated on flat PMMA brush-coated Au substrate. Compared with MHA acted resist layer, the PMMA brushes of the substrate decreased the stretching effect, may increase the nanodisplacement efficiency, and brought a tightness effect to the second-layer polymer brushes, leading the higher, more tightness, and less collapse of the second-layer polymer brush. This phenomenon indicated that polymer brushes acted resist layer could be a benefit to fabricating well-defined 3D structures of lateral patterned second-layer polymer brush. Then PMMA gradient array was fabricated by

1D p-DNL, and the binary 3D PGMA@PMMA brush patterns were therefore produced by *in-suit* second-time p-DNL and second-step SI-ATRP. The key critical positioning problem of *in-suit* technique was captured by manual adjustment of the AFM sample stage. The binary 3D polymer brush structures contain more chemical, topographical, and mechanical properties, which may have great potential in manipulating cell behaviors and other applications (e.g. biosensors).

CHAPTER 6 THERMORESPONSIVE NANO-MICRO BINARY POLYMER BRUSH PATTERNS FOR CONTROLLING CELL ORIENTATION AND Smart DETACHMENT

6.1 Introduction

Cells of many normal tissues *in vivo*, such as tendon cells [206], bone cells [207], myocardial cells [208], vascular endothelial cells [209] and smooth muscle cells [210], are oriented in order to make such tissues perform well. Thorough understanding of how to efficiently control cell orientation on an artificial surface is critical in materials and life sciences such as advanced biomedical engineering, tissue engineering, and cell-based bioassay.

It is well known that the ECM, a complicated network of proteins and proteoglycans, guide cell behaviors including cell orientation [211-212] via surface topographical, chemical, and mechanical cues [213-214]. Therefore, researchers have designed artificial ECM with controlled three cues to study and regulate the cell orientation. Two major methods of designing and fabricating the artificial ECM for controlling cell orientation have been reported so far. One is generating a cell-adhesive surface with structural and directional topography as the artificial ECM (i.e. aligned nanofibers [210], microgrooves [207, 215], microstripes [148, 216], and nanogrooves [217-219]). Under this situation, well-distributed cells will orient and adhere to the entire surface. Another method is using both cell-adhesive and cell-inert materials to create micropatterned chemical cues on the surface, i.e., micro-sized cell-adhesive materials separated by cell-inert microstripes. As such, cells prefer to adhere and align firstly on the cell-adhesive part and subsequently spread to cell-inert areas [148]. However, the natural ECM is cell-adhesive materials containing both directional nano- and

microscale architectures [8, 211]. The uniformly patterned surfaces in these two methods do not mimic the real ECM well. It would be better to use cell-adhesive materials to design biomimetic surfaces with multiscale topography for well-control cell alignment systems.

Several very recent papers have demonstrated the uniqueness of these multiscale surfaces in regulating cell adhesion [220], migration [221], orientation [222], and differentiation [223]. Therefore, such multiscale surfaces are more preferred for better studying cell behaviors and then developing more efficient artificial ECM for biomedical applications. Nevertheless, the development and applications of these complex surfaces are limited due to the lack of a user-friendly tool to generate these complex surfaces with well-defined multiscale topography, and versatile chemical cues.

Herein, to address the challenges, we combined p-DNL technique and SI-ATRP to develop a biomimetic nano-micro binary polymer brushes patterns for controlling cell behaviors. These nano-micro binary polymer brushes patterns consisted of cell-adhesive materials, i.e. gelatin-modified PGMA (gelatin-PGMA) brushes nanolines separated by a thin microstripes of the thermoresponsive PNIPAm brusheses. Cells cultured on this artificial ECM of the binary polymer brushes patterns were not only effective adhered at 37 ºC but also aligned along the gelatin-PGMA nanolines. Meanwhile, the thermal responsive behavior of the microscale pitch of PNIPAm brushes caused the adhered and oriented cells to spontaneously detach from the substrate at low temperature (26 ºC), in which PNIPAm became cell-repellent.

6.2 Materials

ATRP initiator MUDBr was kindly provided by Prof. Hongwei Ma, Suzhou Institute of Nano-Tech and Nano-Bionics. phosphate buffered saline (PBS, pH 7.4, 1 X; Gibco™), Dulbecco's Modified Eagle Medium (DMEM, with high glucose; Gibco™), trypsin-EDTA (0.5%, Gibco™), fetal bovine serum (FBS, South America origin; Gibco™), penicillin-streptomycin (10,000 U/mL; Gibco™), 4-(1,1,3,3-Tetramethylbutyl) phenyl-polyethylene glycol (Triton™ X-100, Sigma), albumin

bovine V (BSA, from bovine serum, Mw 66,000; Sigma-Aldrich), rhodamine phalloidin (Rhod-phalloidin, Cytoskeleton Inc.). All other chemicals were obtained from Sigma-Aldrich and used as received. Au substrates were prepared by thermal evaporation of 15 nm Au/2 nm Cr on the glass wafer. The contact mode and non-contact mode AFM tips were purchased from NanoSensors Inc. The 2D 55,000-tip cantilever array [173, 224] was obtained from NanoInk Inc.

6.3 Experimental

6.3.1 Substrate Modification

The MUDBr-Au substrate was prepared at room temperature and dried via nitrogen stream, and PNIPAm brusheses were then grown from MUDBr-Au via SI-ATRP. The reaction time of polymerization was 5 min. Then passivation of the terminal Br of PNIPAm brushes-coated Au-glass substrate was carried out in 0.1 M DMF solution of NaN3 at 50 °C for more than 6 hrs. The procedures above were proceeded as the receipt mentioned in section 3.1.2.

6.3.2 Fabrication of Initiator Patterns by P-DNL Technique

A 2D 55,000-tip cantilever array (square centimeter array of 55000 tips) was used to perform the experiments. In the 2D p-DNL process, the 2D 55,000-tip cantilever array was inked with MUDBr by being immersed it in MUDBr solution 0.1mM) for 10 s and drying in air for more than 1 hr. Then the 2D 55,000-tip cantilever array was loaded to the *z*-piezo scanner of the XE-100 AFM. And the pre-made PNIPAm brushes-coated Au-glass substrate was put onto the sample stage. Then the leveling of the 2D 55,000-tip cantilever array and the substrate was proceeded by manual manipulation [224] for massively parallel patterning. The movement of the 55,000 tips was precisely controlled by programming the *x*-*y*, and *z*-piezo of the AFM with XEP lithography mode. The PNIPAm chains of the substrate on the patterned area were scraped by the tips while the MUDBr molecules self-assembled onto the bare Au surface at the same time

to obtain lateral patterned MUDBr on the PNIPAm brushes-coated Au-glass. The relative humidity for all p-DNL writing experiments was 50 ± 3%, and the temperature was 25 ± 0.5 °C.

6.3.3 Synthesis of PGMA Brushes via SI-ATRP

The PGMA nanolines were synthesis by synthesized by placing the MUDBr patterned PNIPAm brushes-coated Au-glass substrate in a 50 mL of Schlenk tubes with reaction solution for SI-ATRP. The polymerization proceeded as the receipt mentioned in section 3.1.2. After the reaction, the resultant PGMA@PNIPAm substrate was then rinsed with methanol, deionized water, and dichloromethane, and dried via nitrogen stream.

6.3.4 Gelatin Immobilization

The PGMA@PNIPAm substrate was immersed into 10 mg/mL of gelatin in PBS at 37 °C for 24 h to immobilize gelatin. The resultant gelatin modified PGMA@ PNIPAm (gelatin-PGMA@PNIPAm) substrate was repeated washed by PBS solution to move the unfixed gelatin, and dried under nitrogen stream.

6.3.5 Cell Adhesion and Orientation Experiments

NIH-3T3 were incubated on TCPS dishes in high glucose of DMEM medium with 5 % fetal bovine serum (FBS) and 1 % penicillin-streptomycin. And the cells were placed in an incubator with 75 % humidity and 5 % CO2 at 37 °C. For cell behaviors study, the unpatterned PNIPAm brushes-coated Au-glass, unpatterned gelatin modified PGMA brushes-coated Au-glass, patterned gelatin-PGMA@PNIPAm, and patterned PGMA@PNIPAm without gelatin modification substrates were put on 90 mm of TCPS dishes. Then cultured cells were trypsinized and seeded onto the various substrates at a density of 3 x 10^5 cells/mL or 1 x 10^5 cells/mL.

6.3.6 Fluorescence Dying of Aligned Cells on Nano-Micro Binary Polymer Brush Patterns

Oriented cells on the patterned gelatin-PGMA@PNIPAm surface were washed with PBS and fixed with 4% paraformaldehyde in PBS for 10 min at room temperature. Then the fixed cells were permeabilized with 0.1% Triton™ X-100 in PBS for 3 min at room temperature and washed with PBS. These steps were repeated for three times. Next, the permeabilized cells were blocked with 1% BSA in PBS for 20 min. After being washed with PBS, the cells were incubated with 5 μg/mL of Rhod-phalloidin in PBS in dark place at 37 °C for 1 hr. Finally, the cells were rinsed with PBS and treated with 2.5 μg/mL of DAPI for 15 min at 37 °C for nuclei staining.

6.3.7 Smart Detachment of Cells

The aligned NIH-3T3 cells on the patterned gelatin-PGMA@PNIPAm surface were placed in an incubator with 75 % humidity and 5 % CO_2 at 26 °C and then observed with visual inspection and microscope every 30 min.

6.3.8 Characterization

The ATR-FTIR spectra were used to detect the surface chemistry of polymer brushes-coated Au-glass substrates and the binary polymer brushes patterns. The XPS spectra were applied to test the nitrogen of passive PNIPAm brushes-coated Au-glass substrate. The optical microscope with the bright field was employed to observe the nano-micro binary polymer brushes patterns and the growth of the cultured cells. AFM topography in the air was measured by XE-100 AFM with the non-contact mode at ambient conditions. While equipped with a liquid cell and a heating stage, the XE-100 AFM was able to detect the conformational transition of PNIPAm brushes at a different temperature. The drop shape analyzer was applied to detect the water contact angle of

gelatin-PGMA@PNIPAm at 37 °C and 26 °C. The fluorescent microscopy was used to observe the stained cells.

6.4 Results and Discussions

6.4.1 Fabrication of Binary Polymer Brush Patterns by P-DNL and SI-ATRP

A thin layer of the homogeneous PNIPAm brushes (~8 nm) was grafted onto a transparent Au-glass substrate by SI-ATRP and then terminated by NaN_3 to prepare PNIPAm brushes-coated Au-glass substrate which would be used in the further p-DNL fabrication. From the N1s XPS spectra of PNIPAm brushes-coated Au substrate (before termination, Figure 6.1 a), the single N1s peak at 400.5 eV showed the presence of PNIPAm brushes [225-226] and the single chemical environment of N element in PNIPAm chains. The ATR-FTIR result also found the N-H characteristic peak at 3341 cm^{-1} which were attributable to grafted PNIPAm brushes. Nevertheless, after termination, another N1s peak (N=N=N, at 401.5 eV) [227] was appeared, indicating the successful termination reaction.

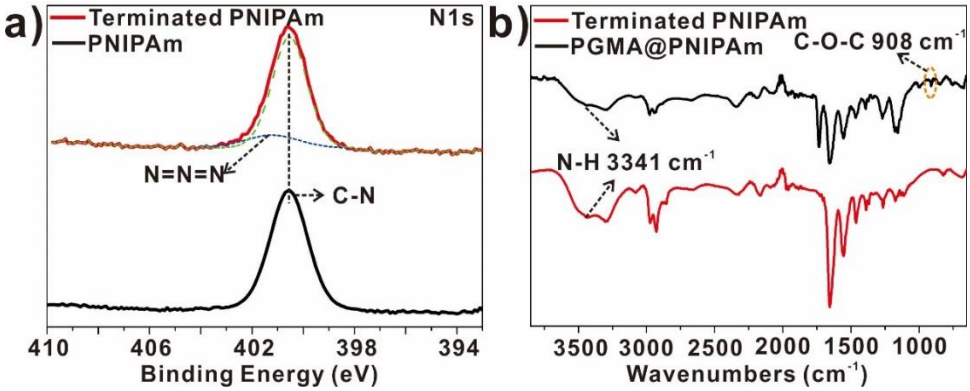

Figure 6.1. (A) The N1s XPS spectra of PNIPAm and terminated PNIPAm brushes on Au surface. (b) ATR-FTIR of terminated PNIPAm and patterned PGMA@PNIPAm.

Then PNIPAm brushes-coated Au-glass substrate was put onto AFM sample stage to continue the 2D p-DNL process. After leveling the MUDBr inked 55,000-tip array

(Figure 6.2b) on the *z*-piezo scanner against the underlying PNIPAm modified Au-glass substrate, the tips were forced with suitable *z* extension to indent into the PNIPAm brushes and cleave the brushes chains off from the Au surface. Meanwhile, the MUDBr initiator inked on the tips self-assembled simultaneously onto the uncovered Au areas via S-Au bonding, forming the MUDBr nanopatterns laterally on the PNIPAm brushes modified Au-glass substrate. Subsequently, a square centimeter of PGMA nanoline array was grown from the MUDBr nanopatterns via performing a second-step SI-ATRP.

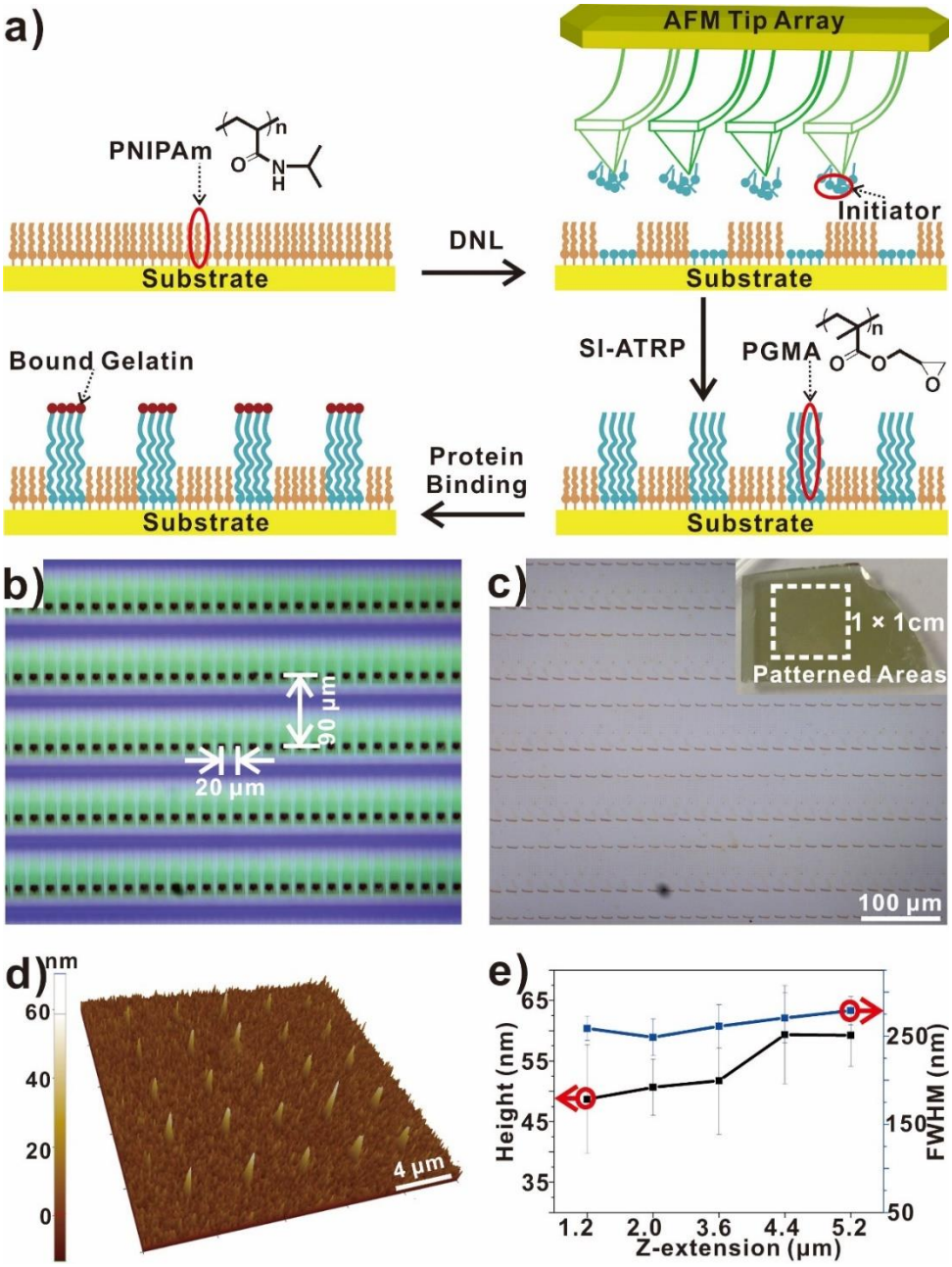

Figure 6.2. (a) Schematic illustration of fabrication of the nano-micro binary polymer brushes system by DNL. (b) Optical image of the 55,000-tip cantilever array. (c) Optical

image and photo image (top right corner) of large-area PGMA nanodot arrays on PNIPAm modified Au substrate. (d) AFM topographic view of PGMA nanodot array. (e) Statistical results of the average heights and FWHM of the PGMA nanodot arrays fabricated by the 55,000 tips in p-DNL.

As a proof-of-concept, a 5 × 5 dot array of the binary PGMA@PNIPAm system (Figure 6.2c) was fabricated with different indentation forces controlled by *z* extension to investigate the brushes shapes. The chemical structures of the binary PGMA@PNIPAm system were studied by ATR-FTIR (Figure 6.1b). The appearance of a C-O-C peak at 908 cm^{-1} [228] illustrated PGMA brushes was grown on PNIPAm brushes-coated Au-glass substrate successfully. The AFM topography (Figure 6.2d and e) showed the height of the PGMA nanodots (additional to the PNIPAm background) increased from 48 nm to 60 nm with increasing *z* extension (1.2, 2.0, 3.6, 4.4 and 5.2 μm), while the full width at half maximum (FWHM) of each nanodot was widened from ~260 nm to ~280 nm. The larger *z* extension resulted in more effective nanodisplacement, leading denser nanopatterned PGMA brushes which forces the polymer chains to stretch up vertically and spread out laterally. Consequently, the 5.2-μm *z* extension was chosen in future p-DNL for controlling cell behaviors.

6.4.2 Cell Adhesion and Orientation on Nano-Micro Binary Polymer Brush Patterns

In the control experiments, PGMA brushes were found to be cell-inert. Therefore, we modified the PGMA brushes with gelatin which improves cell adhesion. Due to a facile reaction between the epoxide groups of the PGMA chains and the amino groups of the proteins [229-230], gelatin was bonded onto PGMA chains, resulting in a cell-adhesive transformation of gelatin-PGMA. The cell culture experiments showed that although cells could adhere to both gelatin-PGMA and thin PNIPAm brushes surfaces at cell growing conditions (37 ºC), the cells were a random orientation (Figure 6.3).

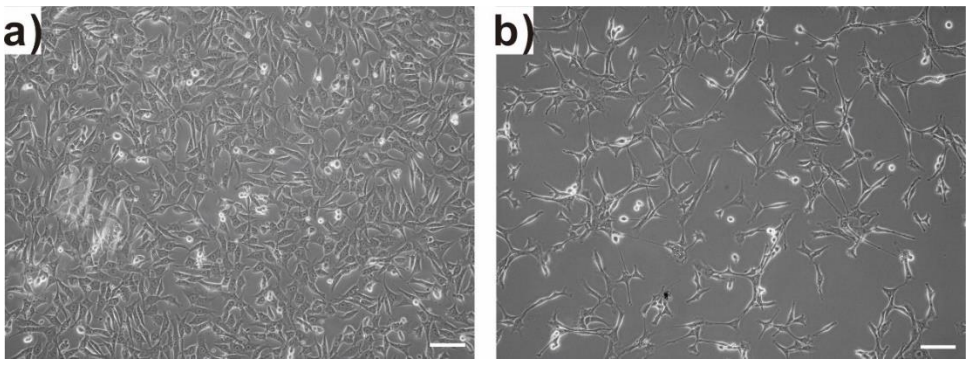

Figure 6.3. (a) Optical image of NIH-3T3 cells incubated on PNIPAm brushes-coated Au-glass substrate (thickness of PNIPAm: 8 nm) for 24 h. Seeding density: 3 x 10^5 cells/mL. (b) Optical image of NIH-3T3 cells incubated on gelatin modified PGMA brushes-coated Au-glass substrate (thickness of PGMA: 70 nm) for 24 h. Seeding density: 1 x 10^5 cells/mL. Scale bar: 100 μm.

To control cell orientation, the directional gelatin-PGMA nanoline array on thin PNIPAm brushes surface (gelatin-PGMA@PNIPAm) was fabricated by 2D p-DNL and SI-ATRP as the methods mentioned above. As shown in Figure 6.4a, each writing tip of the 55,000-tips cantilever array was programmed as the bitmap to make three gelatin-PGMA nanolines. The 92 μm-long nanoline consisted of 510 rows (spaced by 180 nm) × 2 columns (spaced by 70 nm) of nanodots. When done properly, these 92 μm-long nanolines made by each writing tip were connected head-to-tail, resulting ultralong gelatin-PGMA nanolines (Figure 6.4b) which traveled across centimeter distance. From the AFM scanning, the height and FWHM of these gelatin-PGMA nanolines were found to be ~70 nm and ~300 nm respectively (Figure 6.4c).

NIH-3T3 cells showed clearly oriented morphology and uniform distribution (Figure 6.4d) when cultured on the binary surface for 24 hrs. Additionally, the cells kept oriented morphology on patterned areas after 48 hrs but were random orientation outside the patterned area (Figure 6.4e and g). The Rhod-phalloidin stained cytoskeleton of NIH-3T3 cells was also found to be aligned along the gelatin-PGMA nanolines (Figure 6.4f). On the other hand, it was found in the control experiment that cells adhered but were not oriented on the binary surface which included original PGMA nanolines without gelatin modification (Figure 6.5). These results indicated that

although the PNIPAm microstripe allowed cells to adhere, only the cell-adhesive gelatin-PGMA nanolines could apply nanoscale chemical cues to regulate focal adhesion and lead cell orientation.

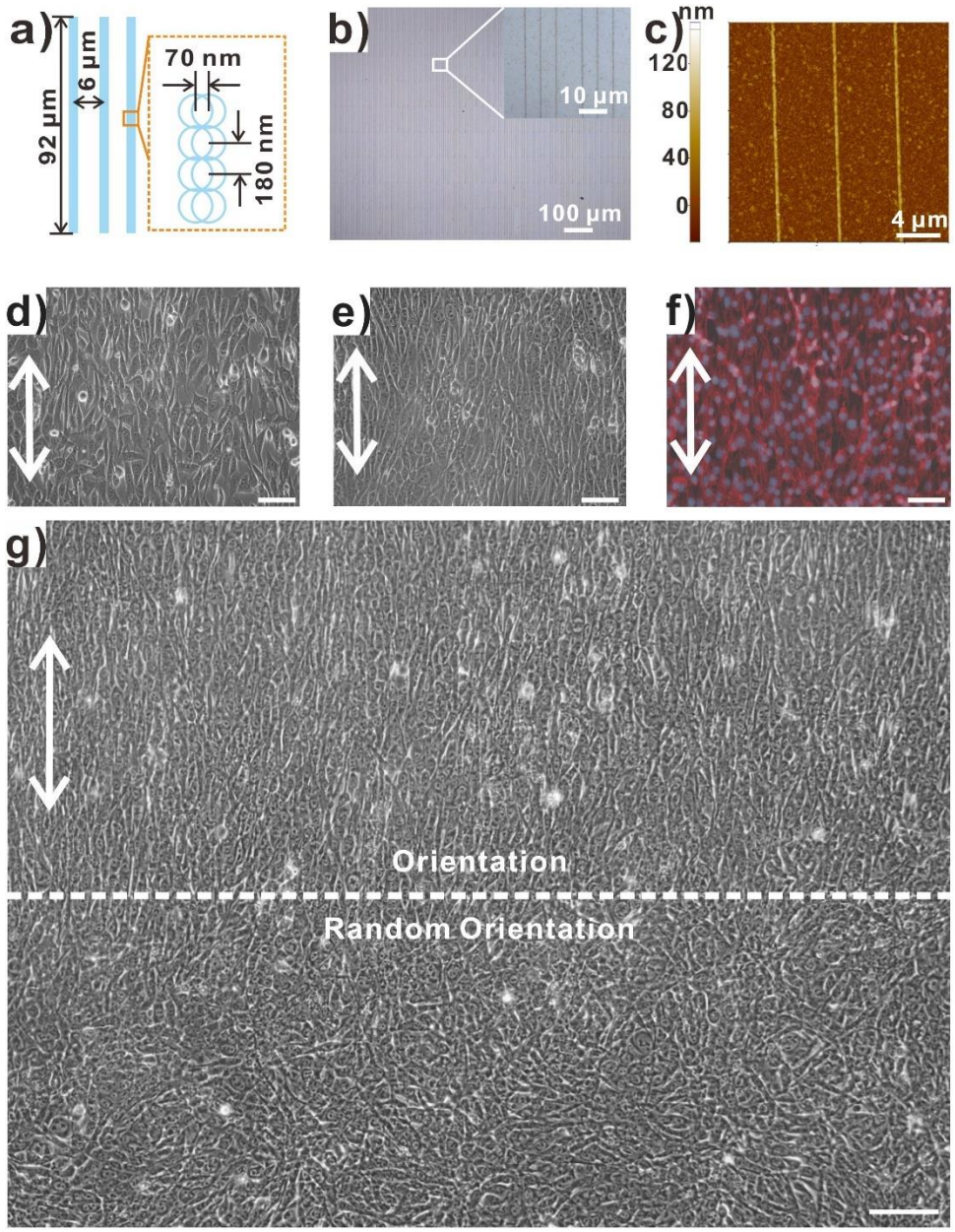

Figure 6.4. (a) Designed pattern parameters for the nanoline array. (b-c) Optical images and AFM topographic view of the gelatin-PGMA@PNIPAm sample. (d-e, g) Optical images of NIH-3T3 incubated on gelatin-PGMA@PNIPAm surface for 24 hrs and 48 hrs. (d) 24 hrs; (e, g) 48 hrs. (f) Fluorescence microscopy images of NIH-3T3 incubated on the gelatin-PGMA@PNIPAm surface for 48 hrs. Red and blue colors were the cell cytoskeleton and nucleus respectively. Scale bar of d-g: 100 μm.

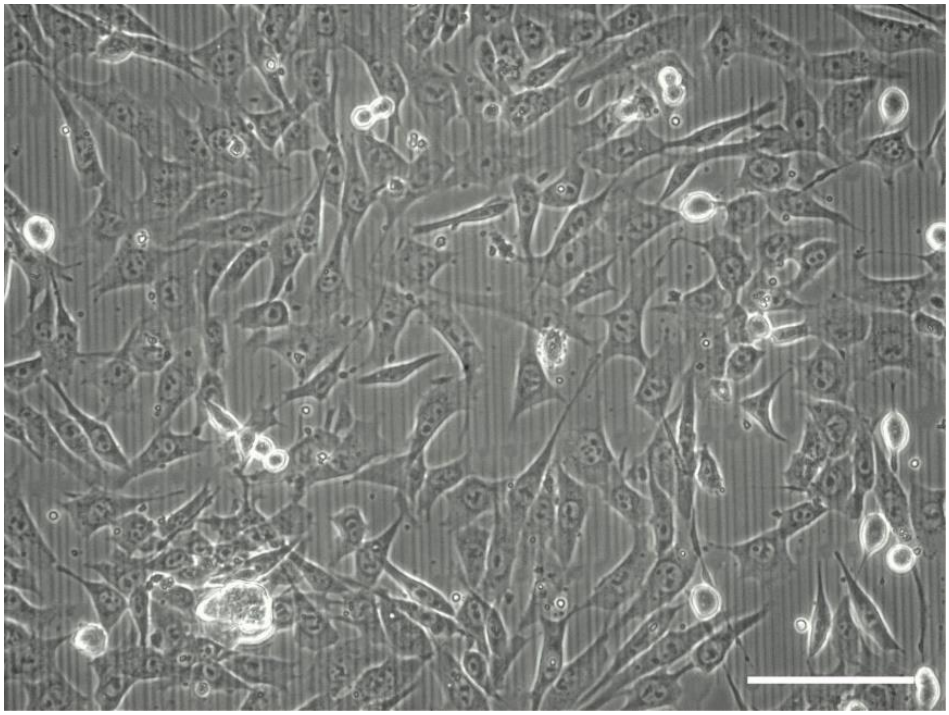

Figure 6.5. Optical image of NIH-3T3 cells incubated on patterned PGMA without gelatin immobilization on PNIPAm brushes-coated Au-glass substrate for 24 h. Seeding density: 3 x 10^5 cells/mL. Scale bar: 100 μm.

6.4.3 Smart Cell Detachment on Nano-Micro Binary Polymer Brush Patterns

Importantly, the PNIPAm microstripes in the nano-micro binary system did not only improve cell adhesion but also led a smart detachment of the oriented cells due to the thermosensitivity of PNIPAm. PNIPAm possesses a lower critical solution temperature (LCST) of 32 °C in aqueous [231-232]. When the temperature is above 32 °C, the intramolecular hydrogen bonds between C=O and N-H groups of the PNIPAm chains make the chains turn to compact and collapsed conformation [233], and then a small molecular mobility. So the PNIPAm chains extensively dehydrate and become hydrophobic. At a temperature below 32 °C, most of the hydrogen bonds of PNIPAm chains are intermolecular bonding between the C=O and N-H groups and water molecules, so the PNIPAm chains have an increase in the conformation of the extended chain, and become fully hydrated. Generally, the competition between intermolecular

and intramolecular hydrogen bonding below and above the LCST results to the hydrophilic-hydrophobic transformation of PNIPAm. Such conformation change and hydrophilic-hydrophobic transformation were visualized through underwater AFM topography and contact angle test respectively. As shown in Figure 6.6a and b, the PNIPAm brushes in the binary system collapsed at 37 °C, while swelled about 40 nm at 26 °C. Accordingly, the water contact angle decreased from 83 ° to 60 ° with the temperature decrease.

Normally, cells reject to adhere on the highly hydrated hydrophilic surface, resulting cell detachment from such surface. Due to the suitable LCST and the highly hydrated hydrophilic-hydrophobic transformation, PNIPAm is widely utilized for controlling smart cell attachment and detachment. Cells can adhere on the thin PNIPAm surface at 37 °C and spontaneously detach by decreasing the temperature to under 32 °C (Figure 6.6c). To verify the smart detachment phenomenon, the oriented NIH-3T3 cells on the directional gelatin-PGMA/PNIPAm binary surface were incubated at 37 °C for 5 days and then removed to another incubator at 26 °C. After 40 min, we found the cells started to score around the edges, as shown in Figure 6.6d. With the time increasing, more and more cells detached from the surface of the substrate, and the cell sheet scrolled due to the mechanical stress (Figure 6.6e). Most of the cells detached from the surface in 4 hrs. Moreover, the detached cells still maintain the orientation morphology. Remarkably, this smart nano-micro binary polymer brushes template is reusable. After cell detachment, the gelatin-PGMA@PNIPAm was washed by trypsin and PBS and then used to culture cells again. It was found that cells could still be well-aligned (Figure 6.7) and smart-released by the same substrate

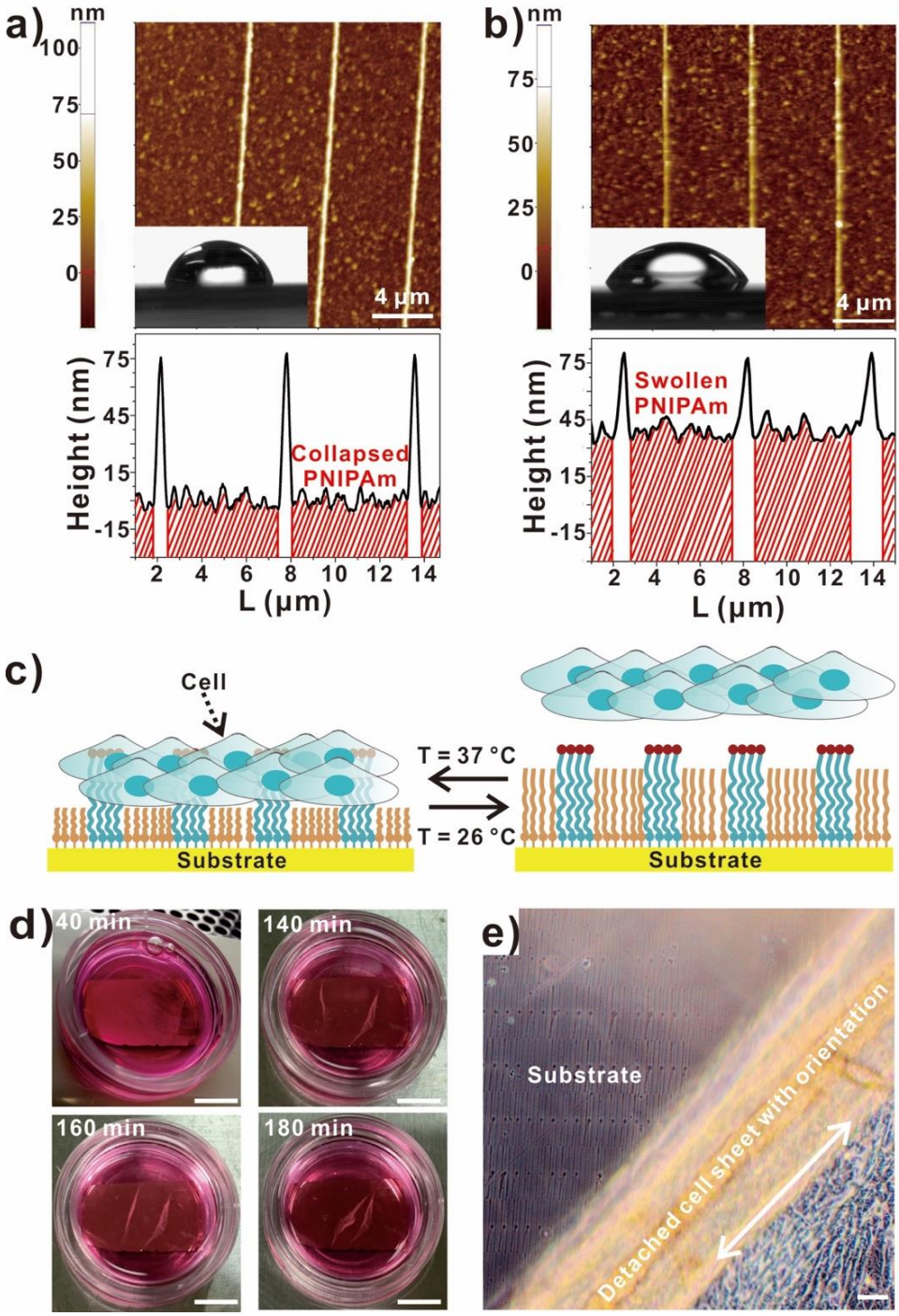

Figure 6.6. (a-b) Underwater AFM topographic view, the corresponding cross-sectional profile and the contact angles of nanoline arrays of the gelatin-PGMA@PNIPAm sample in 37 °C and 26 °C of water. (a) 37 °C; (b) 26 °C. (c) Schematic illustration of the transformation of cell attachment and detachment with temperature variation. (d) Images of NIH-3T3 cells on gelatin-PGMA@PNIPAm substrate incubating in 26 °C. The cell film gradually fell off from the surface from the edges. Scale bars: 1 cm. (e) Optical image of detaching NIH-3T3 cells from the gelatin-PGMA@PNIPAm surface.

Scale bar: 50 μm.

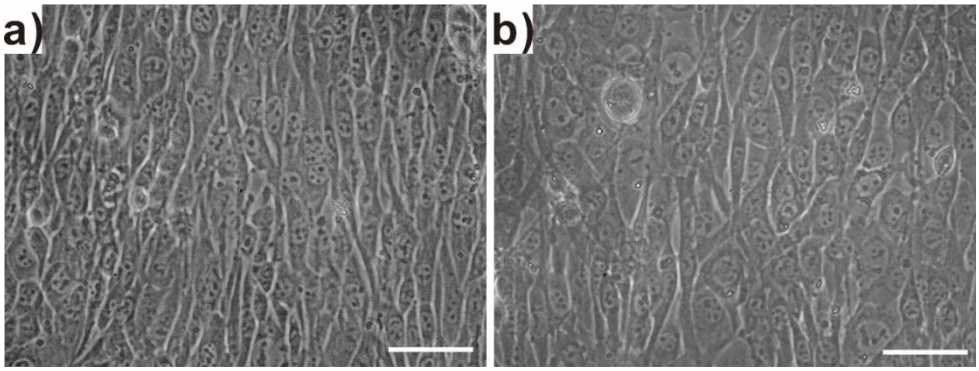

Figure 6.7. Optical image of oriented NIH-3T3 cells on reused gelatin-PGMA@PNIPAm surface. (a) Oriented cells on the surface reused for two times. (b) Oriented cells on the surface reused for three times. Scale bars: 50 μm.

6.4.4 Study of Orientation Mechanism on Nano-Micro Binary Polymer Brush Patterns

Based on the previous results, the cell orientation was proved to be manipulated by the nanoscale chemical cues of gelatin-PGMA nanolines. As a proof-of-concept experiments to study the orientation mechanism, the nano-micro binary polymer brushes patterns with different gelatin-PGMA nanoline space (2, 4, 6.7, 10 and 20 μm) were prepared as former methods. The cell culture experiments showed that cells were oriented on the substrates with 2, 4, 6.7 and 10 μm of space respectively (Figure 6.8a-d), while random distribution on the substrate which had 20-μm nanoline space (Figure 6.8e). After statistical analyzing by Image J software, it was found the angular distribution between cell axes and nanoline of 90 % of cells on the substrate with 6.7-μm nanoline space was less 5 °. The angular distribution between cell axes and nanoline of all cells on the substrates with 2-μm, 4-μm, and 10-μm nanoline space was less 20 °, 20 ° and 10 ° respectively. These results of statistical analysis quantitative showed the 6.7-μm nanoline space could apply the best orientation effect to the cells, and the 10-μm nanoline space took the second one.

The space of gelatin-PGMA nanoline was related to the gelatin density. Dense gelatin, i.e. 2-μm and 4-μm space which was less than cell size, could improve cell

adhesion while lost some ability of orientation control. However, sparse gelatin, such as 20-μm nanoline space that was large than cell size, could not induce a cell to orient well either. Remarkably, only moderate gelatin density, i.e. the nanoline space was close to cell size, could apply a suitable quantity of the nanoscale chemical cues, and induce optimum cell orientation effect.

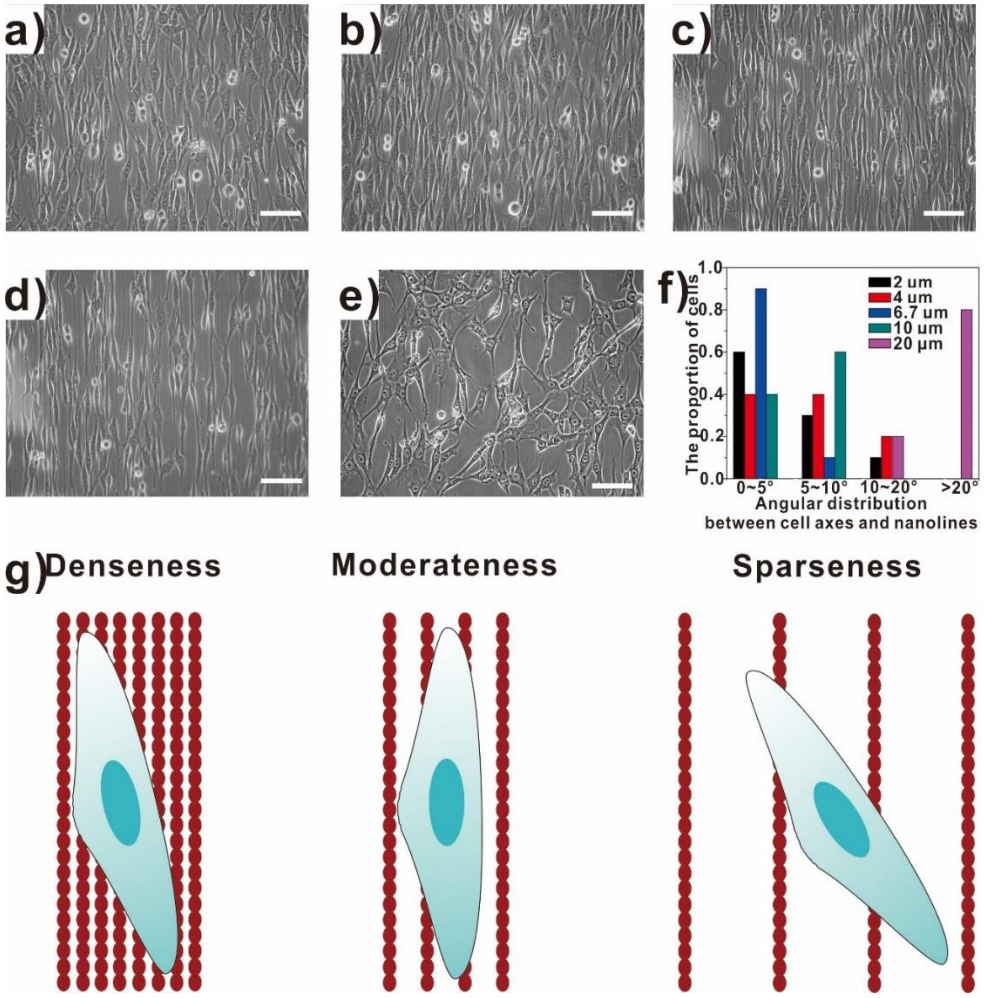

Figure 6.8. (a-e) Optical images of NIH-3T3 incubated on different nanoline space of gelatin-PGMA@PNIPAm surface for 24 hrs. (a) 2 μm; (b) 4 μm; (c) 6.7 μm; (d) 10 μm; (f) 20 μm. Scale bar: 100 μm. (f) Histogram of orientation effect on different nanoline space of the gelatin-PGMA@PNIPAm surface. (g) Mechanism schematic of the influence of nanoline space on cell orientation control effect.

6.5 Conclusions

In summary, biomimetic centimeter-sized nano-micro binary gelatin-

PGMA@PNIPAm brushes patterns, i.e. gelatin-PGMA nanolines spaced by microstriped PNIPAm brushes, were fabricated by 2D p-DNL and SI-ATRP. Such binary polymer brushes patterns provided ideal artificial ECM and showed excellent capability and flexibility to regulate cell orientation and attachment/detachment. As a proof-of-concept, NIH-3T3 cells were uniformly aligned on the binary gelatin-PGMA@PNIPAm brushes patterns, in which the gelatin-PGMA nanolines induced cell orientation. Therefore, the space of gelatin-PGMA nanoline is an important cue for well orientation effect. Only suitable nanoline space which is close to cell size could apply best orientation effect. Moreover, the PNIPAm brushes in the binary system were not only benefited to cell adhesion at 37 °C, but also employed to realize spontaneous cell detachment of the oriented cells from the substrate activated by decreasing temperature to 26 °C. Notably, the gelatin-PGMA@PNIPAm substrate with good cell orientation control and smart cell detachment properties could be reused at least three times. The smart detachment which led the cells to maintain oriented morphology is highly significant for regenerative engineering. Due to the abundant chemistry and topographical structures, this nano-micro binary polymer brushes patterns can be useful to control more kinds of cell behaviors in the future. Otherwise, such multi-scale and multi-component polymer brushes surfaces can be mass produced by using massively multiplexed lithography techniques [234-237] to promoting the study and applications of biomedical engineering in the future.

CHAPTER 7 BINARY POLYMER BRUSH PATTERNS FROM FACILE INITIATOR STICKINESS FOR CELL MICROPATTERNING STUDY

7.1 Introduction

The cellular microenvironment *in vivo* is the local surroundings of cells, such as extracellular matrix (ECM) and neighboring cells. It not only affects cell architecture, dynamics, and mechanics but also decides cell shape, gene expression and cell function [238]. For example, the size of microenvironment can limit cell volume and spread, while the orientation of microenvironment can induce cell alignment.

Historically, much of the understanding of cell biology comes from cell culture that cells are incubated in traditional cell culture dish. However, physiological cellular microenvironment contains highly complex composition and structure of the surfaces that contact cells [239]. When cells are incubated in tissue culture petri dish, although the cells can alive and proliferate, the adhesion surface of the traditional petri dish is simple, homogeneous, flat and rigid, leading to limited expression of cell functions. By contrast, micropatterning strategies for cell culture, which is called cell micropatterning technique, can mimic cellular microenvironment and control living cells selectively placing on a pre-patterned substrate surface [240-243]. Via cell micropatterning techniques, researchers can efficiently study cell sensitivity and response to specific environmental cues [238, 244], which are greatly useful in a range of applications (such as tissue engineering, cell-based drug screening, and fundamental cell biology studies) [240].

To target cell micropatterning, surface chemistry is widely used to generate a patterned surface to make cells selectively adhere. Polymer thin film [245-248], polymer gel [249], polymer brushes [160, 250-252] and SAMs [253] of small molecules as building blocks can be applied to modify the surface chemical properties of substrates. Among

them, the utilization of polymer brushes densely grafted on a substrate surface provides versatility on surface morphology control. Furthermore, polymer brushes possess superior advantages such as long-term stability, excellent mechanical and chemical robustness, and convenient processability [15]. The free-moving chains of polymer brushes can apply unique physical properties to the modified surface. In the last 15 years, several lithography methods, such as ion beam micropatterning [245], EBL [150], PL [247], and μCP [160], which are used to prepare polymer brushes micropatterns for cell micropatterning have been reported.

To successfully induce selective adhesion of cells, the substrate for cell micropatterning should be hybrid cell-adhesive and cell-inert materials. For example, Ober and co-workers [106] have used cell-adhesive PMATEC brushes micropatterns separated by cell-inert short PEG chains by photolithography to spatial control the growth of rat hippocampal neurons. Huck's group [254] used μCP to prepare ECM proteins micropatterns which were surrounded by cell-inert POEGMA brushes for directing the spreading of single cells. Most of the previous reports used one-component polymer brushes for cell micropatterning.

However, due to the excellent advantages of polymer brushes, the future development of this field will pay more attention to multi-component or binary polymer brushes with different chemistries systems. To date, limited references about binary polymer brushes patterns for cell micropatterning have been reported. The combination of SIP and expensive lithography techniques that based on light irradiation is the most commonly used method for fabricating such biomimetic binary polymer brushes patterns. The lack of a facile and cheap fabrication method for generating complex binary polymer brushes systems with well-designed topography and chemical cues has significantly impeded the development of this field.

Herein, we report a new and extremely simple method to fabricate micropatterned binary polymer brush systems for cell micropatterning. During previous binary polymer brush patterns study, we stumbled across a new phenomenon that the MUDBr initiator could be adsorbed by some kinds of polymer brushes (POEGMA, PGMA, and PHEMA). Accordingly, MUDBr micropatterns are easy to be transferred onto these

polymer brushes surfaces via a μCP technique which was fast, simple, cheap, and without light irradiation. The vertically patterned polymer brushes were then grown from the MUDBr micropatterns to form a binary polymer brush patterns. As a proof-of-concept, Human cervical carcinoma (HeLa) and NIH-3T3 cell micropatterning were demonstrated on the prepared binary polymer brush patterns.

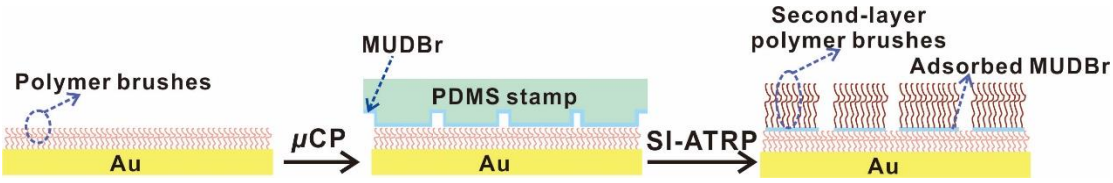

Figure 7.1. Schematic illustration of fabrication of vertically micropatterned binary polymer brush systems by μCP.

7.2 Materials

ATRP initiator MUDBr was kindly provided by Prof. Hongwei Ma, Suzhou Institute of Nano-Tech and Nano-Bionics. PBS (pH 7.4, 1 X; Gibco™), DMEM with high glucose (Gibco™), trypsin-EDTA (0.5%, Gibco™), FBS (South America origin; Gibco™), and penicillin-streptomycin (10,000 U/mL; Gibco™) were purchased from Thermo Fisher Scientific Inc. Rhod-phalloidin was obtained from Cytoskeleton Inc. NR9-8000 negative photoresist was brought from Futurrex Inc. All other chemicals were obtained from Sigma-Aldrich and used as received. Au substrates were prepared by thermal evaporation of 25 nm Au/5 nm Cr on <100> Si wafers with 500 nm SiO_2 on one side, and 15 nm Au/2 nm Cr on the glass wafer. The non-contact mode AFM tip was purchased from NanoSensors Inc.

7.3 Experimental

7.3.1 Substrate Modification

The various homogeneous polymer brushes (PMMA, POEGMA, PNIPAm, PGMA, PHEMA, PMAA, PSPM, and PMATEC) modified Au substrate were prepared

by SI-ATRP as the receipt mentioned in section 3.1.2, and then passivated by 0.1 M NaN_3 solution at 50 °C for more than 6 hrs.

7.3.2 Preparation of Vertically Patterned Binary Polymer Brushes Based on Facile Initiator Stickiness via *μ*CP and SI-ATRP

According to the MUDBr initiator-sticky property of some kinds of polymer brushes, the MUDBr micropatterns were generated on those polymer brushes coated-Au substrates by *μ*CP technique. The vertically patterned second-layer polymer brushes were then grown from the MUDBr micropatterns by SI-ATRP to obtain the binary polymer brush systems. The detailed procedures of the *μ*CP process and SI-ATRP proceeded as the strategies mentioned in section 3.1.2.

7.3.3 Gelatin Immobilization

The PGMA micropatterns on POEGMA brushes coated-Au substrate (PGMA@POEGMA) substrate were immersed into 10 mg/mL of gelatin in PBS at 37 °C for 24 h to immobilize gelatin. The resultant gelatin modified PGMA@ POEGMA (gelatin-PGMA@POEGMA) substrate was repeated washed by PBS solution to move the unfixed gelatin, and dried by nitrogen stream for cell culture experiments.

7.3.4 Cell Micropatterning

HeLa and NIH-3T3 cells were incubated in TCPS dishes in high glucose of DMEM medium with 5 % FBS and 1 % penicillin-streptomycin, and placed in an incubator with 75 % humidity and 5 % CO_2 at 37 °C. For cell behaviors study, the micropatterned gelatin-PGMA@POEGMA were put in 90 mm of TCPS dishes, and seeded with cells at a density of 3 x 10^5 cells/mL.

7.3.5 Fluorescence Dying of Cell micropatterning

Cells on micropatterned gelatin-PGMA@POEGMA surface were washed with PBS and fixed with 4% paraformaldehyde in PBS for 10 min at room temperature, and then permeabilized with 0.1% Triton™ X-100 in PBS for 3 min at room temperature and washed with PBS. These steps were repeated for three times. Next, the permeabilized cells were blocked with 1% BSA in PBS for 20 min. After being washed with PBS, the cells were incubated with 5 μg/mL of Rhod-phalloidin in dark place at 37 °C for 1 hr. Finally, the cells were rinsed with PBS and treated with 2.5 μg/mL of DAPI for 15 min at 37 °C for nuclei staining.

7.3.6 Characterization

The ATR-FTIR spectra were used to detect the surface chemistry of various polymer brushes coated-Au substrates and the vertically patterned binary polymer brushes. The drop shape analyzer was applied to detect the water contact angle of various polymer brushes coated-Au substrates. The optical microscope with the bright field was employed to observe the binary polymer brushes micropatterns and cell micropatterns. AFM topography in the air was measured by XE-100 AFM with the non-contact mode at ambient conditions. The CLSM microscopy was used to observe the stained cells.

7.4 Results and Discussions

7.4.1 Preparation of Various Polymer Brushes coated-Au substrates

In our previous experiments, we found that MUDBr could be adsorbed by POEGMA brushes by accident. And based this phenomenon, it would be very easy to fabricate binary polymer brushes system by simple binding MUDBr to POEGMA brushes surface. But how about another polymer brushes? Do another polymer brushes also can adsorb MUDBr initiator? Therefore, we prepared various polymer brushes

(PMMA, POEGMA, PNIPAm, PGMA, PHEMA, PMAA, PSPM, and PMATEC) surfaces and tried to find the answers. The SI-ATRP was applied to prepare various polymer brushes coated-Au substrates for the MUDBr stickiness study. The water contact angles of PMMA, POEGMA, PNIPAm, PGMA, and PHEMA at room temperature were 80 º, 45 º, 70 º, 77 º, and 46 º respectively.

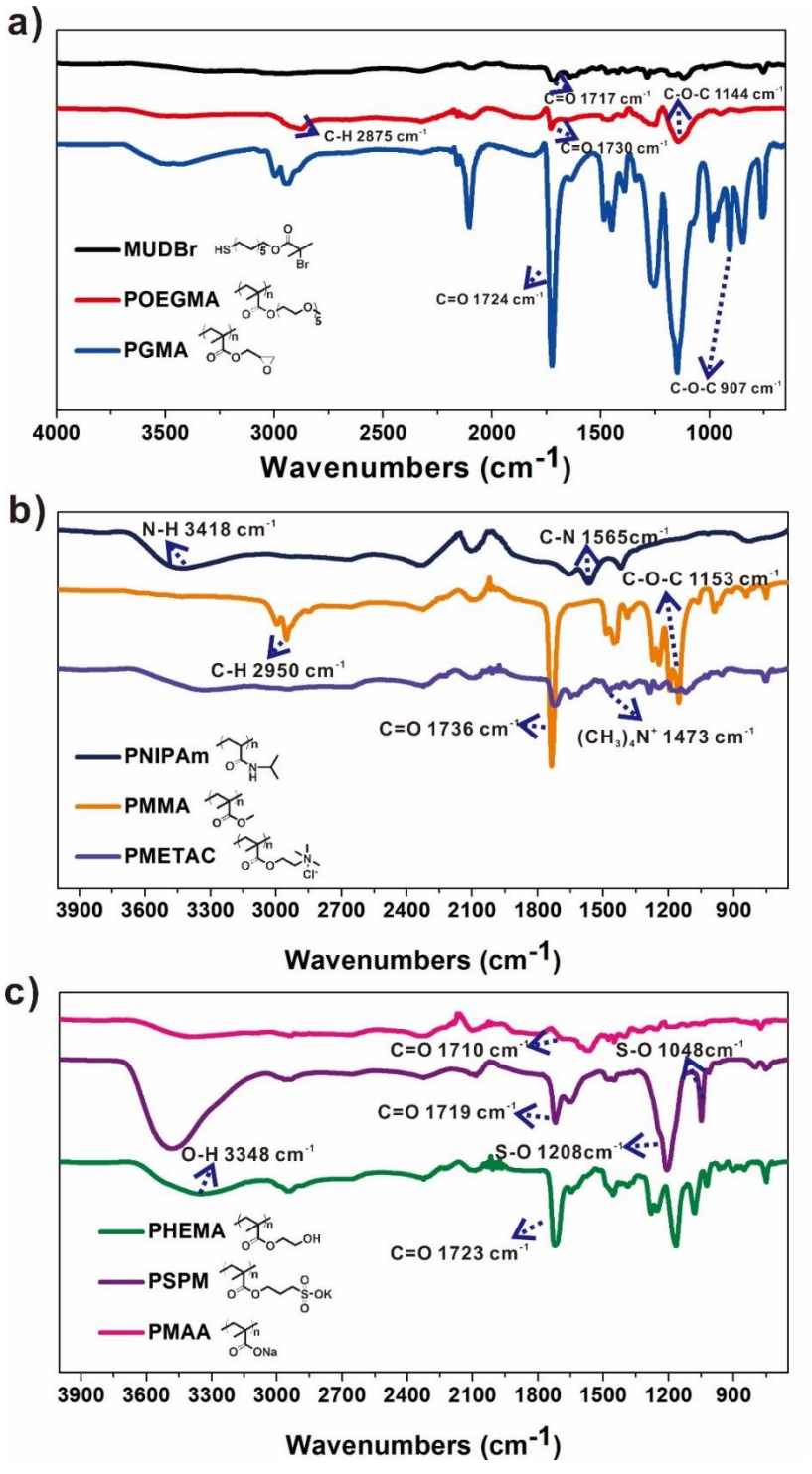

Figure 7.2. (a-c) ATR-FTIR spectra of MUDBr SAM and various polymer brushes

coated-Au substrates.

As shown in Figure 7.2, the ATR-FTIR was used to detect the surface chemistry of the various polymer brushes coated-Au substrates. A clear peak of C=O stretching of the carboxyl group at 1717 cm^{-1} was detected, indicating the successful binding of MUDBr initiator on Au surface for the next SI-ATRP. Furthermore, after SI-ATRP, the characteristic peaks of POEGMA, PGMA, PNIPAm, PMMA, PMETAC, PHEMA, PSPM, and PMAA brushes were observed at 1730 cm^{-1} (C=O stretching) [255], 907 cm^{-1} (C-O-C of epoxy group), 1565 cm^{-1} (C-N bond), 1736 cm^{-1} (C=O stretching) [256], 1473 cm^{-1} [$(CH_3)_4N^+$ bond bending vibration] [257], 3348 cm^{-1} (O-H bond) [258], 1248 and1048 cm^{-1} (O-S bond), and 1710 cm^{-1} (C=O stretching), respectively, indicating the successful polymerizations.

7.4.2 the Initiator Sticky Properties of Various Polymer Brushes coated-Au substrates

To study the initiator stickiness, the μCP method was employed. The μCP is a kind of soft lithographic technique that uses the relief patterns on an elastomeric PDMS stamp to fabricate patterns on a substrate surface by conformal contact. Briefly, the MUDBr initiator inked PDMS stamps contacted the polymer brushes surfaces for 30 s. With MUDBr initiator stickiness, the MUDBr micropatterns should be left on some polymer brushes surfaces after removing PDMS stamp. The vertically micropatterned binary polymer brushes systems were therefore prepared by second-step SI-ATRP of those surfaces that the polymer brushes adsorbed the MUDBr.

The results were observed by the optical microscopy (Figure 7.3a-f). It was clearly seen that the PGMA brushes squares on POEGMA brushes surface (PGMA@POEGMA), PGMA brushes grid on PHEMA brushes surface (PGMA@PHEMA), and second-layer PGMA brushes on PGMA brushes surface (PGMA@PGMA). These results indicated that binary polymer brushes systems could be prepared by our method on POEGMA, PGMA, and PHEMA brushes surfaces, i.e.

POEGMA, PGMA, and PHEMA brushes had MUDBr initiator-sticky ability. On the other hand, the surface of other polymer brushes coated-Au substrates had not vertically micropatterns after μCP and second-step SI-ATRP, meaning the other polymer brushes (PNIPAm, PMMA, PMETAC, PSPM, and PMAA) had not or very low initiator-sticky ability.

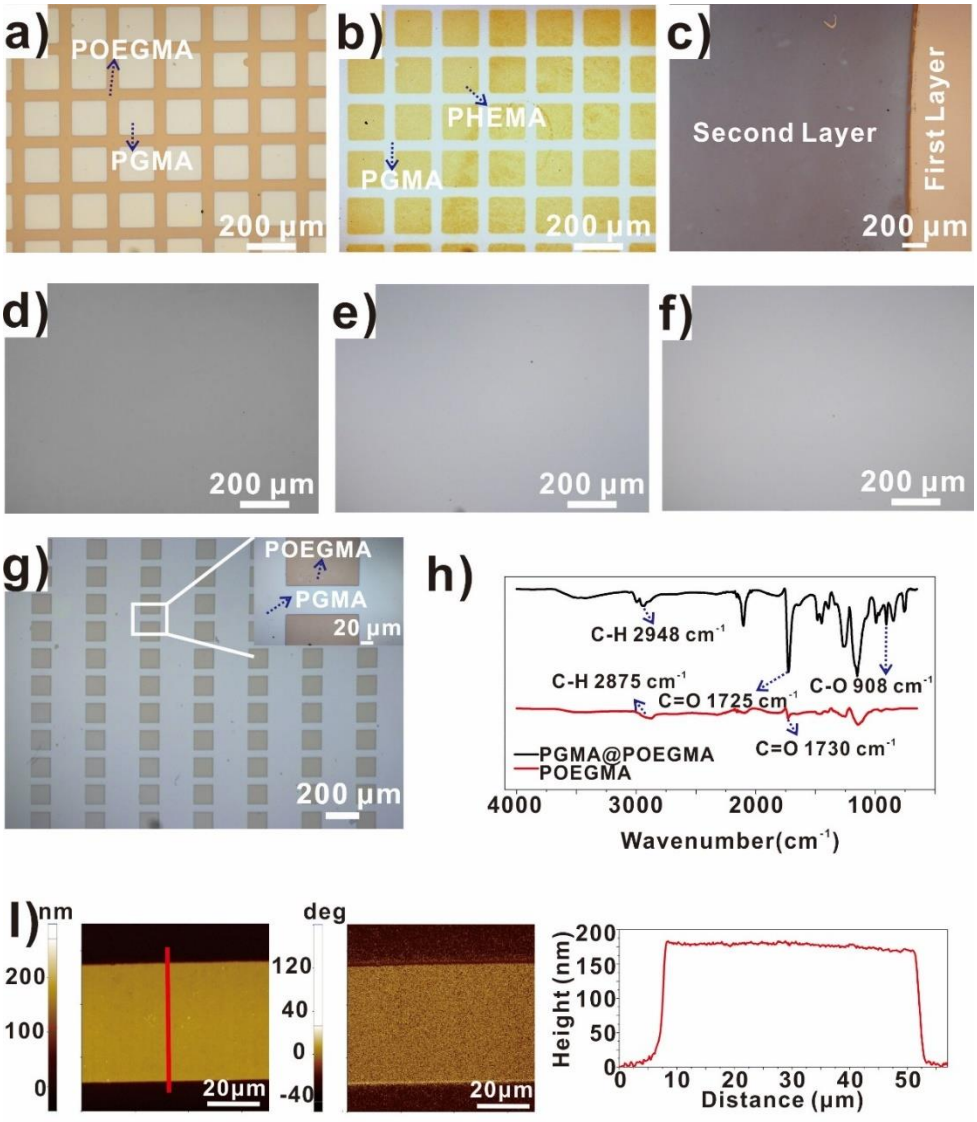

Figure 7.3. (a-f) Optical microscopic images of (a) POEGMA, (b) PHEMA, (c) PGMA (d) PMMA, (e) PMETAC and (f) PNIPAm brushes coated-Au substrates after microcontact printing of initiator and SI-ATRP process. (g) Optical microscopic images of PGMA grid on POEGMA surface, called PGMA@POEGMA. (h) ATR-FTIR spectra of POEGMA brushes coated Au substrate and PGMA@POEGMA sample. (i) AFM topographic view, corresponding phase view and cross-sectional profile of the PGMA

grid on POEGMA surface.

To study the details of the vertically micropatterned binary polymer brushes systems, PGMA@POEGMA sample was chosen to be observed due to its well-fabricated micropatterns showing a good initiator-sticky ability of POEGMA brushes which was the easiest to repeat. As a proof-of-concept, the ATR-FTIR of PGMA@POEGMA was detected (Figure 7.3h). Compared with the spectrum of POEGMA, main feature peaks of POEGMA were also found on the spectrum of PGMA@POEGMA. Also, C-O stretching of the epoxy group at 908 cm-1 became the evidence of the successful grafting of PGMA brushes. The AFM characterization (Figure 7.3i) showed that the PGMA microgrids on the POEGMA brushes surface were well-spatial controlled with a 175 nm-thickness additional the POEGMA layer.

The mechanism of the MUDBr initiator stickiness on POEGMA, PGMA, and PHEMA brushes surfaces were not very clear, maybe the possible hydrogen bond interaction between MUDBr and the three kinds of polymer brushes. However, the contact time during the μCP process could affect the quantity of adsorbed MUDBr on the three kinds of polymer brushes surfaces. As shown in Figure 7.4a-f, the thickness of PGMA grids on the POEGMA brushes surface increased from 14 nm to about 90 nm with the increase of contact time (5s to 60s). The longer contact time resulted in the more MUDBr adsorption. Otherwise, although the sticky mechanism was not clearly, the vertically micropatterned binary polymer brushes system was very stable. The PGMA squares on POEGMA brushes were still robust even being an ultrasonic treatment for 40 min (Figure 7.4g and h). Furthermore, we have used this simple method to prepare binary POEGMA@POEGMA, PMMA@POEGMA, PNIPAm@POEGMA successfully, and PMETAC@POEGMA brushes systems (Figure 7.4a-d). When using this facile method, we were easy to design versatile polymer micropatterns on the initiator-sticky polymer brushes surfaces for many applications in cell micropatterning. For the stability of such binary polymer brushes system, 80 nm-thick copper grid (the sheet resistance of copper grids was 1.85 Ω/□) could be deposed on the binary

PMETAC@POEGMA brushes surfaces by electroless deposition (ELD) [259].

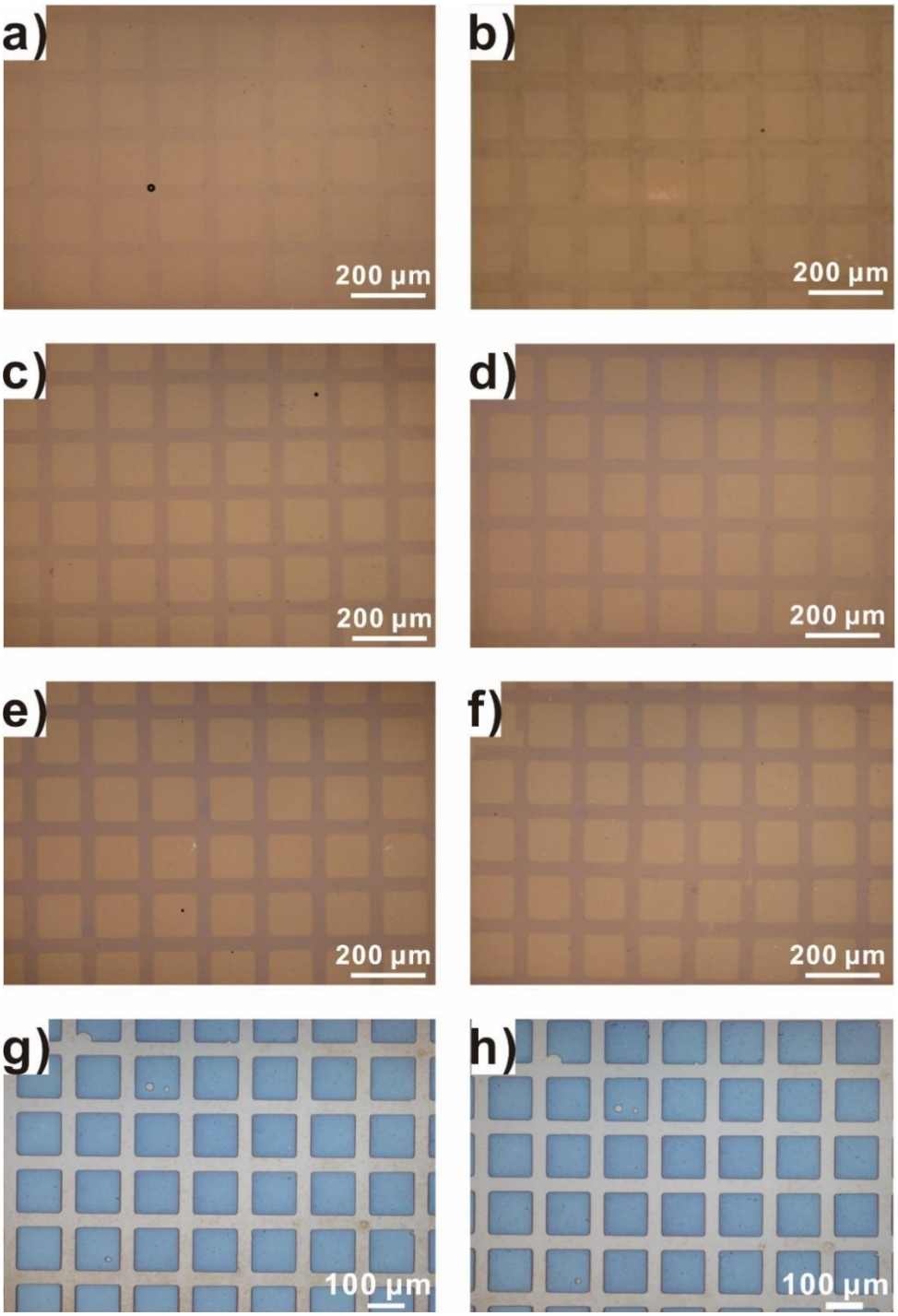

Figure 7.4. (a-f) Optical microscope images of the patterned PGMA brushes grid with a different contact time of PDMS stamp on POEGMA brushes coated Au substrate. (a) 5 s, (b) 10 s, (c) 15 s, (d) 20 s, (e) 45 s and (f) 60 s. (g-h) The stability of binary PGMA@POEGMA substrate in mix solution with ultrasonic. (g) 10 min of ultrasonic, (h) 40 min of ultrasonic.

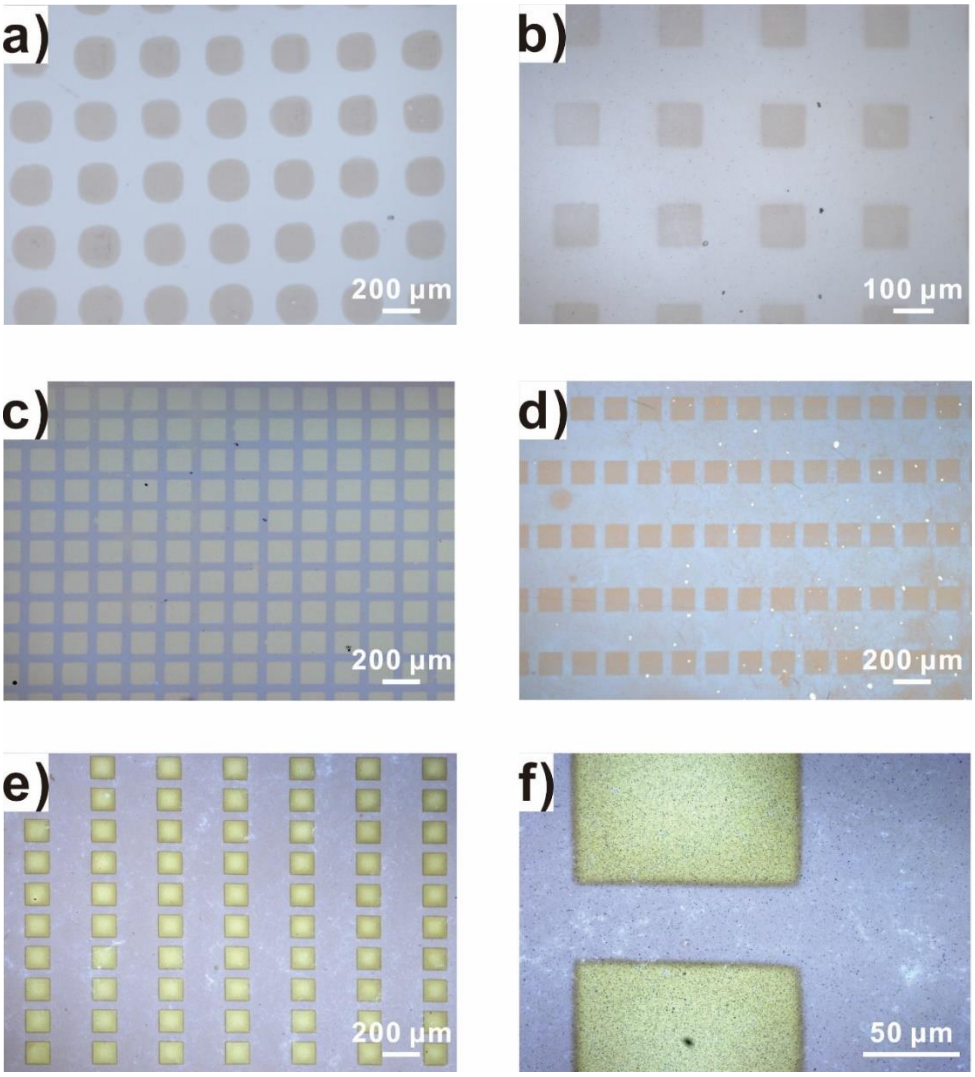

Figure 7.5. (a-d) Optical microscope images of the various binary system. (a) POEGMA dot array on POEGMA surface, called POEGMA@POEGMA, (b) PNIPAm square array on POEGMA surface, called PNIPAm@POEGMA, (c) PMMA grid on POEGMA surface, called PMMA@POEGMA and (d) PMETAC grid on POEGMA surface, called PMETAC@POEGMA. (e-f) Optical microscope images of copper deposition on PMETAC@POEGMA substrate. (e) 5X. (f) 50X.

7.4.3 Cell Micropatterning on Vertically Micropatterned Binary Polymer Brushes Substrates

To study the cell micropatterning on the binary system, the binary PGMA@POEGMA brushes systems on transparent Au substrates were chosen. As our previous experiments proved the PGMA brushes was cell-inert, the gelatin was bonded to the PGMA brushes for improving cell adhesion. Therefore, HeLa and NIH-3T3 cells were cultured on the gelatin-PGMA@POEGMA (micropatterned cell-adhesive gelatin-PGMA brushes separated by cell-inert POEGMA) brushes surface for cell micropatterning. For 24 hrs incubation, the HeLa cells adhered on the gelatin-PGMA grids, forming the cell micropatterning (Figure 7.6b) which could be maintained for even 5 days (Figure 7.6f).

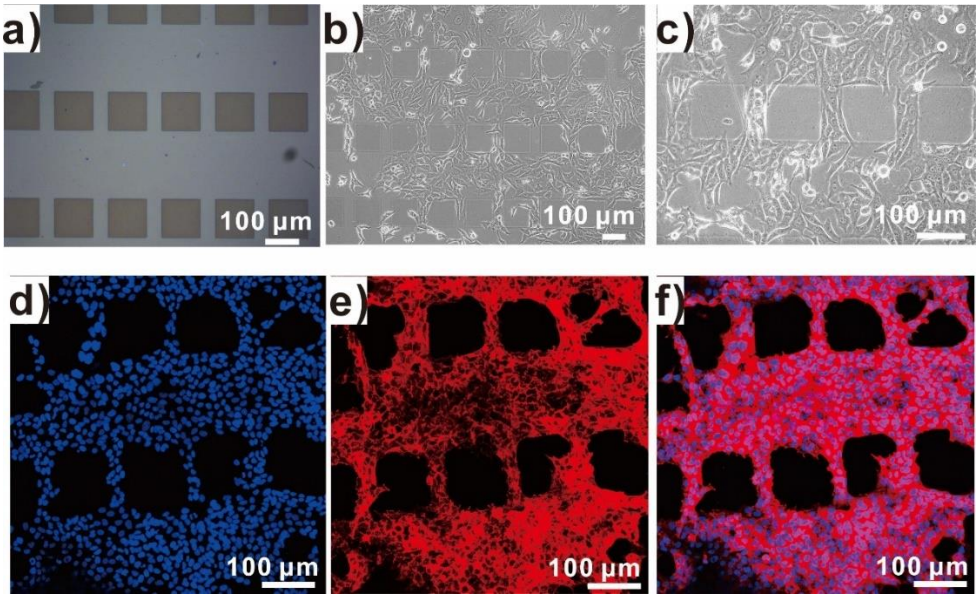

Figure 7.6. (a-c) Optical microscope images of (a) gelatin modified PGMA@POEGMA substrate, called gelatin-PGMA@POEGMA and (b-c) cell micropatterning of NIH-3T3 cells on gelatin-PGMA@POEGMA for 24 hrs. (d-f) CLSM images of NIH-3T3 cells incubated on the gelatin-PGMA@PNIPAm surface for 48 hr. Red and blue colors were the cell cytoskeleton and nucleus respectively.

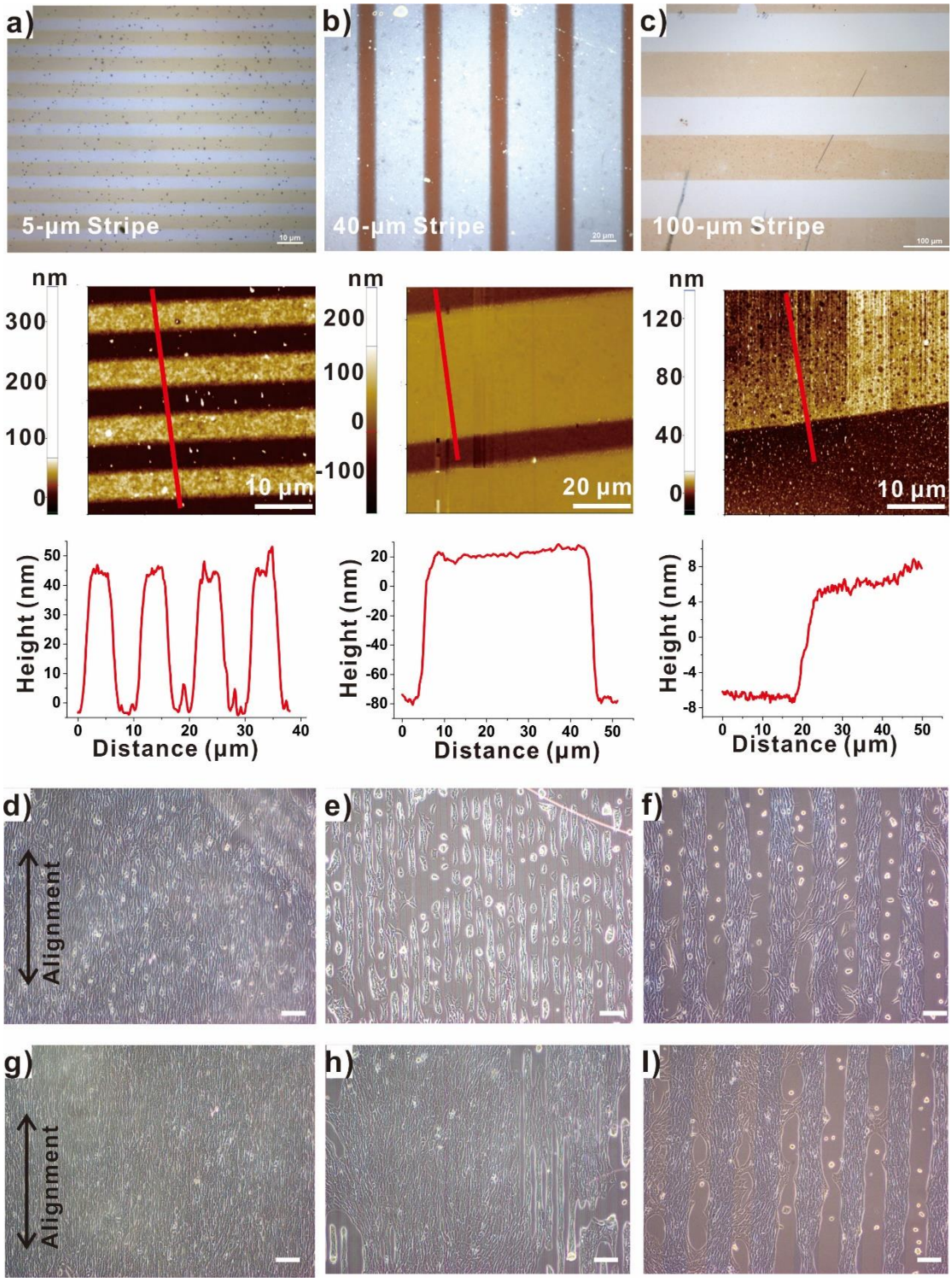

Figure 7.7. (a-c) The optical images, AFM topography and cross-section profiles of gelatin-PGMA stripes (5-, 40, 100-μm width) on POEGMA-glass. (d-i) The optical images of NIH-3T3 cells cultured on gelatin-PGMA stripes (5-, 40, 100-μm width) for 24 hrs (d-f) and 48 hrs (g-i).

Inspired by the cell orientation study on microstripes [148], we designed 100-, 40-,

and 5-μm width of gelatin-PGMA stripe patterns on POEGMA brushes surfaces. After incubated for 6 hrs on 100-, 40-microstriped gelatin-PGMA@POEGMA substrates, NIH-3T3 cells adhered without orientation on the gelatin-PGMA microstripes and started to form cell micropatterning when the width of microstripes was greater than cell width. Whereas, NIH-3T3 cells uniformly adhered on the gelatin-PGMA 5-μm microstripes the space was too narrow for cells to fabricating patterning, but cells were oriented regulated by the microstripes. After 24 hrs, clear cell micropatterning was formed on 100-, and 40-width of gelatin-PGMA stripe pattern, and cell orientation was still found well controlled on the 5-μm microstripes. These results could be attributed to 5 μm was slightly less than cell's width which applied suitable focal adhesion amount and was greatly benefited to regulate cell behaviors.

7.5 Conclusions

In this chapter, we utilized the MUDBr initiator-sticky ability of POEGMA, PHEMA, and PGMA brushes to fabricate vertically micropatterned binary polymer brushes substrates for cell micropatterning study. Notably, this new method was extremely simple and first time to be reported. The MUDBr micropatterns were vertically fabricated by μCP technique, and the second-layer polymer brushes of the binary system were then grown from the pre-patterned MUDBr by SI-ATRP. The thickness of second-layer polymer brushes depended on the print time of μCP. The robust adsorbed MUDBr increased with the contact time of the μCP process. Remarkedly, cell-inert POEGMA brushes had the most stable MUDBr initiator-sticky ability, allowing to grow multiple polymer brushes on its surface and continuous copper deposition. The binary polymer brushes patterns prepared by this extremely simple method, containing vertically micropatterned cell-adhesive gelatin-PGMA on cell-inert POEGMA brushes surface, were successfully applied for cell micropatterning and cell orientation. The stickiness of the original MUDBr micropattern on POEGMA, PHEMA and PGMA brushes surfaces is believed to have a range amount of applications, such as fundamental cell biology study, biosensors, and the understanding of cell behaviors.

CHAPTER 8 CONCLUSIONS AND SUGGESTIONS FOR FUTURE WORK

8.1 Conclusions

In this thesis, two lithography methods, i.e. DNL and μCP have been developed to fabricate large-area and high-resolution binary polymer brush patterns. The well-designed structures and surface chemistry of those binary polymer brush patterns have been studied by a series of characterization techniques, such as ATR-FTIR, XPS, optical microscopy and AFM. Furthermore, the applications of the obtained binary polymer brush patterns for precisely controlling cell behaviors have been demonstrated by NIH-3T3 and HeLa cells. The specific summary of each research chapter is discussed as follows.

In chapter 4, we have introduced the technical essential of DNL technique. The high-resolution, large-area, uniform and serial fabrication of one-component 2D and 3D polymer brush structures were then fabricated by single-tip DNL, 1D p-DNL, and 2D p-DNL. The MHA SAMs successfully prevented the Au surfaces from volatile initiators, which effectively improved the resolution of the patterned polymer brushes. With 2D p-DNL, we even could fabricate crossed Au nanorings with 220 nm-width on entire 1x 1 cm^2. It indicated that we could prepare high-resolution patterns with enough pattern areas for controlling cell behaviors. The understanding of the fundamental DNL technique was very important for the further improvement of DNL.

In Chapter 5, the *in-suit* repeated 1D p-DNL technique with manual alignment was developed to produced laterally patterned binary 3D PGMA@PMMA polymer brush structures. Different with one-component polymer brush patterns, the binary polymer brush patterns were required to be fabricated on a PMMA brush surface. The first-layer of PMMA chains made the second-layer polymer brushes more tightness and less collapse. Therefore, polymer brushes as resist layer can improve lateral resolution. The

binary 3D polymer brush structures contain more chemical, topographical, and mechanical properties, which may have great potential in manipulating cell behaviors and other applications.

In Chapter 6, biomimetic centimeter-sized nano-micro binary gelatin-PGMA@PNIPAm brush patterns were fabricated by integrating 2D p-DNL and SI-ATRP. Such binary polymer brush patterns were composed of cell-adhesive gelatin-PGMA nanolines spaced by microstriped cell-adhesive thin PNIPAm brush. In the cell culture experiments, NIH-3T3 cells uniformly adhered and were aligned on the reused binary gelatin-PGMA@PNIPAm brush patterns at 37 °C. The nanoscale chemistry cues of the gelatin-PGMA nanolines were proved to control cell orientation. When the space between two nanolines was close to cell size, the nanolines could apply preferable orientation effect. Furthermore, due to the conformation transformation of PNIPAm chains based on the thermal sensitivity, oriented cell could spontaneously detach from the substrate activated by decreasing temperature to 26 °C. This novel nano-micro binary polymer brush patterns are believed to be a promising low-cost, mass produced, and easy-accessible artificial ECM for biological applications in the future.

In Chapter 7, the serendipitous MUDBr initiator-sticky ability of POEGMA, PHEMA, and PGMA brushes allowed to develop a novel binary polymer brush patterns by simple μCP technique and SI-ATRP. With the increase of contact time (5 s to 60 s), the thickness of obtained second-layer PGMA brush increased from 14 nm to 90 nm. Cell micropatterning was successfully realized on gelatin-PGMA@POEGMA surface. Moreover, cell orientation could be controlled by 5 μm-width microstriped gelatin-PGMA@POEGMA. The stickiness of the original MUDBr micropattern on POEGMA, PHEMA, and PGMA brush surfaces is believed to have a range amount of applications, such as fundamental cell biology study, biosensors, and the understanding of cell behaviors.

8.2 Suggestions for Future Work

This research project focuses on the fabrication of different binary polymer brush

patterns and their applications in manipulating cell behaviors. We have developed a thermoresponsive nano-micro binary PGMA@PNIPAm brush patterns generated by 2D p-DNL and SI-ATRP to study cell orientation and smart detachment, and a binary PGMA@POEGMA brush micropatterns prepared by simple μCP technique and SI-ATRP to prepare cell micropatterning and control cell orientation. It should be noted that these works are the first attempt of its kind. Therefore, there are many challenges as well as opportunities to address in the future, e.g., the designation of binary and multi-component polymer brush systems, the adjustment of more complicated polymer structures and combinations, and the manipulation of other cell behaviors (such as cell differentiation). Detail outlooks are given as follows.

1. To date, the NIH-3T3 cells could align on the thermoresponsive nano-micro binary gelatin-PGMA@PNIPAm brush patterns generated by 2D p-DNL and SI-ATRP. It is well known that elongated morphology on line patterns is in favor of cardiomyocyte and osteogenic differentiation. Therefore, this nano-micro binary polymer brush patterns can be continually used for controlling stem cell orientation and next differentiation.

2. With the p-DNL technique, binary polymer brush patterns are. Accordingly, this method can be further developed to prepare multi-component and multiscale patterned polymer brushes in the future for better mimicking the real ECM and manipulating complex cell behaviors, such as cell migration and separation.

3. For the MUDBr initiator-sticky ability of POEGMA, PHEMA, and PGMA brushes, the sticky mechanism still has not been figured out. Although we have done some experiments, such as water contact angle test and XPS, the results are not adequate to give a clear clue to the sticky mechanism. More chemical analyses (such as energy dispersive X-ray detector and XPS) are needed for further investigation.

REFERENCE

[1] C. M. Niemeyer, C. A. Mirkin, *Nanobiotechnology: concepts, applications and perspectives, Vol. 1*, John Wiley & Sons, **2004**.

[2] N. M. Alves, I. Pashkuleva, R. L. Reis, J. F. Mano, *Small* **2010**, *6*, 2208-2220.

[3] D. K. Eric, Anchor Books, **1986**.

[4] R. Ogaki, M. Alexander, P. Kingshott, *Materials Today* **2010**, *13*, 22-35.

[5] D. F. Williams, *Biomaterials* **2008**, *29*, 2941-2953.

[6] P. Viswanathan, E. Themistou, K. Ngamkham, G. C. Reilly, S. P. Armes, G. Battaglia, *Biomacromolecules* **2014**, *16*, 66-75.

[7] E. K. Yim, K. W. Leong, *Nanomedicine: Nanotechnology, biology and medicine* **2005**, *1*, 10-21.

[8] D.-H. Kim, P. P. Provenzano, C. L. Smith, A. Levchenko, *The Journal of cell biology* **2012**, *197*, 351-360.

[9] R. O. Hynes, *Cell* **2002**, *110*, 673-687.

[10] C. A. Parent, P. N. Devreotes, *Science* **1999**, *284*, 765-770.

[11] J. P. Spatz, B. Geiger, *Methods in cell biology* **2007**, *83*, 89-111.

[12] T. Dvir, B. P. Timko, D. S. Kohane, R. Langer, *Nature nanotechnology* **2011**, *6*, 13-22.

[13] A. T. Nguyen, S. R. Sathe, E. K. Yim, *Journal of Physics: Condensed Matter* **2016**, *28*, 183001.

[14] A. Rastogi, M. Y. Paik, M. Tanaka, C. K. Ober, *ACS nano* **2010**, *4*, 771-780.

[15] S. Edmondson, V. L. Osborne, W. T. Huck, *Chemical society reviews* **2004**, *33*, 14-22.

[16] B. Geiger, J. P. Spatz, A. D. Bershadsky, *Nature reviews Molecular cell biology* **2009**, *10*, 21-33.

[17] M. M. Stevens, J. H. George, *Science* **2005**, *310*, 1135-1138.

[18] A. Curtis, C. Wilkinson, *Biomaterials* **1997**, *18*, 1573-1583.

[19] S. Ji, C.-C. Liu, G. Liu, P. F. Nealey, *ACS nano* **2009**, *4*, 599-609.

[20] O. Azzaroni, *Journal of Polymer Science Part A: Polymer Chemistry* **2012**, *50*, 3225-3258.

[21] F. Zhou, P. M. Biesheuvel, E.-Y. Choi, W. Shu, R. Poetes, U. Steiner, W. T. Huck, *Nano letters* **2008**, *8*, 725-730.

[22] J. Bünsow, T. S. Kelby, W. T. Huck, *Accounts of chemical research* **2009**, *43*, 466-474.

[23] A.-J. Wang, J.-J. Feng, J. Fan, *Journal of Chromatography A* **2008**, *1192*, 173-179.

[24] R. Barbey, H.-A. Klok, *Langmuir* **2010**, *26*, 18219-18230.

[25] P. Paoprasert, J. W. Spalenka, D. L. Peterson, R. E. Ruther, R. J. Hamers, P. G. Evans, P. Gopalan, *Journal of Materials Chemistry* **2010**, *20*, 2651-2658.

[26] F. Zhou, W. T. Huck, *Chemical communications* **2005**, 5999-6001.

[27] Y. Shen, L. Qi, X. Wei, R. Zhang, L. Mao, *Polymer* **2011**, *52*, 3725-3731.

[28] Z. Li, J. Wei, F. Shan, J. Yang, X. Wang, *Journal of Polymer Science Part B: Polymer Physics* **2008**, *46*, 751-758.

[29] C. Rodriguez-Emmenegger, E. Brynda, T. Riedel, M. Houska, V. Šubr, A. B. Alles, E. Hasan, J. E. Gautrot, W. T. Huck, *Macromolecular rapid communications* **2011**, *32*, 952-957.

[30] A. Hucknall, S. Rangarajan, A. Chilkoti, *Advanced Materials* **2009**, *21*, 2441-2446.

[31] P. Akkahat, V. P. Hoven, *Colloids and Surfaces B: Biointerfaces* **2011**, *86*, 198-205.

[32] G. Gao, D. Lange, K. Hilpert, J. Kindrachuk, Y. Zou, J. T. Cheng, M. Kazemzadeh-Narbat, K. Yu, R. Wang, S. K. Straus, *Biomaterials* **2011**, *32*, 3899-3909.
[33] M. Welch, A. Rastogi, C. Ober, *Soft Matter* **2011**, *7*, 297-302.
[34] N. Ayres, *Polymer Chemistry* **2010**, *1*, 769-777.
[35] P. M. Mendes, *Chemical Society Reviews* **2008**, *37*, 2512-2529.
[36] R. Barbey, E. Kauffmann, M. Ehrat, H.-A. Klok, *Biomacromolecules* **2010**, *11*, 3467-3479.
[37] S. Tugulu, A. Arnold, I. Sielaff, K. Johnsson, H.-A. Klok, *Biomacromolecules* **2005**, *6*, 1602-1607.
[38] S. Tugulu, P. Silacci, N. Stergiopulos, H.-A. Klok, *Biomaterials* **2007**, *28*, 2536-2546.
[39] R. Oren, Z. Liang, J. S. Barnard, S. C. Warren, U. Wiesner, W. T. Huck, *Journal of the American Chemical Society* **2009**, *131*, 1670-1671.
[40] X. Wang, H. Hu, Y. Shen, X. Zhou, Z. Zheng, *Advanced Materials* **2011**, *23*, 3090-3094.
[41] X. Liu, H. Chang, Y. Li, W. T. Huck, Z. Zheng, *ACS applied materials & interfaces* **2010**, *2*, 529-535.
[42] D. Paripovic, H.-A. Klok, *ACS applied materials & interfaces* **2011**, *3*, 910-917.
[43] Z. Liu, H. Hu, B. Yu, M. Chen, Z. Zheng, F. Zhou, *Electrochemistry Communications* **2009**, *11*, 492-495.
[44] O. Azzaroni, Z. Zheng, Z. Yang, W. T. Huck, *Langmuir* **2006**, *22*, 6730-6733.
[45] X. Zhou, X. Liu, Z. Xie, Z. Zheng, *Nanoscale* **2011**, *3*, 4929-4939.
[46] N. Yamada, T. Okano, H. Sakai, F. Karikusa, Y. Sawasaki, Y. Sakurai, *Die Makromolekulare Chemie, Rapid Communications* **1990**, *11*, 571-576.
[47] J. O. Zoppe, N. C. Ataman, P. Mocny, J. Wang, J. Moraes, H.-A. Klok, *Chemical Reviews* **2017**, *117*, 1105-1318.
[48] B. Zdyrko, I. Luzinov, *Macromolecular rapid communications* **2011**, *32*, 859-869.
[49] R. Barbey, L. Lavanant, D. Paripovic, N. Schüwer, C. Sugnaux, S. Tugulu, H.-A. Klok, *Chemical reviews* **2009**, *109*, 5437-5527.
[50] Y. Tsujii, K. Ohno, S. Yamamoto, A. Goto, T. Fukuda, in *Surface-initiated polymerization I*, Springer, **2006**, pp. 1-45.
[51] B. Yameen, A. Farrukh, *Chemistry, an Asian journal* **2013**, *8*, 1736-1753.
[52] K. Matyjaszewski, J. Xia, *Chemical reviews* **2001**, *101*, 2921-2990.
[53] K. Matyjaszewski, *Macromolecules* **2012**, *45*, 4015-4039.
[54] G. Morandi, L. Heath, W. Thielemans, *Langmuir* **2009**, *25*, 8280-8286.
[55] J. Raula, J. Shan, M. Nuopponen, A. Niskanen, H. Jiang, E. I. Kauppinen, H. Tenhu, *Langmuir* **2003**, *19*, 3499-3504.
[56] G. Zhai, W. Yu, E. Kang, K. Neoh, C. Huang, D. Liaw, *Industrial & engineering chemistry research* **2004**, *43*, 1673-1680.
[57] R. Matsuno, K. Yamamoto, H. Otsuka, A. Takahara, *Macromolecules* **2004**, *37*, 2203-2209.
[58] L. Ghannam, J. Parvole, G. Laruelle, J. Francois, L. Billon, *Polymer international* **2006**, *55*, 1199-1207.
[59] J. E. Krause, N. D. Brault, Y. Li, H. Xue, Y. Zhou, S. Jiang, *Macromolecules* **2011**, *44*, 9213-9220.
[60] N. Luo, J. B. Hutchison, K. S. Anseth, C. N. Bowman, *Macromolecules* **2002**, *35*, 2487-2493.
[61] A. Simakova, S. E. Averick, D. Konkolewicz, K. Matyjaszewski, *Macromolecules* **2012**, *45*, 6371-6379.

[62] B. T. Cheesman, J. D. Willott, G. B. Webber, S. Edmondson, E. J. Wanless, *ACS Macro Letters* **2012**, *1*, 1161-1165.

[63] M. M. Pradas, M. J. Vicent, *Polymers in Regenerative Medicine: Biomedical Applications from Nano-to Macro-structures*, John Wiley & Sons, **2015**.

[64] A. A. Khalili, M. R. Ahmad, *International journal of molecular sciences* **2015**, *16*, 18149-18184.

[65] G. Margaret, S. Ulrich, *Journal of Physics: Condensed Matter* **2010**, *22*, 190301.

[66] L. De Bartolo, A. Bader, *Biomaterials for Stem Cell Therapy: State of Art and Vision for the Future*, CRC Press, **2013**.

[67] A. Kikuchi, T. Okano, *Journal of Controlled Release* **2005**, *101*, 69-84.

[68] E. Ito, K. Suzuki, M. Yamato, M. Yokoyama, Y. Sakurai, T. Okano, *Journal of biomedical materials research* **1998**, *42*, 148-155.

[69] C. Nojiri, T. Okano, H. Koyanagi, S. Nakahama, K. D. Park, S. W. Kim, *Journal of Biomaterials Science, Polymer Edition* **1993**, *4*, 75-88.

[70] J. D. Sipe, *Annals of the New York Academy of Sciences* **2002**, *961*, 1-9.

[71] F. Grinnell, *The Journal of cell biology* **1986**, *103*, 2697-2706.

[72] A. J. García, in *Polymers for regenerative medicine*, Springer, **2006**, pp. 171-190.

[73] X. Liu, L. Yuan, D. Li, Z. Tang, Y. Wang, G. Chen, H. Chen, J. L. Brash, *Journal of Materials Chemistry B* **2014**, *2*, 5718-5738.

[74] H. Chen, L. Yuan, W. Song, Z. Wu, D. Li, *Progress in Polymer Science* **2008**, *33*, 1059-1087.

[75] A. Rosenhahn, S. Schilp, H. J. Kreuzer, M. Grunze, *Physical Chemistry Chemical Physics* **2010**, *12*, 4275-4286.

[76] T. Okano, N. Yamada, M. Okuhara, H. Sakai, Y. Sakurai, *Biomaterials* **1995**, *16*, 297-303.

[77] R. E. Holmlin, X. Chen, R. G. Chapman, S. Takayama, G. M. Whitesides, *Langmuir* **2001**, *17*, 2841-2850.

[78] E. Lih, S. H. Oh, Y. K. Joung, J. H. Lee, D. K. Han, *Progress in Polymer Science* **2015**, *44*, 28-61.

[79] Y. Higaki, M. Kobayashi, D. Murakami, A. Takahara, *Polymer Journal* **2016**, *48*, 325-331.

[80] E. H. Leduc, S. Holt, *The Journal of cell biology* **1965**, *26*, 137-155.

[81] C. Leng, H.-C. Hung, S. Sun, D. Wang, Y. Li, S. Jiang, Z. Chen, *ACS applied materials & interfaces* **2015**, *7*, 16881-16888.

[82] N. D. Winblade, I. D. Nikolic, A. S. Hoffman, J. A. Hubbell, *Biomacromolecules* **2000**, *1*, 523-533.

[83] K. L. Prime, G. M. Whitesides, *Science* **1991**, *252*, 1164.

[84] Y. Wei, J. Zhang, H. Li, L. Zhang, H. Bi, *Journal of Biomaterials Science, Polymer Edition* **2015**, *26*, 1357-1371.

[85] N. Zhang, T. Pompe, I. Amin, R. Luxenhofer, C. Werner, R. Jordan, *Macromolecular bioscience* **2012**, *12*, 926-936.

[86] R. Konradi, B. Pidhatika, A. Mühlebach, M. Textor, *Langmuir* **2008**, *24*, 613-616.

[87] N. Zhang, T. Pompe, I. Amin, R. Luxenhofer, C. Werner, R. Jordan, *Macromolecular Bioscience* **2012**, *12*, 926-936.

[88] A. de los Santos Pereira, S. Sheikh, C. Blaszykowski, O. Pop-Georgievski, K. Fedorov, M. Thompson, C. Rodriguez-Emmenegger, *Biomacromolecules* **2016**, *17*, 1179-1185.

[89] D. Fairhurst, R. Rowell, I. Monahan, S. Key, D. Stieh, F. McNeil-Watson, A. Morfesis, M. Mitchnick, R. Shattock, *Langmuir* **2007**, *23*, 2680-2687.

[90] Y. Xia, C. Cheng, R. Wang, C. He, L. Ma, C. Zhao, *Colloids and Surfaces B: Biointerfaces* **2016**, *139*, 199-210.
[91] K. Chen, S. Zhou, L. Wu, *RSC Advances* **2015**, *5*, 104907-104914.
[92] W. Zheng, W. Zhang, X. Jiang, *Advanced healthcare materials* **2013**, *2*, 95-108.
[93] F. Xu, Z. Wang, W. Yang, *Biomaterials* **2010**, *31*, 3139-3147.
[94] S. Yuan, G. Xiong, A. Roguin, C. Choong, *Biointerphases* **2012**, *7*, 30.
[95] F. Grinnell, M. Feld, *J Biol Chem* **1982**, *257*, 4888-4893.
[96] K. Hazen, D. Brawner, M. Riesselman, M. Jutila, J. Cutler, *Infection and immunity* **1991**, *59*, 907-912.
[97] Y. Arima, H. Iwata, *Biomaterials* **2007**, *28*, 3074-3082.
[98] D. S. Benoit, M. P. Schwartz, A. R. Durney, K. S. Anseth, *Nature materials* **2008**, *7*, 816-823.
[99] J. Y. Lim, M. C. Shaughnessy, Z. Zhou, H. Noh, E. A. Vogler, H. J. Donahue, *Biomaterials* **2008**, *29*, 1776-1784.
[100] W. Feng, S. Zhu, K. Ishihara, J. L. Brash, *Langmuir* **2005**, *21*, 5980-5987.
[101] Y. Inoue, T. Nakanishi, K. Ishihara, *Langmuir* **2013**, *29*, 10752-10758.
[102] R. Iwata, P. Suk-In, V. P. Hoven, A. Takahara, K. Akiyoshi, Y. Iwasaki, *Biomacromolecules* **2004**, *5*, 2308.
[103] Y. Inoue, K. Ishihara, *Colloids and Surfaces B: Biointerfaces* **2010**, *81*, 350-357.
[104] K. Fukazawa, A. Nakao, M. Maeda, K. Ishihara, *ACS Applied Materials & Interfaces* **2016**, *8*, 24994-24998.
[105] J. Wei, M. Yoshinari, S. Takemoto, M. Hattori, E. Kawada, B. Liu, Y. Oda, *Journal of Biomedical Materials Research Part B: Applied Biomaterials* **2007**, *81B*, 66-75.
[106] R. Dong, R. P. Molloy, M. Lindau, C. K. Ober, *Biomacromolecules* **2010**, *11*, 2027-2032.
[107] M. M. Gentleman, E. Gentleman, *International Materials Reviews* **2014**, *59*, 417-429.
[108] J. Schakenraad, H. Busscher, *Colloids and surfaces* **1989**, *42*, 331-343.
[109] Y. Yang, K. Kulangara, R. T. Lam, R. Dharmawan, K. W. Leong, *ACS nano* **2012**, *6*, 8591-8598.
[110] A. H. Poulsson, S. A. Mitchell, M. R. Davidson, A. J. Johnstone, N. Emmison, R. H. Bradley, *Langmuir* **2009**, *25*, 3718-3727.
[111] J. Wei, T. Igarashi, N. Okumori, T. Igarashi, T. Maetani, B. Liu, M. Yoshinari, *Biomedical Materials* **2009**, *4*, 045002.
[112] E. Bolbasov, L. Antonova, V. Matveeva, V. Novikov, E. Shesterikov, N. Bogomolova, A. Golovkin, S. Tverdohlebov, O. Barbarash, L. Barbarash, *Biomeditsinskaia khimiia* **2016**, *62*, 56-63.
[113] J. Comelles, M. Estévez, E. Martínez, J. Samitier, *Nanomedicine: Nanotechnology, Biology and Medicine* **2010**, *6*, 44-51.
[114] N. J. Hallab, K. J. Bundy, K. O'Connor, R. L. Moses, J. J. Jacobs, *Tissue engineering* **2001**, *7*, 55-71.
[115] E. M. Harnett, J. Alderman, T. Wood, *Colloids and surfaces B: Biointerfaces* **2007**, *55*, 90-97.
[116] L. Ponsonnet, K. Reybier, N. Jaffrezic, V. Comte, C. Lagneau, M. Lissac, C. Martelet, *Materials Science and Engineering: C* **2003**, *23*, 551-560.
[117] S. A. Redey, M. Nardin, D. Bernache–Assolant, C. Rey, P. Delannoy, L. Sedel, P. J. Marie, *Journal of biomedical materials research* **2000**, *50*, 353-364.
[118] E. S. Gil, S. M. Hudson, *Progress in polymer science* **2004**, *29*, 1173-1222.
[119] J. F. Mano, *Advanced Engineering Materials* **2008**, *10*, 515-527.

[120] K. Nagase, J. Kobayashi, T. Okano, *Journal of the Royal Society Interface* **2009**, *6*, S293-S309.
[121] N. Yamada, T. Okano, H. Sakai, F. Karikusa, Y. Sawasaki, Y. Sakurai, *Die Makromolekulare Chemie, Rapid Communications* **1990**, *11*, 571-576.
[122] J. Yang, M. Yamato, C. Kohno, A. Nishimoto, H. Sekine, F. Fukai, T. Okano, *Biomaterials* **2005**, *26*, 6415-6422.
[123] M. Yamato, T. Okano, *Materials Today* **2004**, *7*, 42-47.
[124] E. Wischerhoff, K. Uhlig, A. Lankenau, H. G. Börner, A. Laschewsky, C. Duschl, J. F. Lutz, *Angewandte Chemie International Edition* **2008**, *47*, 5666-5668.
[125] A. Dworak, A. Utrata-Wesołek, D. Szweda, A. Kowalczuk, B. Trzebicka, J. Anioł, A. L. Sieroń, A. Klama-Baryła, M. Kawecki, *ACS applied materials & interfaces* **2013**, *5*, 2197-2207.
[126] B. Byambaa, T. Konno, K. Ishihara, *Reactive and Functional Polymers* **2016**, *104*, 30-37.
[127] J.-F. Lutz, Ö. Akdemir, A. Hoth, *Journal of the American Chemical Society* **2006**, *128*, 13046-13047.
[128] J.-i. Edahiro, K. Sumaru, Y. Tada, K. Ohi, T. Takagi, M. Kameda, T. Shinbo, T. Kanamori, Y. Yoshimi, *Biomacromolecules* **2005**, *6*, 970-974.
[129] A. J. Engler, S. Sen, H. L. Sweeney, D. E. Discher, *Cell* **2006**, *126*, 677-689.
[130] R. K. Das, O. F. Zouani, *Biomaterials* **2014**, *35*, 5278-5293.
[131] P.-Y. Wang, W.-B. Tsai, N. H. Voelcker, *Acta biomaterialia* **2012**, *8*, 519-530.
[132] S. V. Plotnikov, A. M. Pasapera, B. Sabass, C. M. Waterman, *Cell* **2012**, *151*, 1513-1527.
[133] K. Nam, R. Fukaya, Y. Hashimoto, Y. Ito, T. Kimura, A. Kishida, *Chemistry letters* **2010**, *39*, 1164-1165.
[134] C. Yoshikawa, A. Goto, Y. Tsujii, T. Fukuda, T. Kimura, K. Yamamoto, A. Kishida, *Macromolecules* **2006**, *39*, 2284-2290.
[135] I. Lilge, H. Schönherr, *Angewandte Chemie* **2016**, *128*, 13308-13311.
[136] X. Liu, S. Wang, *Chemical Society Reviews* **2014**, *43*, 2385-2401.
[137] J. Ouyang, M. Chen, W.-J. Bao, Q.-W. Zhang, K. Wang, X.-H. Xia, *Advanced Functional Materials* **2015**, *25*, 6122-6130.
[138] L. Hao, J. Lawrence, *Proceedings of the Institution of Mechanical Engineers, Part H: Journal of Engineering in Medicine* **2006**, *220*, 47-55.
[139] F. J. O'Brien, B. A. Harley, I. V. Yannas, L. J. Gibson, *Biomaterials* **2005**, *26*, 433-441.
[140] J.-Q. Meng, C.-L. Chen, L.-P. Huang, Q.-Y. Du, Y.-F. Zhang, *Applied Surface Science* **2011**, *257*, 6282-6290.
[141] X. Shi, Y. Wang, D. Li, L. Yuan, F. Zhou, Y. Wang, B. Song, Z. Wu, H. Chen, J. L. Brash, *Langmuir* **2012**, *28*, 17011-17018.
[142] T. Azuma, Y. Teramura, M. Takai, *ACS applied materials & interfaces* **2016**, *8*, 10710-10716.
[143] T.-H. Kim, S. Shah, L. Yang, P. T. Yin, M. K. Hossain, B. Conley, J.-W. Choi, K.-B. Lee, *ACS nano* **2015**, *9*, 3780-3790.
[144] M. P. Prabhakaran, E. Vatankhah, D. Kai, S. Ramakrishna, *International Journal of Polymeric Materials and Polymeric Biomaterials* **2015**, *64*, 338-353.
[145] Q. Yu, L. K. Ista, R. Gu, S. Zauscher, G. P. López, *Nanoscale* **2016**, *8*, 680-700.
[146] T. Chen, I. Amin, R. Jordan, *Chemical Society Reviews* **2012**, *41*, 3280-3296.
[147] M. Han, W. Lee, S.-K. Lee, S. S. Lee, *Sensors and Actuators A: Physical* **2004**, *111*, 14-20.
[148] H. Takahashi, M. Nakayama, K. Itoga, M. Yamato, T. Okano, *Biomacromolecules* **2011**, *12*, 1414-1418.

[149] F. Yu, P. Li, H. Shen, S. Mathur, C.-M. Lehr, U. Bakowsky, F. Mücklich, *Biomaterials* **2005**, *26*, 2307-2312.
[150] Q. Yu, L. M. Johnson, G. P. López, *Advanced Functional Materials* **2014**, *24*, 3751-3759.
[151] T. Kamada, Y. Yamazawa, T. Nakaji-Hirabayashi, H. Kitano, Y. Usui, Y. Hiroi, T. Kishioka, *Colloids and Surfaces B: Biointerfaces* **2014**, *123*, 878-886.
[152] Q. Yu, L. K. Ista, R. Gu, S. Zauscher, G. P. Lopez, *Nanoscale* **2016**, *8*, 680-700.
[153] C. Vieu, F. Carcenac, A. Pepin, Y. Chen, M. Mejias, A. Lebib, L. Manin-Ferlazzo, L. Couraud, H. Launois, *Appl. Surf. Sci.* **2000**, *164*, 111-117.
[154] N. Idota, T. Tsukahara, K. Sato, T. Okano, T. Kitamori, *Biomaterials* **2009**, *30*, 2095-2101.
[155] N. Gomez, J. Y. Lee, J. D. Nickels, C. E. Schmidt, *Advanced functional materials* **2007**, *17*, 1645-1653.
[156] G. M. Whitesides, E. Ostuni, S. Takayama, X. Jiang, D. E. Ingber, *Annual review of biomedical engineering* **2001**, *3*, 335-373.
[157] A. Kumar, G. M. Whitesides, *Appl. Phys. Lett.* **1993**, *63*, 2002-2004.
[158] H.-W. Li, B. V. Muir, G. Fichet, W. T. Huck, *Langmuir* **2003**, *19*, 1963-1965.
[159] J. E. Gautrot, B. Trappmann, F. Oceguera-Yanez, J. Connelly, X. He, F. M. Watt, W. T. S. Huck, *Biomaterials* **2010**, *31*, 5030-5041.
[160] K. Y. Tan, H. Lin, M. Ramstedt, F. M. Watt, W. T. Huck, J. E. Gautrot, *Integr. Biol.* **2013**, *5*, 899-910.
[161] S. H. Lee, H. E. Jeong, M. C. Park, J. Y. Hur, H. S. Cho, S. H. Park, K. Y. Suh, *Adv. Mater.* **2008**, *20*, 788-792.
[162] C. Carbonell, A. B. Braunschweig, *Acc. Chem. Res.* **2016**.
[163] S. Sekula, J. Fuchs, S. Weg-Remers, P. Nagel, S. Schuppler, J. Fragala, N. Theilacker, M. Franzreb, C. Wingren, P. Ellmark, C. A. K. Borrebaeck, C. A. Mirkin, H. Fuchs, S. Lenhert, *Small* **2008**, *4*, 1785-1793.
[164] G. Arrabito, S. Reisewitz, L. Dehmelt, P. I. Bastiaens, B. Pignataro, H. Schroeder, C. M. Niemeyer, *Small* **2013**, *9*, 4243-4249.
[165] S. Laing, R. Suriano, D. A. Lamprou, C.-A. Smith, M. J. Dalby, S. Mabbott, K. Faulds, D. Graham, *ACS Appl. Mat. Inter.* **2016**, *8*, 24844-24852.
[166] Z. Xie, C. Chen, X. Zhou, T. Gao, D. Liu, Q. Miao, Z. Zheng, *ACS Applied Materials & Interfaces* **2014**, *6*, 11955-11964.
[167] R. R. Shah, D. Merreceyes, M. Husemann, I. Rees, N. L. Abbott, C. J. Hawker, J. L. Hedrick, *Macromolecules* **2000**, *33*, 597-605.
[168] X. Liu, Y. Li, Z. Zheng, *Nanoscale* **2010**, *2*, 2614-2618.
[169] G. Binnig, C. F. Quate, C. Gerber, *Physical review letters* **1986**, *56*, 930.
[170] X. Zhou, Z. Liu, Z. Xie, X. Liu, Z. Zheng, *Small* **2012**, *8*, 3568-3572.
[171] C. Chen, X. Zhou, Z. Xie, T. Gao, Z. Zheng, *Small* **2015**, *11*, 613-621.
[172] X. Zhou, X. Wang, Y. Shen, Z. Xie, Z. Zheng, *Angew. Chem. Int. Ed. Engl.* **2011**, *50*, 6506-6510.
[173] J. Haaheim, V. Val, J. Bussan, S. Rozhok, J. W. Jang, J. Fragala, M. Nelson, *Scanning* **2010**, *32*, 49-59.
[174] Q. He, A. Kueller, S. Schilp, F. Leisten, H.-A. Kolb, M. Grunze, J. Li, *Small* **2007**, *3*, 1860-1865.
[175] S. Schilp, N. Ballav, M. Zharnikov, *Angew. Chem. Int. Ed.* **2008**, *47*, 6786-6789.
[176] M. Steenackers, R. Jordan, A. Kuller, M. Grunze, *Adv. Mater.* **2009**, *21*, 2921-2925.

[177] M. Steenackers, A. Kueller, N. Ballav, M. Zharnikov, M. Grunze, R. Jordan, *Small* **2007**, *3*, 1764-1773.
[178] X. G. Liu, S. W. Guo, C. A. Mirkin, *Angew. Chem. Int. Ed.* **2003**, *42*, 4785-4789.
[179] H. W. Ma, J. H. Hyun, P. Stiller, A. Chilkoti, *Adv. Mater.* **2004**, *16*, 338-341.
[180] X. C. Zhou, X. L. Wang, Y. D. Shen, Z. Xie, Z. J. Zheng, *Angew. Chem. Int. Ed. Engl.* **2011**, *50*, 6506-6510.
[181] M. Hirtz, M. K. Brinks, S. Miele, A. Studer, H. Fuchs, L. Chi, *Small* **2009**, *5*, 919-923.
[182] T. Gan, X. Zhou, C. Ma, X. Liu, Z. Xie, G. Zhang, Z. Zheng, *Small* **2013**, *9*, 2851-2856.
[183] C. Schuh, S. Santer, O. Prucker, J. Ruhe, *Adv. Mater.* **2009**, *21*, 4706-4710.
[184] J. E. Poelma, B. P. Fors, G. F. Meyers, J. W. Kramer, C. J. Hawker, *Angew. Chem. Int. Ed.* **2013**, *52*, 6844-6848.
[185] B. P. Fors, J. E. Poelma, M. S. Menyo, M. J. Robb, D. M. Spokoyny, J. W. Kramer, J. H. Waite, C. J. Hawker, *J. Am. Chem. Soc.* **2013**, *135*, 14106-14109.
[186] E. M. Benetti, C. Acikgoz, X. Sui, B. Vratzov, M. A. Hempenius, J. Huskens, G. J. Vancso, *Adv. Funct. Mater.* **2011**, *21*, 2088-2095.
[187] I. W. Moran, J. R. Ell, K. R. Carter, *Small* **2011**, *7*, 2669-2674.
[188] Y. F. Li, J. H. Zhang, L. P. Fang, L. M. Jiang, W. D. Liu, T. Q. Wang, L. Y. Cui, H. C. Sun, B. Yang, *J. Mater. Chem.* **2012**, *22*, 25116-25122.
[189] M. Wang, J. E. Comrie, Y. P. Bai, X. M. He, S. Y. Guo, W. T. S. Huck, *Adv. Funct. Mater.* **2009**, *19*, 2236-2243.
[190] T. Chen, J. M. Zhong, D. P. Chang, A. Carcia, S. Zauscher, *Adv. Mater.* **2009**, *21*, 1825-1829.
[191] T. Chen, R. Jordan, S. Zauscher, *Small* **2011**, *7*, 2148-2152.
[192] T. T. Gao, X. L. Wang, B. Yu, Q. B. Wei, Y. Q. Xia, F. Zhou, *Langmuir* **2013**, *29*, 1054-1060.
[193] Z. Xie, X. Zhou, X. Tao, Z. Zheng, *Macromolecular rapid communications* **2012**, *33*, 359-373.
[194] A. M. Jonas, Z. Hu, K. Glinel, W. T. Huck, *Nano letters* **2008**, *8*, 3819-3824.
[195] A. M. Jonas, Z. Hu, K. Glinel, W. T. Huck, *Macromolecules* **2008**, *41*, 6859-6863.
[196] C. Chen, X. Zhou, Z. Xie, T. Gao, Z. Zheng, *Small* **2015**, *11*, 613-621.
[197] R. Advincula, W. Brittain, K. Caster, J. Rühe, *Federal Republic of Germany Weinheim: Wiley-VCH* **1983**, *483*.
[198] W. Senaratne, L. Andruzzi, C. K. Ober, *Biomacromolecules* **2005**, *6*, 2427-2448.
[199] D. J. Dyer, *Advanced Functional Materials* **2003**, *13*, 667-670.
[200] A. Sidorenko, I. Tokarev, S. Minko, M. Stamm, *Journal of the American Chemical Society* **2003**, *125*, 12211-12216.
[201] J. Pahnke, J. Rühe, *Macromolecular rapid communications* **2004**, *25*, 1396-1401.
[202] M. Husemann, M. Morrison, D. Benoit, J. Frommer, C. M. Mate, W. D. Hinsberg, J. L. Hedrick, C. J. Hawker, *Journal of the American Chemical Society* **2000**, *122*, 1844-1845.
[203] F. Zhou, L. Jiang, W. Liu, Q. Xue, *Macromolecular Rapid Communications* **2004**, *25*, 1979-1983.
[204] Q. Wei, B. Yu, X. Wang, F. Zhou, *Macromolecular Rapid Communications* **2014**, *35*, 1046-1054.
[205] F. Zhou, Z. Zheng, B. Yu, W. Liu, W. T. Huck, *Journal of the American Chemical Society* **2006**, *128*, 16253-16258.
[206] S. Woo, K. An, S. Arnoczky, J. Wayne, D. Fithian, B. Myers, *Orthopaedic basic science* **1994**, 45-87.
[207] J. H. C. Wang, E. S. Grood, J. Florer, R. Wenstrup, *Journal of Biomechanics* **2000**, *33*, 729-735.

[208] G. C. Engelmayr, M. Cheng, C. J. Bettinger, J. T. Borenstein, R. Langer, L. E. Freed, *Nature materials* **2008**, *7*, 1003-1010.

[209] J. Lu, M. P. Rao, N. C. MacDonald, D. Khang, T. J. Webster, *Acta biomaterialia* **2008**, *4*, 192-201.

[210] C. Y. Xu, R. Inai, M. Kotaki, S. Ramakrishna, *Biomaterials* **2004**, *25*, 877-886.

[211] K. Gerald, **2005**.

[212] P. A. Soucy, L. H. Romer, *Matrix Biology* **2009**, *28*, 273-283.

[213] M. Gardel, U. Schwarz, *Journal of Physics: Condensed Matter* **2010**, *22*, 190301.

[214] N. J. Sniadecki, R. A. Desai, S. A. Ruiz, C. S. Chen, *Annals of biomedical engineering* **2006**, *34*, 59-74.

[215] J. H. C. Wang, F. Jia, T. W. Gilbert, S. L. Y. Woo, *Journal of Biomechanics* **2003**, *36*, 97-102.

[216] C. Williams, Y. Tsuda, B. C. Isenberg, M. Yamato, T. Shimizu, T. Okano, J. Y. Wong, *Advanced Materials* **2009**, *21*, 2161-2164.

[217] B. Zhu, Q. Lu, J. Yin, J. Hu, Z. Wang, *Tissue engineering* **2005**, *11*, 825-834.

[218] W. Loesberg, J. Te Riet, F. van Delft, P. Schön, C. Figdor, S. Speller, J. van Loon, X. Walboomers, J. Jansen, *Biomaterials* **2007**, *28*, 3944-3951.

[219] P. Uttayarat, G. K. Toworfe, F. Dietrich, P. I. Lelkes, R. J. Composto, *Journal of Biomedical Materials Research Part A* **2005**, *75*, 668-680.

[220] U. Horzum, B. Ozdil, D. Pesen-Okvur, *Nano letters* **2015**, *15*, 5393-5403.

[221] H. Jeon, S. Koo, W. M. Reese, P. Loskill, C. P. Grigoropoulos, K. E. Healy, *Nat Mater* **2015**, *14*, 918-923.

[222] W.-G. Bae, J. Kim, Y.-H. Choung, Y. Chung, K. Y. Suh, C. Pang, J. H. Chung, H. E. Jeong, *Biomaterials* **2015**, *69*, 158-164.

[223] J. Kim, W.-G. Bae, H.-W. Choung, K. T. Lim, H. Seonwoo, H. E. Jeong, K.-Y. Suh, N. L. Jeon, P.-H. Choung, J. H. Chung, *Biomaterials* **2014**, *35*, 9058-9067.

[224] J. Haaheim, O. A. Nafday, *Scanning* **2008**, *30*, 137-150.

[225] Y.-P. Wang, K. Yuan, Q.-L. Li, L.-P. Wang, S.-J. Gu, X.-W. Pei, *Materials Letters* **2005**, *59*, 1736-1740.

[226] A. Maringa, P. Mashazi, T. Nyokong, *Electrochimica Acta* **2014**, *145*, 237-244.

[227] I. Alves, I. Kurylo, Y. Coffinier, A. Siriwardena, V. Zaitsev, E. Harté, R. Boukherroub, S. Szunerits, *Analytica Chimica Acta* **2015**, *873*, 71-79.

[228] T. Gao, S.-W. Ng, X. Liu, L. Niu, Z. Xie, R. Guo, C. Chen, X. Zhou, J. Ma, W. Jin, *NPG Asian Mater* **2014**, *6*, e130.

[229] F. Xu, Q. Cai, Y. Li, E. Kang, K. Neoh, *Biomacromolecules* **2005**, *6*, 1012-1020.

[230] Z. Xie, C. Chen, X. Zhou, T. Gao, D. Liu, Q. Miao, Z. Zheng, *ACS applied materials & interfaces* **2014**, *6*, 11955-1196.

[231] M. Heskins, J. E. Guillet, *Journal of Macromolecular Science—Chemistry* **1968**, *2*, 1441-1455.

[232] Y. H. Bae, T. Okano, S. W. Kim, *Journal of Polymer Science Part B: Polymer Physics* **1990**, *28*, 923-936.

[233] T. Sun, G. Wang, L. Feng, B. Liu, Y. Ma, L. Jiang, D. Zhu, *Angewandte Chemie International Edition* **2004**, *43*, 357-360.

[234] Y. Zhou, Z. Xie, K. A. Brown, D. J. Park, X. Zhou, P. C. Chen, M. Hirtz, Q. Y. Lin, V. P. Dravid, G. C. Schatz, *small* **2015**, *11*, 913-918.

[235] X. Liao, K. A. Brown, A. L. Schmucker, G. Liu, S. He, W. Shim, C. A. Mirkin, *Nature*

communications **2013**, *4*.

[236] Z. Zheng, W. L. Daniel, L. R. Giam, F. Huo, A. J. Senesi, G. Zheng, C. A. Mirkin, *Angewandte Chemie* **2009**, *121*, 7762-7765.

[237] L. R. Giam, M. D. Massich, L. Hao, L. S. Wong, C. C. Mader, C. A. Mirkin, *Proceedings of the National Academy of Sciences* **2012**, *109*, 4377-4382.

[238] M. Théry, *Journal of cell science* **2010**, *123*, 4201-4213.

[239] X. Jiang, G. M. Whitesides, *Engineering in life sciences* **2003**, *3*, 475-480.

[240] J. Nakanishi, T. Takarada, K. Yamaguchi, M. Maeda, *Analytical sciences* **2008**, *24*, 67-72.

[241] J. S. Choi, T. S. Seo, *Biomaterials* **2016**, *84*, 315-322.

[242] M. Mrksich, G. M. Whitesides, *Annual review of biophysics and biomolecular structure* **1996**, *25*, 55-78.

[243] D. Falconnet, G. Csucs, H. M. Grandin, M. Textor, *Biomaterials* **2006**, *27*, 3044-3063.

[244] E. D'Arcangelo, A. P. McGuigan, *BioTechniques* **2015**, *58*, 13-23.

[245] I.-T. Hwang, C.-H. Jung, C.-H. Jung, J.-H. Choi, K. Shin, Y.-D. Yoo, *Journal of Biomedical Nanotechnology* **2016**, *12*, 387-393.

[246] K. Kuroda, H. Miyoshi, S. Fujii, T. Hirai, A. Takahara, A. Nakao, Y. Iwasaki, K. Morigaki, K. Ishihara, S.-i. Yusa, *RSC Advances* **2015**, *5*, 46686-46693.

[247] Y. Kumashiro, J. Ishihara, T. Umemoto, K. Itoga, J. Kobayashi, T. Shimizu, M. Yamato, T. Okano, *Small* **2015**, *11*, 681-687.

[248] Y. Chen, B. Pidhatika, T. von Erlach, R. Konradi, M. Textor, H. Hall, T. Lühmann, *Biointerphases* **2014**, *9*, 031003.

[249] H. Liu, J. Liu, C. Qi, Y. Fang, L. Zhang, R. Zhuo, X. Jiang, *Acta biomaterialia* **2016**, *35*, 228-237.

[250] T. Fujie, H. Haniuda, S. Takeoka, *Journal of Materials Chemistry* **2011**, *21*, 9112-9120.

[251] A. F. Hirschbiel, S. Geyer, B. Yameen, A. Welle, P. Nikolov, S. Giselbrecht, S. Scholpp, G. Delaittre, C. Barner-Kowollik, *Advanced Materials* **2015**, *27*, 2621-2626.

[252] Z. Zhou, P. Yu, H. M. Geller, C. K. Ober, *Biomacromolecules* **2013**, *14*, 529-537.

[253] K. A. Kilian, B. Bugarija, B. T. Lahn, M. Mrksich, *Proceedings of the National Academy of Sciences* **2010**, *107*, 4872-4877.

[254] J. E. Gautrot, B. Trappmann, F. Oceguera-Yanez, J. Connelly, X. M. He, F. M. Watt, W. T. S. Huck, *Biomaterials* **2010**, *31*, 5030-5041.

[255] X. Li, M. Wang, L. Wang, X. Shi, Y. Xu, B. Song, H. Chen, *Langmuir* **2013**, *29*, 1122-1128.

[256] T. K. Mandal, M. S. Fleming, D. R. Walt, *Nano Letters* **2002**, *2*, 3-7.

[257] C. Combellas, F. Kanoufi, S. Sanjuan, C. Slim, Y. Tran, *Langmuir* **2009**, *25*, 5360-5370.

[258] T. Perova, J. Vij, H. Xu, *Colloid and Polymer Science* **1997**, *275*, 323-332.

[259] C. Yan, Z. Zheng, *Journal of Fiber Bioengineering and Informatics* **2013**, *6*, 117-128.